AN ABSTRACT OF THE DISSERTATION OF

Scott A. Klasek for the degree of Doctor of Philosophy in Microbiology presented on March 8, 2019.

Title: Establishment and Dynamics of Methane-oxidizing Microbial Communities in Marine Sediments

Abstract approved: _____

Frederick S. Colwell

Abstract

Marine sediments are vast sources and reservoirs of methane, a potent greenhouse gas. Most of this methane is anaerobically oxidized by archaea before it can reach the overlying ocean, though the efficiency of this process often depends on methane fluxes and mechanisms of fluid transport. Anaerobic methanotrophic archaea, or ANME, often aggregate with sulfate-reducing bacteria in consortia using sulfate as an electron acceptor, and thus are active at sulfate-methane interfaces of marine sediments. ANME are known to double on the order of months, but have not been isolated in pure culture. Their temporal responses to variation in sulfate supply or methane flux as sediment conditions change are not well understood, but would help constrain estimates of methane emission to the hydrosphere.

The focus of this dissertation was to gain an integrated understanding of how ANME, sulfate reducing bacteria, microbial community composition, and rates of methane oxidation change in response to fluctuations in biogeochemical conditions. Using two field studies and one laboratory incubation, we hypothesized that methane influx or addition would increase ANME and sulfate-reducing bacteria populations and abundances as well as methane oxidation rates,

but only after lag periods of several months. Samples were collected from Storfjordrenna, offshore Svalbard in the high Arctic, where increases in methane flux inferred from reactive-transport modeling brought methane into shallower sediment horizons. Sediments from this area were also incubated at *in situ* temperature and pressure for different lengths of time and under different methane concentrations. At the active Venere mud volcano in the Mediterranean, microbial communities from a freshly extruded summit mud breccia flow were analyzed in combination with geochemical data to infer the development of methanotrophy and examine whether deep-sourced fluids hosted unique microbial communities.

At Venere mud volcano, methane and sulfate structured microbial communities to a greater extent than deep-sourced fluids, and methanotrophs present in mud flows consisted of aerobic Gammaproteobacteria. These low-biomass fresh mud flows, probably a few years old, are likely too young for active ANME populations to develop. In contrast, at Storfjordrenna, ANME were most abundant near sulfate-methane transitions where methane was moving up the sediment column, suggesting these populations can respond after a year or less of methane intrusion. This methane intrusion fueled a boom in ANME and sulfate-reducing bacteria and decreased community diversity, which reverted after methane influx stopped. Some parallels were also observed in incubations: rates of anaerobic methane oxidation and ANME percent abundances increased with added methane concentrations, but only in a sediment from an active area of seepage and after a few months. These results provide a path forward for understanding the dynamics and capacity of this globally significant microbial subseafloor methane filter, and further the understanding of how microbial community structures and activities are linked.

Establishment and Dynamics of Methane-oxidizing Microbial Communities in Marine Sediments

by
Scott A. Klasek

A DISSERTATION

submitted to

Oregon State University

in partial fulfillment of
the requirements for the
degree of

Doctor of Philosophy

Presented March 8, 2019
Commencement June 2019

Doctor of Philosophy dissertation of Scott A. Klasek presented on March 8, 2019

APPROVED:

Major Professor, representing Microbiology

Head of the Department of Microbiology

Dean of the Graduate School

I understand that my dissertation will become part of the permanent collection of Oregon State University libraries. My signature below authorizes release of my dissertation to any reader upon request.

Scott A. Klasek, Author

ACKNOWLEDGEMENTS

A friend recently mentioned to me that “it takes a village to raise a graduate student”. I would first like to thank Rick Colwell for being such a fantastic and supportive advisor, and for his willingness and patience in taking on a student who at the time had very little background in both microbiology and earth sciences. Marta Torres likewise provided me with essential guidance and support, and her passion for marine geochemistry has become contagious. My other committee members, Ryan Mueller, Peter Bottomley, and Sandra Loesgen, have also given me useful guidance and furthered my development as a scientist.

I have also had the great pleasure to work with such a wonderful and diverse team of researchers in the Geomicro group throughout my graduate studies, in particular Byron Crump, Clare Reimers, and Andrew Thurber. My friends and colleagues, in particular Michael Graw, Amy Smith, Juliette Ohan, Rosie Gradoville, and Peter Chace, have been extremely thoughtful, supportive, and willing to listen to new ideas. I would also like to thank Stella Ross, Madeline Tyler, and Katie Hostetler for all of their hard work and positive attitudes while helping me in the laboratory.

Wei-Li Hong deserves a special mention for his assistance with geochemistry and modeling, but more broadly as a tremendously collaborative colleague and friend whose ideas and creativity have strongly shaped this dissertation. I am also grateful to Doug Bartlett and Fengping Wang for providing me the opportunities to work in their labs in addition to their useful comments, suggestions, and ideas. I would also like to recognize Simon Gilroy, Sarah Swanson, George Reed, Nancy Keller, and Scott Kennedy for allowing me to work in their laboratories as an

undergrad/postgrad and for fostering my interest in research. My path to graduate school would not have been possible without their mentorship.

To the friends I've made in Corvallis who have filled my life here with strange music, volleyball, trail runs, hatch chili peppers, and thought-provoking radio shows, thank you all so much. My family have been an enormous source of love and support from the very beginning of this journey, and I am grateful to my parents in particular for instilling in me a curiosity for the natural world. Lastly, to my fiancée, Connie, for being such a wonderful, caring partner regardless of the physical distance between us. I love you dearly.

CONTRIBUTION OF AUTHORS

Chapter 2:

Scott A. Klasek and Wei-Li Hong designed the study and participated in fieldwork, and analyzed results. Wei-Li Hong provided geochemical analyses and numerical modeling, while Scott A. Klasek conducted labwork, data analysis, and wrote the manuscript. Friederike Gründger participated in fieldwork and contributed methane measurements. Alexey Portnov participated in fieldwork and provided bathymetric mapping. Stella Ross and Katelyn Hostetler assisted with labwork. Marta E. Torres and Frederick S. Colwell secured funding for the project, discussed and interpreted results, and helped edit the manuscript.

Chapter 3:

Scott A. Klasek designed the experiment, collected samples in the field, conducted labwork, analyzed data, interpreted results, and wrote the manuscript. Marta E. Torres secured funding and provided study design, interpretation, and manuscript editing. Douglas H. Bartlett contributed funding, equipment, and laboratory space for incubations. Madeline Tyler assisted with labwork, and Wei-Li Hong provided additional geochemical data and interpretation of results. Frederick S. Colwell also helped fund this work, and provided assistance with data interpretation and manuscript editing.

Chapter 4:

Scott A. Klasek designed the study, conducted labwork, analyzed data, interpreted results, and wrote the manuscript. Marta E. Torres collected samples, provided geochemical data and

analysis, and helped edit the manuscript. Markus Loher provided mapping data and geophysical and geochemical interpretations. Gerhard Bohrmann served as chief scientist on the research cruise to the field site and provided additional geochemistry data. Thomas Pape contributed methane measurements and additional interpretations. Frederick S. Colwell helped with data interpretation and manuscript editing.

TABLE OF CONTENTS

TABLE OF CONTENTS (CONTINUED)

Page

LIST OF FIGURES

LIST OF FIGURES (CONTINUED)

Figure Page

LIST OF FIGURES (CONTINUED)

LIST OF TABLES

Establishment and dynamics of methane-oxidizing microbial communities in marine sediments

Chapter 1: Introduction

Microbial metabolism in marine sediments

Bacteria and archaea represent the vast majority of the diversity of life on Earth (Hug et al., 2016). Members of either of these domains of life mediate biogeochemical cycles in nearly every environment, though recent estimates of global biomass suggest bacteria and archaea dominate deep subsurface habitats (Bar-On et al., 2018). The existence of active bacteria in marine sediments has been known for over 80 years (Zobell, 1938), and marine sediments are currently estimated to contain 2.9×10^{29} microbial cells, making them comparable in magnitude to soils and seawater (Kallmeyer et al., 2012).

As organic carbon is deposited into marine sediments, it is metabolized by microbes according to available sources of electron acceptors that are consecutively exhausted with increasing depth through the sediment column. Organic carbon is predominantly oxidized using the electron acceptor that releases the highest amount of free energy (Claypool and Kaplan, 1974; Froelich et al., 1979). As such, aerobic respiration generally depletes oxygen in shallowest sediment regimes. Underneath, this is followed by denitrification, iron and manganese reduction, and then sulfate reduction, leaving methanogenesis as the most predominant metabolism after sulfate has been exhausted (Stumm and Morgan, 1996). The actual depths at which these metabolisms occur depend on a suite of biological and geophysical parameters which include primary production in overlying waters (Kallmeyer et al., 2012), sedimentation and diffusion rates, grain sizes, pressure gradients, and fluid flow through pore waters (Burdige,

2006). In addition, subseafloor chemolithotrophic processes like anaerobic ammonium oxidation coupled to nitrite reduction, or anammox (Dalsgaard et al., 2005) and denitrification coupled to sulfide or iron (II) oxidation (Hedrich et al., 2011; Marzocchi et al., 2014) expand the diversity of microbial metabolism beyond the scope of organic carbon mineralization.

Deeper into the sediment column, the party comes to an end. Widespread decreases in cell numbers (Kallmeyer et al., 2012) are attributed to the ability of comparably few bacterial and archaeal taxa to persist under extraordinary energy limitation (Starnawski et al., 2017) which may consist of methanogenesis and fermentation of organic material (D'Hondt et al., 2003). But this is not the case everywhere: basaltic aquifers can deliver waters rich in electron acceptors to overlying sediment columns (D'Hondt et al., 2004), and geothermal breakdown of recalcitrant organic material can release volatile substrates that fuel microbial activity (Horsfield et al., 2006).

Methane in the marine subsurface

Methane is a metabolite of particular interest because it connects subseafloor environments to the atmosphere, wherein it is the most abundant hydrocarbon and second most important anthropogenic greenhouse gas, with a global warming potential 25 times that of carbon dioxide over a 100-year period (Boucher et al., 2009; Eggleston et al., 2006). The mixing ratio of methane in the atmosphere has increased by around 1% every year since the 1970s, though its residence time is under 10 years (Rasmussen and Khalil, 1981; Reeburgh, 2007). However, it would be a mistake to conclude that marine systems are the cause of this increase, because fossil fuels, agriculture, and wetlands all emit far higher amounts of methane (Saunois et al., 2016). Rather, the oceans, and marine sediments in particular, can be thought of as biofilters

that oxidize the vast majority of the methane before it can reach the atmosphere (Reeburgh, 2007).

This capacity for methane oxidation is impressive, considering the marine subsurface produces an estimated 85 Tg methane per year (Reeburgh, 2007). Much of this methane is diffuse, formed by microbial degradation of buried organic matter using hydrogen and either acetate, carbon dioxide, or methylated organic compounds (Conrad, 1999; Henrichs and Reeburgh, 1987; Summons et al., 1998; Zinder, 1993). Thermogenic degradation of buried organic material at high temperatures and pressures also produces large amounts of methane, which can be distinguished from biogenic methane by stable isotope analysis (Etiope et al., 2008; Whiticar, 1999).

If present at high enough concentrations at sufficient pressure, methane can form hydrates, ice-like solids that trap gas molecules within a water lattice. These deposits constitute a large (500-2500 Gt) reservoir of methane in sediments (Milkov, 2004). Their sensitivity to temperature has triggered concern that warming bottom waters could release massive amounts of methane into the oceans or even the atmosphere in a response analogous to thawing of permafrost (Shakhova et al., 2010; Westbrook et al., 2009), though recent studies have demonstrated that this is not currently occurring (Berndt et al., 2014; Hong et al., 2017; Mau et al., 2017). Instead, hydrate-derived methane that reaches the water column undergoes aerobic oxidation to carbon dioxide (Leonte et al., 2017; Sparrow et al., 2018), a process mediated by several clades of aerobic bacteria, most of which belong to the class Gammaproteobacteria (Dedysh and Knief, 2018):

$CH_4 + 2\ O_2 \rightarrow CO_2 + 2\ H_2O$ (Equation 1.1)

In the sediment column, hydrate methane is more easily consumed (Treude et al., 2003). Whether hydrates are present or not, the upper extent of the methanogenic zone often coincides with the depth of sulfate depletion, forming a sulfate-methane transition zone (SMTZ). Here, anaerobic oxidation of methane (AOM) to bicarbonate is coupled to sulfate reduction to sulfide:

$CH_4 + SO_4^{2-} \rightarrow HCO_3^- + HS^- + H_2O$ (Equation 1.2)

This process of anaerobic methane oxidation (AOM) is globally distributed in anoxic sediments, responsible for removing anywhere between 60-90% of the methane before it can reach the overlying ocean (Hinrichs and Boetius, 2003; Reeburgh, 2007). The efficiency of this biological anaerobic methane filter is dependent on methane flux from below. While small fluxes of shallow, microbially-derived methane migrate diffusively and are often completely consumed at the SMTZ, larger fluxes may additionally migrate advectively through fractures and conduits, allowing a higher percentage to escape into the hydrosphere (Hong et al., 2016; Reeburgh, 2007). These seeps may be associated with pockmarks, craters, gas hydrate mounds, or other sub-kilometer sized seafloor features (Andreassen et al., 2017; Paull et al., 2007). Highest methane fluxes are contributed by seafloor mud volcanoes, which are larger structures overlying convergent margins that mobilize methane, fluids, and muds sourced from kilometers deep into the subsurface (Kopf, 2002). Reactive transport modeling studies show positive relationships between methane fluxes and rates of AOM, and as a consequence, sulfate is drawn down, shoaling the SMTZ until an equilibrium is reached (Hong et al., 2016; Regnier et al., 2011).

Anaerobic methanotrophic archaea

The microorganisms responsible for AOM include anaerobic methanotrophic archaea (ANME) that often, but not always, partner with sulfate-reducing bacteria (SRB) in consortia of hundreds to thousands of cells (Knittel and Boetius, 2009). Geochemical and laboratory incubation evidence for this syntrophy (Hoehler et al., 1994) was later supported by analysis of archaeal lipid biomarkers, fluorescent in-situ hybridization, and 16S rRNA gene sequencing (Boetius et al., 2000; Hinrichs et al., 1999; Orphan et al., 2001). ANME have not yet been isolated in pure culture, and their doubling times range on the order of months, likely a result of the extremely low free energy yield of AOM (Girguis et al., 2005; Hoehler et al., 1994; Nauhaus et al., 2007). Molecular studies reveal that they consist of three clades (ANME-1, -2, and -3) that group into the phylum Euryarchaeota, closely related to canonical methanogens (Knittel and Boetius, 2009). ANME contain the same methanogenesis pathway, but generally operate it in reverse to oxidize methane (Hallam et al., 2004; Wang et al., 2013), though net methanogenesis can predominate under sulfate-limiting conditions (Lloyd et al., 2011; Yoshinaga et al., 2014). SRB that associate with ANME group within several clades of Deltaproteobacteria (Knittel et al., 2003). ANME are now thought to be globally dispersed keystone microbial taxa in anoxic marine sediments where methane is present (Ruff et al., 2015). In cold seep environments, the fixation of methane and reduction of sulfate provide fundamental energy sources that can sustain diverse macrofaunal communities of chemosynthetic microbial mats, clams, and tubeworms (Boetius and Suess, 2004; Sibuet and Olu, 1998).

Additional research on ANME has revealed that they are able to use other electron acceptors in addition to sulfate, including iron, manganese, and nitrate (Beal et al., 2009; Haroon et al., 2013). They are thought to employ direct interspecies electron transfer in aggregations with SRB (McGlynn et al., 2015), though they can also associate with other types of cells (Chen et al., 2014; Pernthaler et al., 2008). ANME have also been described inhabiting diverse seafloor sediment environments, including hydrothermally-influenced sediments (Kellermann et al., 2012; Teske et al., 2002), and mud volcanoes (Niemann et al., 2006b).

In summary, the wide distribution of ANME and their ability to mediate AOM across diverse marine sediment environments shows they are capable of removing high amounts of methane (tens of Tg/yr) from the seafloor. Modeling studies suggest that growth and activity of methanotrophic populations could significantly mitigate methane emissions into the seafloor caused by large-scale gas hydrate dissolution events (Biastoch et al., 2011; Dale et al., 2008). However, how sediment microbial communities, and methanotrophs in particular, respond to spatiotemporal changes in energy supply are poorly constrained. Marine sediments are not often thought of as dynamic environments, but changes in subseafloor methane fluxes (Borowski et al., 1996), submarine landslides (Hensen et al., 2003), bioturbation from macrofauna (Berner and Westrich, 1985), and deposition of deeply-sourced muds from mud volcanoes (Werne et al., 2004) can perturb established SMTZs and effectively reset the interfaces at which these communities thrive. These phenomena allow us to inferentially understand the timescales and other environmental factors that affect the development and activity of methanotrophic communities.

Research questions

Addressing questions of how methanotrophs react to these changes lays a foundation for establishing ecological links between microbial communities and ecosystem function at cold seeps, and more accurately constraining methane emissions from the marine subsurface. I began to address this by asking three broad questions:

- On what timescales do ANME grow and rates of AOM change as methane supply increases?
- How do microbial communities change during methane influx, and what other biogeochemical cycles might they be capable of?
- How does sediment geochemistry structure microbial communities in transitional systems where methane oxidation may be expected to occur?

Dissertation structure

In chapter 2, we investigate Arctic seafloor gas hydrate mounds offshore Svalbard where methane fluxes are increasing and reaching into shallower sediment horizons (Hong et al., 2017; Serov et al., 2017). By pairing reactive transport modeling of porewater sulfate profiles with microbial community analyses, we observe increases in ANME/SRB populations occurring within a year after methane has migrated into sulfate reduction zones, and propose a model of microbial community dynamics associated with increases in methane flux.

A laboratory microcosm approach is presented in Chapter 3, where sediment samples from Storfjordrenna were incubated at *in situ* pressure and temperature for different lengths of time and concentrations of methane to understand how rates of sulfate reduction and AOM, microbial community composition, and abundances of sulfate reducers and methanotrophs changed concurrently. Chapter 4, the final manuscript chapter, presents changes in microbial

communities from a recently extruded mud breccia flow from the active Venere Mud Volcano (MV) in the central Mediterranean (Ceramicola et al., 2014; Loher et al., 2018c, 2018a). Methane and sulfate structured communities to a higher degree than deep-sourced fluids, and shallow cores from the flows showed increased percent abundances of aerobic methanotrophic bacteria. In addition, preliminary analysis metagenomes from Venere and Håkon Mosby MVs (Ruff et al., 2018) suggests they contain different gene content from other subseafloor ecosystems, and thus represent a distinct environment.

Chapter 2

Methane-driven microbial community succession in Arctic seafloor gas hydrate mounds

Scott A. Klasek[1], WeiLi Hong[2,3], Marta E. Torres[4], Stella Ross[4], Katelyn Hostetler[1], Alexey Portnov[3,5], Friederike Gründger[3], Frederick S. Colwell[1,4]

1 Department of Microbiology, Oregon State University, Corvallis, OR, USA

2 Geological Survey of Norway, 7491 Trondheim, Norway

3 Centre for Arctic Gas Hydrate, Environment and Climate (CAGE), Department of Geosciences, UiT The Arctic University of Norway, N-9037 Tromsø, Norway

4 College of Earth, Ocean, and Atmospheric Sciences, Oregon State University, Corvallis, OR, USA

5 School of Earth Sciences, The Ohio State University, Columbus, OH, USA

Abstract

Archaea performing anaerobic methane oxidation prevent methane produced in marine sediments from reaching the hydrosphere. How microbial communities respond to changes in methane flux in natural settings remains largely uncharacterized. We investigate gas hydrate-bearing seafloor mounds at Storfjordrenna, offshore Svalbard in the high Arctic, where methane flux ranges from diffusive transport to active gas advection. Populations of anaerobic methanotrophs and sulfate-reducing bacteria were highest at a seep site, and recent methane influx was associated with decreased community diversity. After methane passed into shallower sediment depths and stimulated sulfate-dependent anaerobic methane oxidation, microbial community composition converged, shifting on timescales of years. Despite high methane fluxes and methanotroph doubling times of 5-9 months, microbial responses are largely synchronous with the advancement of the methane front. Community diversity and gene abundance data supplement computationally-derived methane consumption rates, which together provide a framework for interpreting subseafloor microbial responses to methane escape in a changing Arctic.

Introduction

The microbial process of anaerobic methane oxidation (AOM) is responsible for consuming a sizeable majority–up to 90% (Reeburgh, 2007)–of the estimated 10^{13} – 10^{14} g methane produced in marine sediments each year (Hinrichs and Boetius, 2003) before it can escape to the hydrosphere. This globally-dispersed (Ruff et al., 2015) microbial methane filter consists of very slow-growing, currently uncultured clades of anaerobic methanotrophic archaea (ANME)

and often-symbiotic sulfate-reducing bacteria (SRB) that thrive at sulfate-methane transitions (SMTs), depth zones in sediments where methane is oxidized with sulfate (Boetius et al., 2000; Knittel and Boetius, 2009; Orphan et al., 2002). At locations of active methane gas release, some of the methane escapes the microbial filter, even though AOM rates at these sites are quite high (Boetius and Wenzhöfer, 2013).

The study of methane release from the Arctic seafloor has received significant attention over the past two decades (Ruppel, 2011). Seafloor permafrost methane venting to the atmosphere has been documented along a wide portion of the East Siberian Margin (Shakhova et al., 2010) and the South Kara Sea shelf (Portnov et al., 2013). Extensive surveying has characterized thousands of fault-associated seeps below warming waters along the West Spitsbergen (Svalbard) margin (Mau et al., 2017; Westbrook et al., 2009); numerical modeling and U/Th dates from authigenic carbonates revealed that seepage has persisted here for hundreds to thousands of years (Berndt et al., 2014; Hong et al., 2017). The Storfjordrenna trough mouth fan, 50 km south of Svalbard, hosts seafloor gas hydrate-bearing mounds (GHMs) morphologically similar to those described in the Beaufort (Paull et al., 2007) and Kara (Serov et al., 2015) Seas. These GHMs lie below water depths of 370-390 meters (Fig. 2.1), which approach the upper limit of gas hydrate stability in this area (Serov et al., 2017). Gas leakage was observed at four of five GHMs, which are thought to have formed from hydrate accumulation and methane gas overpressure following glacial retreat (Serov et al., 2017). Microbial community responses to subsurface methane release, whether driven by tectonic (Niemann et al., 2006a), climate (Biastoch et al., 2011) and/or oceanographic (Spielhagen et al., 2011) forcings, are important to constrain because they support macrofaunal communities

(Åström et al., 2018; Sen et al., 2018) that have ecological and economic importance (Haug et al., 2017). However, how these microbial communities respond to changes in methane release over time in Arctic cold seeps remains largely uncharacterized.

Changes in concentration gradients of porewater sulfate have been used to constrain the timing of subaqueous landslides (Hensen et al., 2003) and to indicate irrigation (through bioturbation or ascending gas bubbles (Haeckel et al., 2004) or migration of upwards-diffusing methane in sediments (Hong et al., 2017). Under steady-state conditions with a constant methane flux, sulfate decreases linearly with depth until the SMT is reached (Borowski et al., 1996). In non-steady-state settings experiencing increases in methane flux, sulfate deviates from the linear profile, showing an abrupt decrease to < 1 mM within a small depth range. The sulfate reduction (SR) zone thins in response to methane advancement into shallower layers, which stimulates AOM within them. Other geochemical signatures, combined with observations of free gas and gas hydrates, support a model where episodic methane emission occurs in pulses, with distinctive pre- and post-active stages (Hong et al., 2018). However, microbial responses to fluctuating methane regimes in seafloor environments are only beginning to be understood in a successional context (Ruff et al., 2018).

Such knowledge is of immediate importance as environmental changes, from either natural or anthropogenic causes, could potentially result in a sudden increase of methane flux. For example, methane release from the Deepwater Horizon oil spill in the Gulf of Mexico triggered the growth of aerobic methane-oxidizing *Gammaproteobacteria* that led to oxygen drawdown in deep marine waters (Kessler et al., 2011). Microbial successional patterns attributed to redox changes have been described in a variety of environments (Crump et al., 2007; Pett-Ridge et al.,

2006), and spatiotemporally variable interfaces have also been shown to drive community dynamics through changes in organic carbon transport (Stegen et al., 2016). In the Arctic Ocean, abrupt release of methane from the central Barents Sea has been hypothesized (Andreassen et al., 2017). However, whether microbial activity can mitigate such a release of methane in sediment systems is currently unknown.

To fill this knowledge gap, we constrain temporal responses of microbial communities as methane enters increasingly shallow sediment horizons using interdisciplinary geochemical, numerical, and microbiological approaches from Storfjordrenna GHMs, where varying stages of methane transport are evident. We report shifts in AOM rates, ANME/SRB abundances, and microbial communities concomitant with recent changes in methane flux, showing a tightly-coupled microbial response to intensifying subseafloor methane fluxes.

Methods

Fieldwork and Sample Collection

Samples and data were collected aboard the RV Helmer Hanssen on CAGE cruise 16-5, from June 16th to July 4th, 2016. Bathymetric data were acquired with the RV *Helmer Hanssen*'s shipboard Kongsberg Simrad EM 302 multibeam echo sounder using a frequency of 30 Hz and a swath angle of 60 degrees. Gas flares were detected with single (split)-beam EK60 and multibeam EM302 echosounders using 18 and 38 KHz transducers.

Gravity cores were obtained from the RV Helmer Hanssen's gravity coring apparatus. GC1045 was recovered from the south slope of GHM3, and GCs 1068–1070 from three locations at GHM5. GC1081 was collected from gas seepage area at GHM4. Once recovered, the plastic liner

containing the core was removed from the barrel, sectioned into 1 m segments, labeled, and split in half with a table saw to obtain working and archive halves. Core halves were stored horizontally at 4˚C. Following sectioning, Rhizons were used to sample porewater on archive halves. To preserve sediment headspace gas samples for methane measurements, 5 ml bulk sediment was collected with cutoff plastic syringes from the working half of the core, transferred to 20 ml headspace glass vials with 5 ml 1M NaOH and 2 glass beads, capped with rubber septa and aluminum crimpers, and stored at 2˚C until measurements were taken with a gas chromatograph. Total alkalinity (TA) was titrated onboard less than a few hours after the syringes were detached from the Rhizons. Depending on the expected TA, we used 0.1 to 0.5 ml of porewater for titration in an open beaker with constant stirring. pH was manually recorded with every addition of 0.0012M HCl. 7-10 measurements were performed for every sample. TA was calculated from the recorded pH and amount of acid added using the Gran function. Details of the calculation were reported previously (Latour et al., 2018). Increases in porewater alkalinity determined by onboard titrations were used to roughly constrain the SMT depths (within 30 cm) for sampling purposes.

Sediment microbiology samples of 2 cm depth were then taken every 5-10 cm near the SMT and every 20-50 cm above and below it. Less than 12 hours after cores were collected, ethanol-sanitized spatulas were used to scrape away the outer several mm of sediment from the working core half, and ~100 g from the interior of each sample was placed into a sterile whirlpak bag (VWR) and immediately frozen at -80˚C.

Replicate PVC push cores for geochemical and microbiological sampling were collected ~30 cm from the seep at GHM3 using a Sperre Subfighter 30k remotely operated vehicle (ROV)

equipped with a raptor arm from the Centre for Autonomous Marine Operations and Systems (AMOS). Recovery ranged from 23 to 50 cm. Rhizons were used to extract porewater from one core, and microbiology samples were extruded on deck from the other in 2-cm sections using an ethanol-sanitized spatula. These were placed into sterile bags and frozen immediately at -80˚C. Deep-frozen sediment samples were shipped from UiT-Tromsø to Oregon State University in a Cryo Solutions MVE Doble 47 dry shipper and were subsequently stored at -80˚C.

Geochemistry

Sulfate content in porewater was analyzed by a Dionex ICS1100 ion chromatography (IC) in the laboratory of Geological Survey of Norway (NGU). An IonPac AS23 column was equipped on the IC with the eluent (4.5 mM $NaCO_3$ and 0.8 mM $NaHCO_3$) flow set to be 1 mL/min. Due to a dilution issue when analyzing sulfate concentration with IC, measured values were corrected by assuming a constant chloride concentration of 556 mM across the samples. From our previous knowledge of chloride concentration in the region, the concentration can be at most 10% apart from the concentration we assigned for correction (this translates to a few mM uncertainty in the sulfate concentration). However, this correction does not affect our interpretation of non-steady-state sulfate profiles, as we observed concomitant increases in alkalinity from TA measurements.

Total sulfide (ΣHS) concentrations were measured spectrophotometrically following the Cline method (Cline, 1969). Samples were preserved onboard with 23.8 mM $Zn(OAc)_2$ solution < 30 minutes after the syringes were disconnected from the Rhizons. The samples were then kept

frozen until shore-based analysis. Details of the analyses were also given in (Latour et al., 2018). Depending on the factor of dilution, the detection limit is around tens of μM.

To determine the concentration of dissolved methane in the porewater of the sediment matrix, a conventional headspace method was applied (Serov et al., 2017). Gas measurements were performed using a Thermo Scientific Trace 1310 gas chromatograph equipped with a flame ionization detector (GC-FID) and a Thermo Scientific TG-BOND alumina (Na_2SO_4) column (30 m × 0.53 mm × 10 μm).

Modeling

For the sites with non-steady-state porewater profiles (GC1045 and GC1081), we applied the same reduced modeling scheme as described in (Hong et al., 2017). Briefly, only sulfate and methane were considered in the model with AOM as the only reaction consuming both. We assigned the diffusion coefficients of sulfate and methane to be 1.58×10^{-2} and 3.01×10^{-2} m^2/year, respectively, when corrected for tortuosity and temperature. We simulated a 60-meter sediment column, which is the bottom of gas hydrate stability zone in the area. The rates of AOM were controlled by the theoretical maximum rate and the lower boundary condition of methane. The theoretical maximum rate was determined by fitting the porewater profiles around the depth of SMT, which was set to be 2 mole/m^3/yr for all the cores (Hong et al., 2017). Different lower boundary conditions of methane were assigned, which were constrained by the curvatures of the sulfate profiles. A higher concentration of methane for the lower boundary condition results in a more abrupt change in the sulfate concentration gradient, and vice versa.

We assigned seawater sulfate and methane concentrations for the initial and upper boundary conditions; a no-flux lower boundary condition was used for sulfate.

For the sites with steady-state porewater profiles, we applied the comprehensive modeling scheme as described previously (Hong et al., 2017). We coupled the routine CrunchFlow for this simulation. We used the profiles of sulfate, ΣHS, TA, calcium, magnesium, and ammonium to constrain the reaction network. Ammonium concentration measurements were not available for these sites. Therefore, we assumed a similar profile, and therefore the same organic matter degradation rate, as that of GC920 from a previous study (Hong et al., 2017). Seawater composition was used for upper and initial conditions for all solutes. Except for methane, no-flux lower boundary conditions were assigned for all solutes. Methane was produced at the deepest cell in the model from an imaginary mineral. Such a setup is to simulate a methane source that was not produced *in situ* in the sediments, and to overcome the limitation of the software package used that required all solutes to have the same boundary condition. A detailed description of the reaction network can be found in (Hong et al., 2017). Depth-integrated fluxes were calculated by summing the product of modeled AOM rates and the cell thickness, considering all modeled AOM rates from above the methanogenic zone. GC1048 is a special case compared with the other steady-state sites: Its sulfate profile is also slightly bent as in the profiles of non-steady-state sites. To satisfactorily fit this observation, we similarly applied a slightly intensifying methane flux when we modeled GC1048. However, the increase in methane flux we assigned for GC1048 is much smaller than those from other non-steady-state sites. For this reason, and other geochemical and microbiological similarities observed between this site and steady-state areas, we discuss GC1048 together with other steady-state

sites. To eliminate concerns that only three porewater samples were collected above the SMTs which may lead to misinterpretation of the status of pore fluid system (i.e., steady-state vs. non-steady-state), we also fit the porewater profiles from the four steady-state sites with model results for non-steady-state scenarios (Fig. 2.2). Despite the scarcity of this sulfate data collected, we conclude it is difficult to misinterpret these as steady-state sites.

DNA Extraction, Amplification, Sequencing, and Analysis

DNA was extracted from sediments in a clean laminar flow hood using a Qiagen DNeasy PowerSoil kit following the manufacturer's protocol. The Earth Microbiome Project 16S Illumina Protocol was used to prepare amplicons for sequencing. Briefly, V4 regions of bacterial and archaeal 16s rRNA genes were amplified in triplicate 25 ul reactions using universal 515-forward and 806-reverse primers (Caporaso et al., 2011) modified with dual-indexed Illumina sequencing adapters (Kozich et al., 2013). The thermal cycling protocol of (Caporaso et al., 2011) was followed without modifications. After confirming amplification with agarose gel electrophoresis, triplicate PCR products were pooled and purified with a Qiagen QIAquick PCR purification kit. Amplicon concentrations were quantified with a Qubit fluorometer using the Qubit dsDNA high sensitivity assay kit and pooled in equimolar amounts. Illumina Miseq V2 paired-end 250 bp sequencing was performed by technicians at Oregon State University's Center for Genome Research and Biocomputing (CGRB). Two sediment-free DNA extraction blanks were amplified and included in the sequencing run.

16S gene sequences were processed with mothur v.1.39.3 (Schloss et al., 2009) following an established pipeline (Kozich et al., 2013). Reads were clustered into OTUs at a 97% similarity

level and taxonomically classified using the SILVA database v. 128 (Quast et al., 2013). Sequences representing potential contaminants previously reported in DNA extraction kits (Salter et al., 2014) and present in sediment-free DNA extraction blanks were removed. Sequences from the genus Brachybacterium were also removed, which represented 10% of reads from one of the extraction blanks but only 0.06% of the total reads in the dataset. After removal of singleton OTUs, communities were rarefied to 3,622 reads and relative abundances were calculated. Alpha diversity metrics (number of OTUs, Chao1, Shannon, and Simpson indices) were then determined. To compare beta diversity, a tree file containing the most common individual sequence from each OTU was constructed using clearcut (Evans et al., 2006), and weighted unifrac (Lozupone et al., 2007) distances were calculated from the untransformed OTU table. Weighted unifrac distance files were generated for each set of samples tested for differences in community structure using AMOVA (Excoffier et al., 1992) with a Bonferroni correction for multiple pairwise comparisons. (PC1029 samples were considered above-SMT, because sulfate did not drop to 0 mM). Metastats (White et al., 2009) was used to determine whether individual OTUs were differentially abundant between groups of samples.

Droplet Digital PCR

Droplet digital PCR (ddPCR) was used to quantify abundances of functional genes *dsrAB* and *mcrA* using primer pairs described by (Kondo et al., 2004) and (Luton et al., 2002), respectively. Reactions of 22 ul volume were prepared in a clean PCR hood in 96-well plates using 1x Bio-Rad QX200 ddPCR EvaGreen Supermix, 200 nM primers, and and 0.88 ul of tenfold-diluted genomic

DNA. Droplets were generated on a QX200 AutoDG Droplet Generator using automated droplet generation oil for EvaGreen Supermix (Bio-Rad). Thermal cycling was performed immediately afterwards on a Veriti 96-well thermal cycler. Protocols began with a single initialization step at 95˚C for 5 minutes and then proceeded to 40 cycles of denaturation at 95˚C for 30 seconds, annealing for 1 minute (at a temperature of 53 for *mcrA* and 58 for *dsrAB*), and for *mcrA* only, an extension at 72˚C for 75 seconds. Signal stabilization steps (4˚C for 5 minutes, then 90˚C for 5 minutes) were then performed before maintaining a 4˚C hold. To ensure uniform heating of all droplets, the ramp rate for all amplification cycles was set to 2˚C/minute. Reactions were kept at 4˚C overnight and read with the Bio-Rad QX200 Droplet Reader the following morning. Droplet generation and reading were performed by the lead author at OSU's CGRB core facility. Normalization was performed by inspecting fluorescence distributions using Quantasoft software (Bio-Rad). Threshold fluorescence values were manually imposed by visually inspecting distributions of DNA extraction blank and no-template-added control samples. Amplicon copy numbers per well were then converted to copies per gram wet sediment.

Results

Identification of sequential stages of methane flux

To investigate microbial community successional patterns across a range of methane seepage activity in Storfjordrenna GHMs, we collected sediment cores from GHMs representing different stages in seepage (Fig. 2.1, Table 2.1). GHM3 and GHM4 show persistent hydroacoustic gas flares over multi-year surveys and thus represent an active stage of seepage (Serov et al., 2017). Here, ascending free gas is the dominant carrier of methane, with limited

movement in the aqueous phase (Hong et al., 2018). In contrast, GHM5 represents a post-active stage where abundant trace elements in porewaters suggest movement of the aqueous phase at deeper depths, and gaseous methane supply has ceased, likely controlled by the openness of the conduit and/or the activity of the fluid reservoir (Hong et al., 2018). Geochemical data, microbial community, and functional gene abundance data, and numerical modeling results are each presented in Figures 2 through 4, which are grouped according to different stages of methane transport. Downcore changes from a push core precisely taken by a remote-operated vehicle (ROV) from GHM3 capture the biogeochemical signatures that reflect a recent increase in methane flux and gas bubble emission (Fig. 2.3). Next, areas at GHM3 and GHM4 currently experiencing increasing methane flux into shallower sediment horizons, but have not reached steady-state with respect to sulfate-methane dynamics, are considered a separate stage (Fig. 2.4). Finally, four cores from areas exhibiting methane supply where steady-state has been reached (i.e. no changes in methane flux) are presented, with GC1048 representing a low methane flux case from a non-GHM area (Fig. 2.5).

Field descriptions and general patterns

Black-colored glaciomarine sediments were recovered in all cores, reflecting the precipitation of iron sulfide minerals resulting from high sulfide fluxes (Sen et al., 2018). Authigenic carbonate nodules were retrieved in several cores, and chunks of gas hydrates several cm in diameter were observed between 40-50 cm below seafloor in a replicate push core of PC1029. Cores PC1029 and GC1081 were taken from areas of gas seepage indicated by the white polygons in Fig. 2.1. Core recovery lengths ranging from 102 to 335 cm captured SMTs in all cores except for

PC1029 (Table 2.1). Across all cores, alkalinity profiles that contrast with the decline in sulfate provide further support of AOM as the dominant sink for sulfate (Figs. 2.3a, 2.4a, 2.5a). *In situ* methane values are probably higher than those reported, as gas samples were taken from cores at atmospheric pressure.

High-throughput sequencing of bacterial and archaeal 16S rRNA genes recovered 3.13 million sequences and 24,328 OTUs after contaminants and singletons were removed. Bubble plots (Figs. 2.3c, 2.4c, 2.5c, left panels) show the ten most abundant taxonomic classes in the dataset, each of which individually constitute 2% or more of the total sequences, and combined account for 74%. The most common OTU, which alone comprises 24% of total sequences and becomes more abundant below the SMT, belongs to the phylum *Atribacteria*, which is thought to ferment organic matter (Nobu et al., 2016). Two other dominant classes, *Deltaproteobacteria* and *Methanomicrobia*, are subdivided into common genera of sulfate-reducing bacteria (SRB) and anaerobic methanotrophs (ANME), respectively (Figs. 2.3c, 2.4c, 2.5c, right panels). Combined, ANME and SRB make up 22% of total sequences in this dataset. ANME are present in highest relative abundances at or up to tens of cm above SMTs, but correlate most strongly with peak AOM rates derived from numerical modeling. Two clades of sulfate-reducing bacteria that commonly associate with ANME at seeps, Seep-SRB1 and Seep-SRB2 (Kleindienst et al., 2012; Knittel et al., 2003), share similar distribution patterns. Droplet digital PCR counts of the methane-fixing gene *mcrA* and dissimilatory sulfate reduction gene *dsrAB* span several orders of magnitude across cores and depths (Figs. 2.3d, 2.4d, 2.5d).

Seepage stages defined by geochemical and microbial data.

Observations of vigorous gas bubbling and recovery of gas hydrate, coupled with an incomplete drawdown in porewater sulfate and elevated methane concentrations in PC1029, suggest incomplete sulfate reduction resulting from a recent onset of seepage at the center of GHM3 (Fig. 2.3a). Depth-integrated methane flux is two orders of magnitude higher in PC1029 than in any other core (Fig. 2.6). Model-derived rates of anaerobic methane oxidation are the highest by far in PC1029, exceeding 8 mM L^{-1} bulk sediment d^{-1} without decreasing downcore (Fig. 2.3b). ANME-2 occur in noteworthy abundance at 1-3 cm in PC1029, but ANME-1b are dominant at depths with lower sulfate concentrations (Fig. 2.3c). Seep-SRB1 and Seep-SRB2 are present in near-equal percent abundances at PC1029 and in GC1081, the other core from a seep site (Figs. 2.3c, 2.4c). Highest numbers of *mcrA,* exceeding 10^8 copies per gram bulk sediment, were recovered in PC1029, even in depths with high sulfate, low methane, and low alkalinity (Fig. 2.3d); these values are comparable to ANME cell counts reported from other seep sites (Knittel et al., 2005; Ruff et al., 2018). *dsrAB* counts were over an order of magnitude lower than *mcrA* throughout the core, but still higher than in nearly all other samples.

Sulfate profiles from cores GC1045 and GC1081, in addition to PC1029, show concave-up curvature, indicating the system is not at steady-state with regard to methane-sulfate dynamics (Hong et al., 2017), hereafter referred to as non-steady-state cores (Figs. 2.3a, 2.4a). However, porewater sulfate drops off and sulfate-methane transitions are established in GC1045 and GC1081. Total methane fluxes throughout these two cores have increased over the past two decades (Table 2.2). Attributing the curvature of porewater sulfate profiles to increases in methane flux requires several assumptions. Modeling scenarios were constructed on a prior dataset of several porewater species from Storfjordrenna in an attempt to account for other

processes, but only a scenario applying contrasts in methane flux adequately fit these data (Hong et al., 2017). No sedimentological changes, fractures, or evidence of bioturbation were found in the gravity cores analyzed, though we cannot rule out bioturbation at PC1029. Cores experiencing increases in methane flux were initially assumed to be at steady-state before the methane front migrated up through the sediment column. Fluxes are integrated from all modeled AOM rates assuming AOM as the only sink for sulfate.

Modeled AOM rates peak at or up to 20 cm above the SMT depth (Fig. 2.4b). The positions of peak AOM rates in non-steady-state cores currently migrate upwards at an approximately linear rate of 10 cm per year (Fig. 2.4b, Table 2.2) as fluxes increase throughout these cores. Peak rates are much lower than in PC1029, decreasing to less than 200 uM L^{-1} d^{-1}. ANME-1b are the dominant ANME genus in GC1045 and GC1081, though ANME-1a abundances are higher than in PC1029 (Fig. 2.4c). *mcrA* counts reach maxima around 10^7 copies per gram at SMTs from both GC1045 and GC1081 (Fig. 2.4d). Though *dsrAB* counts are also comparable at these SMTs, higher *dsrAB* abundances at shallower depths in GC1045 likely reflect a larger and more diverse sulfate-reducing community than in GC1081.

The remaining four gravity cores showed linear decreases in sulfate, with methane present only below the SMT (Fig. 2.5a). We classify these sites as being at steady-state with respect to sulfate-methane dynamics, and hereafter refer to them as steady-state cores. Sulfide profiles mirror the shape of the alkalinity curves, peaking at SMT depths in steady-state cores. High sulfide concentrations at these locations confirm a complete sulfate reduction pathway. In addition, macroscopic SMT-associated mucoid biofilms, clear-translucent to yellow in color, were observed in split cores at 63 and 68 cm in GC1070 and at 305 cm in GC1048 (Fig. 2.5a).

Total methane fluxes in steady-state cores are comparable to those in non-steady-state cores (Fig. 2.6). As steady-state sulfate-methane dynamics are reached, these peak rates increase to over 500 uM L^{-1} d^{-1} (Fig. 2.5b). Despite this increase, the roughly equal methane fluxes observed in steady-state cores are attributed to the thinning of the AOM zone from roughly 20 to about 10 cm.

Dominance of ANME-1a in steady-state cores suggests ANME-1b initially grow more quickly after methane enters a sediment layer, but are then succeeded by ANME-1a (Fig. 2.7). Percent abundances of Seep-SRBs in sulfate reduction zones are lower here than in cores from non-steady-state areas (Fig. 2.3), though this decline is more drastic in Seep-SRB2. In contrast, sequences belonging to Aminicenantes and the archaeal phyla Lokiarchaeota and Woesearchaeota were more common in cores showing steady-state sulfate-methane dynamics (Fig. S2.3). Abundances of *dsrAB* in cores from steady-state areas do not differ much from GC1045 and GC1081, though *mcrA* is lower in GC1069 and GC1070 (Fig. 2.5d).

Integrating geochemistry, microbiology, and flux measurements in distinct systems.

In non-steady-state areas experiencing increases in methane flux, modeled AOM peaks migrate upward (Fig. 2.4b). Different depths, and thus microbial communities inhabiting them, can be assigned by the time they experienced (or are expected to experience) this upward-moving peak in AOM. At GC1045 and GC1081, AOM fronts migrate upward at roughly 10 cm per year (Fig. 2.4b, Table 2.2); thus GC1045 communities from 66, 76, 86, and 110 cm depths respectively correspond to the time of collection, and one, two, and over four years before. Highest relative abundances of Seep-SRB1 and total ANME, as well as highest concentrations of

mcrA, are seen in the community sampled at 76 cm (Fig. 2.4c, d). This indicates these taxa dominate microbial communities after about a year following an AOM pulse. In contrast, ANME-1b are highest in the community from 66 cm, which suggests they grow more quickly than ANME-1a in this setting. In the timespan from 1 to 4 years after the AOM pulse has passed through, *mcrA* abundances decrease by nearly three orders of magnitude, but *dsrAB* by less than one. In the one to two years after the AOM pulse moves onward and microbial communities are starved of sulfate, ANME and SRB populations rapidly decrease from 46 to 1% and 20 to 3% of the total community respectively.

GC1081 communities from 56.5, 69, and 86 cm correspond to maximum AOM rates from the present, 1.5, and 3 years ago, respectively, while the community at 49 cm is associated with high (but not yet peaking) AOM (Fig. 2.4b). In contrast to communities from GC1045, ANME percent abundances do not decrease as quickly, and Seep-SRB1 actually increases with depth (Fig. 2.4c). A similar trend of ANME-1b growth preceding ANME-1a is noticed, but surprisingly ANME-1b are present in high relative abundance at 24 cm, where AOM rates are not expected to be significant until two years into the future. Concentrations of *mcrA* and *dsrAB* both roughly correspond to the present-day AOM pulse, showing no lag time with respect to methane influx (Fig. 2.4d). Across all cores and samples, *mcrA* gene abundances correlate positively with corresponding modeled AOM rates when plotted on a log-log scale (Fig. 2.8).

Microbial community diversity and analysis.

The clear dominance of the three most abundant classes, the *Methanomicrobia*, *Deltaproteobacteria*, and a class of *Atribacteria*, in non-steady-state sites (cores GC1045 and

GC1081) is noticeable, particularly below the SMT (Fig. 2.4c). Besides these major groups, other poorly-understood taxa of bacteria that inhabit Storfjordrenna GHMs include the Aminicenantes, Anaerolineae, and Phycisphaerae, all thought to be fermentative saccharolytic heterotrophs (Sharon et al., 2015; Spring et al., 2018; Xia et al., 2016). Dehalococcoidia, also present, contain members capable of reductive dehalogenation (Hiraishi, 2008). In communities from non-steady-state cores, Shannon-Weiner alpha diversity indices decrease as depths approach peak model-derived AOM rates (Fig. 2.9a). This decline, particularly noticeable in samples just above the AOM peak, is consistent with depths experiencing recent methane influx. Linear regressions show no such decrease in diversity across AOM peaks from steady-state areas (Fig. 2.9b). Interestingly, contrasting trends are observed near peak AOM rates in steady-state sites GC1069 and GC1070.

We define three geochemical zones by the shapes of porewater sulfate profiles: these include the linear sulfate reduction (SR) zone, non-steady-state SR zone, and below-SMT. To test whether microbial communities inhabiting these groups have similar structures, we used the analysis of molecular variance (AMOVA), which examines whether genetic diversity within groups is significantly different from the average genetic diversity of pooled groups (Schloss, 2008). Results of AMOVA tests are shown in Fig. 2.10.

In cores from non-steady-state areas, differences in community structure were noted between the linear SR zone and others, but not between the non-steady-state SR zone and below-SMT (Fig. 2.10a). This suggests that despite containing high relative abundances of ANME, communities undergoing recent methane influx (i.e., those from the non-steady-state SR zone) are more similar to those below the SMT than those in all linear SR zones. Differences between

steady-state and non-steady-state areas were evident above, but not below, the SMT (Fig. 2.10b). The lack of difference between below-SMT communities in steady-state and non-steady-state cores may be attributed to differential representation in only four common OTUs, compared to nine that show markedly different abundances above the SMT (Fig. 2.7).

Discussion

The presence of distinct stages of methane flux at Storfjordrenna GHMs allows for examination of changes in predicted AOM activity and microbial community successional patterns. We conceptually summarize results from integrated geochemical, numerical, and microbiological analyses that characterize three distinct biogeochemical successional stages corresponding to changes in methane supply in all seven cores analyzed at Storfjordrenna GHMs (Fig. 2.11). Panels A, B, and C illustrate data shown in Figures 3, 4 and 5, respectively.

In panel A, gas seepage and the presence of hydrates at PC1029 indicate methane is at or above saturation in porewaters throughout the core. Despite large uncertainties in estimating when methane flux began to increase at PC1029, sulfate present at 10-30 cm should be entirely consumed within a year given the large supply of methane. Other indirect evidence for this short time frame comes from the high (> 10 μM) Fe^{2+} concentration measured at 1 cm, which should be rapidly consumed in the presence of hydrogen sulfide (30 μM at 1 cmbsf). The abundance of methane and sulfate predicts high AOM rates throughout nearly the entirety of the core, supporting large populations of ANME and SRB based on respective counts of *mcrA* and *dsrAB*. Presumably, these populations have not yet had the time to dominate the entire microbial community, which consists of high cell densities in these shallow sediments. The next

successional stage is illustrated in panel B, where AOM draws down sulfate and an SMT is established, though it has not reached steady-state dynamics. Gas seepage may still be possible if methane is oversaturated. At GC1045, diffusion modeling of sulfate porewater profiles indicate the methane front began around 292 years ago; as it diffused upwards, it stimulated comparatively lower rates of AOM in increasingly shallow sediment layers, which supported the growth of ANME/SRB and decreased microbial community diversity. Steady-state sulfate-methane dynamics are reached once methane consumption is balanced by sulfate diffusion from seawater at the SMT, a process estimated to take 10^2–10^3 years (panel C). Here, AOM rates are localized to a narrow depth window (approx. 10 cm) but are higher than in panel B. ANME and SRB populations exist in comparable abundances to panel B, but are now accompanied by an increased diversity of other microbial groups, many which may be slow-growing anaerobic fermenters of organic matter. Growth of biofilms at SMTs may also be supported over long timescales, if given steady supplies of methane and sulfate.

Model-derived methane fluxes from Storfjordrenna GHM gravity cores are an order of magnitude higher than those from seeps associated with pockmark features at Vestnessa Ridge, west of Svalbard (Hong et al., 2016). When compared to other estimates across continental margins worldwide, the values we report are high but fall within reported ranges (Regnier et al., 2011). The calculated methane flux of 610 mol m^{-1} yr^{-1} at PC1029 exceeds other modeled AOM rates at seep sites by over an order of magnitude (Joye et al., 2004), and surpasses the highest empirically measured AOM rate by 40% (Boetius and Wenzhöfer, 2013). Such a high AOM rate is somewhat unexpected, because porewater sulfate exceeds 10 mM throughout this core and has not yet depleted. This apparently high flux, supported by recovery of gas hydrates, may

reflect a recent methane intrusion, though high *mcrA* and *dsrAB* gene abundances indicate the microbial community has had some time to respond. We acknowledge that the rate estimated from PC1029 is associated with large uncertainties, as we were not able to satisfactorily fit the modeled curve to empirically-derived sulfate data under the current setup of the model. The model currently does not consider gaseous phase transport or bioturbation, which would enhance gas transport from deeper sediments and sulfate infiltration from the bottom water, thus providing additional substrates for SR-AOM.

Per-volume AOM rates from gravity cores ranged from one to four orders of magnitude higher than those reported in deep (>1 m) sediments (Biddle et al., 2006; Orcutt et al., 2013). The highest relative abundances of ANME coincide with peak AOM rates in all steady-state cores except at GC1068 and GC1069, where ANME are positioned well above SMT depths. Higher-resolution alkalinity and sulfate measurements may redefine these SMTs at shallower depths, though a cease in methane supply would allow sulfate to diffuse into a deeper depth without affecting the linearity of the sulfate profile.

If we interpret the downcore increases in *mcrA* concentrations approaching the SMT in non-steady-state cores (Fig. 2.4d) as methane-fueled ANME growth, doubling times of 147 days (GC1081, 23 to 56.5 cm) to 261 days (GC1045, 66 to 76 cm) can be derived by assuming one copy of *mcrA* per ANME genome (Haroon et al., 2013). These values complement the only other estimate of *in situ* ANME doubling time, at approximately 100-200 days (Ruff et al., 2018). Estimated per-cell AOM rates across SMTs averaged 0.65 pmol CH_4 d^{-1}, comparable to the 0.5–1.8 reported in a bioreactor where AOM was stimulated (Girguis et al., 2005). The observation that AOM rates and *mcrA* abundances nevertheless peak at nearly the same depths in areas

experiencing increasing methane flux suggests that despite findings from prior modeling studies (Dale et al., 2006), these notoriously long ANME doubling times do not imply a significant lag (only 0-1 years) in the response of the benthic biogeochemical methane filter.

The high concentrations of *mcrA* seen above the sulfate decline in PC1029 seem unexpected, but AOM rates from 0-5 cm in PC1029 still exceed 80 umol L^{-1} d^{-1} (Fig. 2.3b). This could sustain the elevated presence of ANME-2 here, which compared to ANME-1 are thought to preferentially inhabit surface sediments with higher sulfate concentrations (Knittel and Boetius, 2009). It is unclear why ANME-1 are the dominant ANME clade in all other communities. Genomic explanations may include the lack of an energetically expensive *nifDHK* nitrogenase in ANME-1 (Krukenberg et al.), and fewer multi-heme cytochromes thought to be involved in direct intercellular electron transfer (McGlynn et al., 2015). Additionally, the lack of *mer* in ANME-1 (Hallam et al., 2004; Meyerdierks et al., 2010), and the suggestion of *met* (Stokke et al., 2012) or *fae*, *hps,* and *adh* (Welander and Metcalf, 2008) as functional replacements in the reverse methanogenesis pathway imply that separate niches could exist for these two clades, but this remains an open question.

All three clades of ANME have been found as isolated cells and also in association with SRB or other bacteria, but ANME-1 are most often reported alone (Lloyd et al., 2011). In non-steady-state cores, ANME-1b aligned more closely with modeled AOM peaks than ANME-1a, but the 1a subclade was more dominant in steady-state cores (Figs. 2.4c, 2.5c). Though steady-state cores have higher peak AOM rates, ANME percent abundances and *mcrA* concentrations are mostly lower than in cores experiencing increasing methane flux (Figs. 2.3, 2.4, 2.5). This points towards a boom-and-bust cycle where methane influx into shallower sediment layers quickly

stimulates a large but ultimately unsustainable methanotrophic population, which may decline as sulfate is drawn down or as other community members establish.

In several instances, high abundances of ANME or concentrations of *mcrA* are seen at depths above where methane is expected (in GC1081 and GC1048) or below the SMT (GC1069). These may reflect inactive relic communities, though ANME-1 may still be capable of AOM (Knab et al., 2008; Parkes et al., 2007) or even methanogenesis (Lloyd et al., 2011; Wegener et al., 2016) when starved of sulfate. Co-occurrences between ANME-1b and Seep-SRB2 have been reported (Ruff et al., 2015), and are noteworthy here in GHM4 samples. Both clades of Seep-SRB, as well as *Desulfatiglans*–the most common SRB genus unaffiliated with ANME in our dataset–are presumed to oxidize a wide variety of reduced hydrocarbons (Kleindienst et al., 2012; Suzuki et al., 2014). The presence of several potentially fermentative and saccharolytic clades like the Atribacteria, Aminicenantes, Anaerolineae, and Phycisphaerae may reflect alternate organic matter-dependent metabolic strategies that are interrupted by ANME and SRB when methane enters sulfate-rich porewaters. Hydrogen-dependent CO_2 fixation by Lokiarchaeota (Sousa et al., 2016) may be another concurrent metabolism in these communities, while Woesearchaeotal capabilities may range from heterotrophy to obligate symbiosis or parasitism (Castelle et al., 2015). Macroscopic biofilms found at two SMTs in GC1048 contained *mcrA* in concentrations of up to 7.6×10^{10} g^{-1}. In combination with our geochemical and microbial community data from these depths, we hypothesize these biofilms are comprised predominately of ANME, and reflect sediment regimes experiencing steady methane and sulfate supply over many years. ANME biofilms have been described at SMTs in other subseafloor locations, often in fracture-dominated cores (Briggs et al., 2011).

Microbial communities inhabiting Storfjordrenna GHMs show lower richness and evenness than most other reported communities from methane seeps, sulfate-methane transition zones, and marine subsurface environments (Ruff et al., 2015). Broadly, diversity decreases with depth, but only significantly across depths corresponding to peak AOM rates in non-steady-state areas (Fig. 2.9). This decrease is still seen when other metrics of richness (Chao estimate and number of OTUs) or evenness (inverse Simpson) are used (data not shown).

In marine sediments, cell generation times can decrease by several orders of magnitude throughout the sulfate reduction zone and into the SMT. Starnawski et al. (2017) concluded that community assembly is influenced more by slow growth of the few OTUs capable of thriving in an energy-limited environment than by evolutionary adaptation during burial (Starnawski et al., 2017). Our finding that non-steady-state SR communities experiencing recent methane influx are more similar to those below the SMT than those in linear SR zones (Fig. 2.10a) suggests that taxa common in linear SR zones are outcompeted by ANME/SRB on timescales of years as the methane front progresses and AOM is stimulated. However, in most cases after sulfate is depleted and steady-state conditions are reached, Atribacteria become the most abundant class. Similar patterns of Atribacterial dominance have been reported in methane-rich deep Antarctic marine sediments (Carr et al., 2015) and in a submarine mud volcano off of Japan (Hoshino et al., 2017). Above-SMT differences in microbial community structure between steady-state and non-steady-state areas (Fig. 2.10b) can be linked to the abundance patterns of nine common OTUs (Fig. 2.7). Organic matter fermentation, mediated by Atribacteria, may be more dominant in steady-state sites, while Sulfurovum, which oxidizes elemental sulfur or thiosulfate using oxygen or nitrate as electron acceptor (Inagaki, 2004), may

mediate this cycle above SMTs in non-steady-state areas. These differences may be in some way related to the absence of the sulfide-dependent polychaete *Oligobrachia haakonmosbiensis*, and the decreased prevalence of seafloor bacterial mats at the steady-state GHM5 (Sen et al., 2018). Despite the short (several km) distances between individual GHMs, many interdependent factors, such as physical disturbances, differences in fluid flow regimes, and colonization of foundation species provide heterogeneity across seep ecosystems (Cordes et al., 2010).

Similar successional stages that show a decrease in community diversity have been reported: As the seepage of reducing fluids in sulfides from hydrothermal vents ceased, shifts in metabolic strategies common to oxidizing environments were documented (Sylvan et al., 2012). Aquifers amended with phenol and toluene to stimulate bioremediation of trichloroethene experienced decreases in community diversity attributable to buildup of toxic cometabolites, particularly 1,1-dichloroethene (Fries et al., 1997). Other events that could be considered disturbances, such as petroleum contamination of beach sands, represent added energy inputs for certain microbial taxa and can therefore increase community diversity (Rodriguez-R et al., 2015). Methane encroachment into sediment layers at Storfjordrenna could be considered an analogous disturbance, though one that selects for a single type of metabolism with the result of restricting community diversity.

The incorporation of genomic data into reactive transport models describing other microbially-mediated processes has demonstrated utility in predicting subsurface microbial responses (Scheibe et al., 2009). A modeling scenario that considers the dynamics of ANME growth may be of use in constraining estimates of marine subsurface methane flux into the hydrosphere.

Global microbial methane filter efficiencies of 50-60% (Knittel and Boetius, 2009) have been used in modeling studies (Biastoch et al., 2011), but seep sites display wide heterogeneity (Boetius and Wenzhöfer, 2013). Our finding that *mcrA* gene copy numbers correlate positively with modeled AOM rates provides some justification for coupling these populations and their associated activities (Fig. 2.8). Other studies reported positive correlations between methane fluxes and transcripts of methanogens and aerobic methanotrophs in peat soils, elucidating coupled microbial-biogeochemical processes (Freitag et al., 2010; Freitag and Prosser, 2009). Though microbial community data can provide explanatory power for predicting ecosystem processes, its value is often limited (Bier et al., 2015; Graham et al., 2016). Further studies could also apply the successional framework discussed here to other seep ecosystems, and integrate microbial community activities and changes with methane fluxes into overlying waters.

In summary, our integrated approach allows us to conclude that 1) seepage supports the growth of high populations of anaerobic methanotrophs and sulfate-reducing bacteria on timescales of a few years, with little if any lag time; 2) SMT establishment constrains distributions and abundances of these groups as methane encroaches into shallower sediment horizons, and 3) community diversity rebounds, and organic matter degradation becomes the dominant metabolism as steady-state sulfate-methane dynamics are reached. Cold seeps are dynamic systems that undergo temporal perturbations in methane flux. These results highlight the importance of framing microbial community data and estimates of their metabolic processes within a spatially and temporally constrained geochemical context to more thoroughly understand microbial contributions in structuring habitats and mediating biogeochemical cycles.

Acknowledgements

We thank the officers and crew of R/V Helmer Hanssen on the CAGE cruise 16-5, cruise leader Michael Carroll, chief engineers Bjørn Runar Olsen, Pedro De La Torre, Frode Volden, and researcher Stein Nornæs from the Centre for Autonomous Marine Operations and Systems (AMOS) for helping with the data acquisition and ROV operation. We also thank Stefan Bünz for providing bathymetric data. Data were acquired by the Norwegian Centre of Excellence, Centre for Arctic gas hydrates, Environment, and Climate (CAGE). We also thank Mark Dasenko, Anne-Marie Girard Pohjanpelto, and Jessica Nixon at the Oregon State University Center for Genome Resources and Biocomputing (CGRB) for support with DNA sequencing and droplet digital PCR. This work is supported by the Research Council of Norway (RCN) through its Centres of Excellence funding scheme project no. 223259, and also by the U.S. Department of Energy (DE-FE0013531). S.R. was supported by the US National Science Foundation Research Experience for Undergraduate (REU) program. M.E.T. acknowledges a fellowship from the Hanse-Wissenschaftskolleg (HWK), Germany. W.H. acknowledges the support from the RCN-funded project NORCRUST (grant no. 255150).

Figures

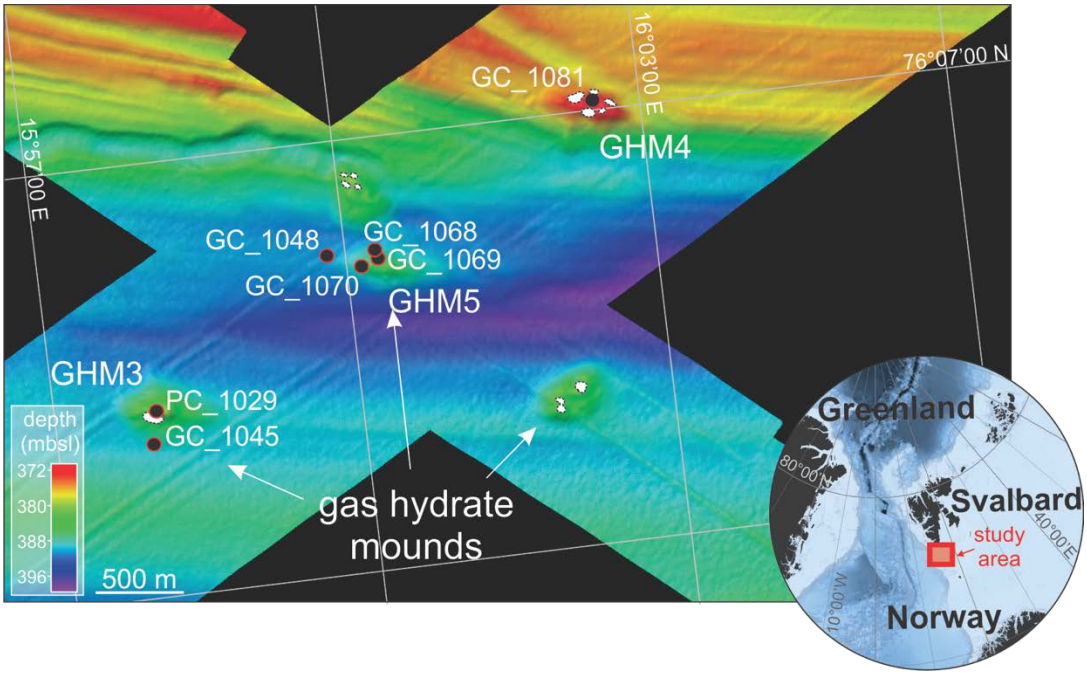

Figure 2.1. Bathymetric map of Storfjordrenna gas hydrate mounds. Storfjordrenna is located south of the Svalbard Archipelago. Locations of cores and gas hydrate mounds (GHMs) are shown. White polygons indicate areas of seafloor gas release observed at the time of the cruise. All cores were collected from GHMs, with the exception of the reference core GC1048.

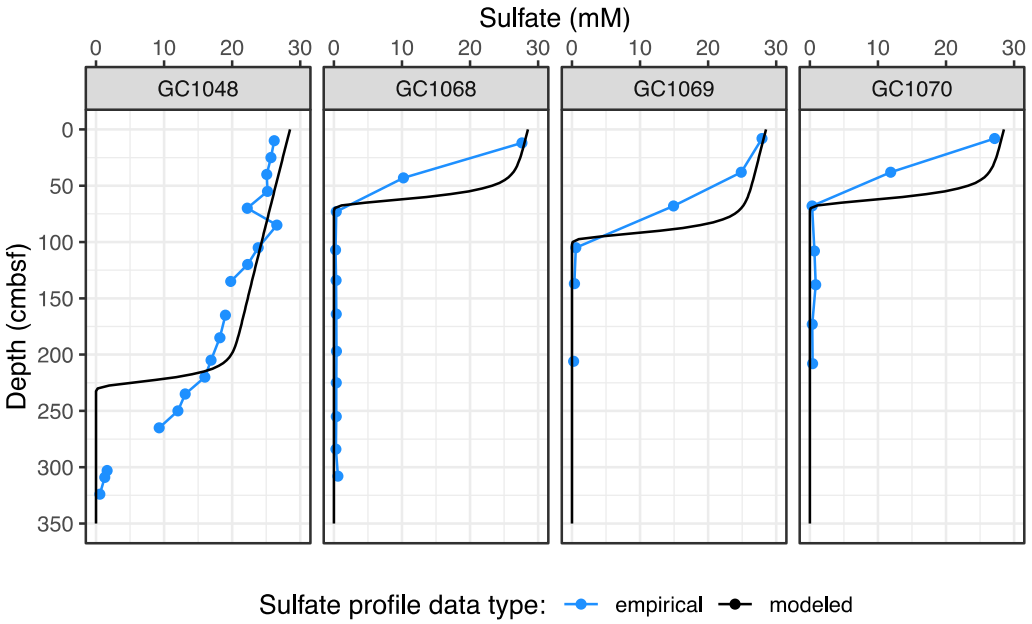

Figure 2.2. Empirically-measured sulfate porewater profiles (in blue) from cores taken from steady-state areas, juxtaposed with the modeled sulfate profiles (in black) assuming a non-

steady state scenario where methane flux is increasing. The mismatches between these two profiles justify designating these four cores under steady-state conditions.

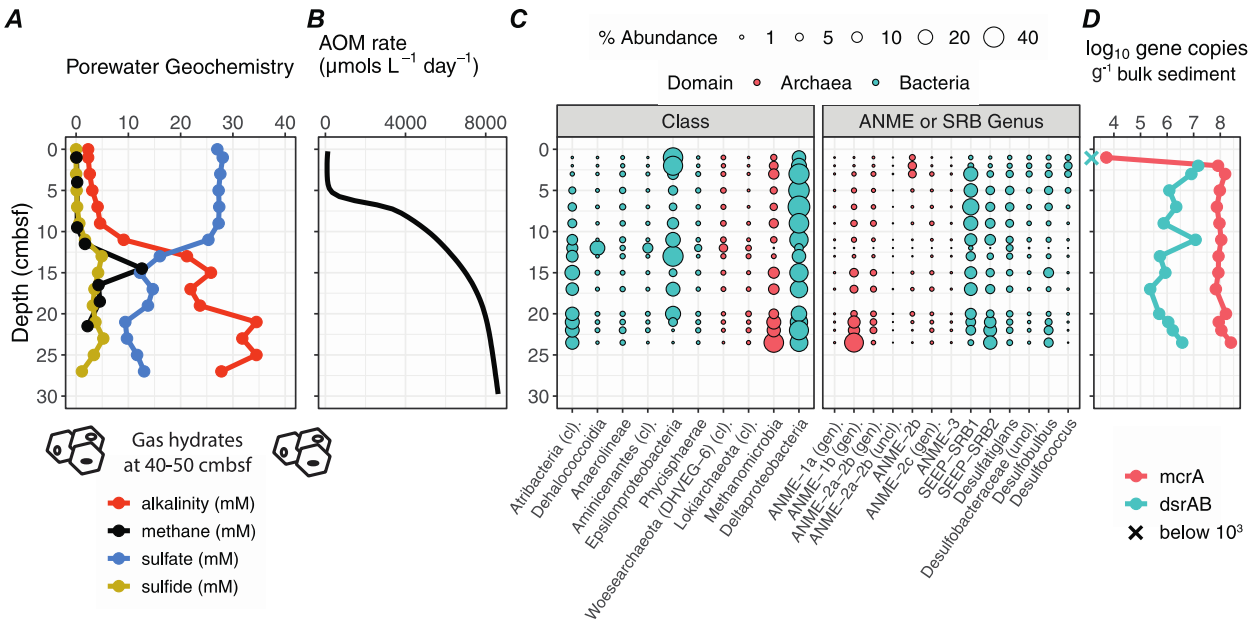

Figure 2.3. Geochemical, numerical, microbial community, and gene abundance data from an active seep site. Push core PC1029 is located at the seep in the center of GHM3. **(A)** shows porewater sulfate, sulfide, and alkalinity, and **(B)** present-day modeled AOM rates. **(C)** depicts percent abundances of dominant bacterial and archaeal classes within the microbial community (left panel), and dominant sulfate-reducing bacterial (SRB) and anaerobic methanotrophic archaeal (ANME) genera (right panel). **(D)** shows copy numbers of *mcrA* and *dsrAB* genes per gram bulk sediment, with values below the detectable limit (10^3 g^{-1}) indicated by X's. Gas hydrate nodules several cm in diameter **(A)** were recovered in a replicate core at 40-50 cm below seafloor.

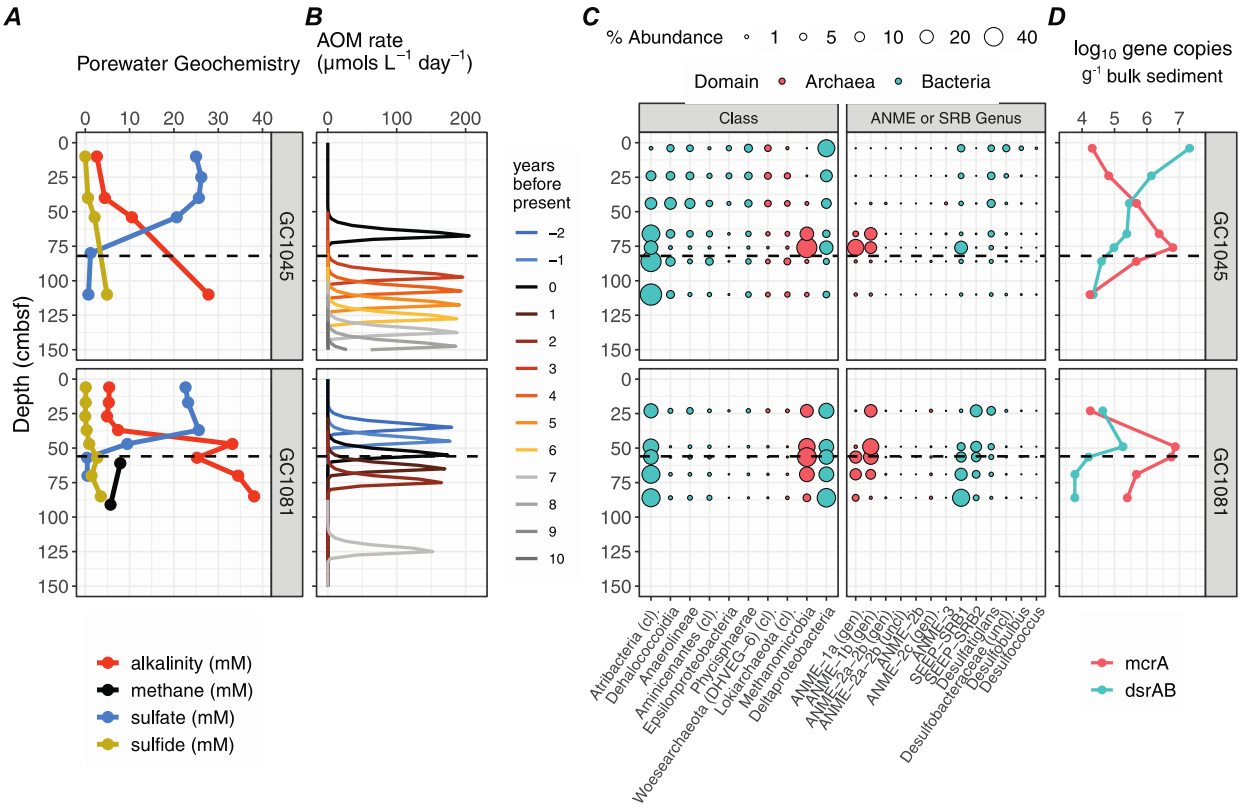

Figure 2.4. Geochemical, numerical, microbial community, and gene abundance data from two sites showing non-steady-state sulfate-methane dynamics. Gravity cores GC1045 and GC1081 are located at GHMs 3 and 4, respectively. Sulfate-methane transition depths are indicated by dashed lines. **(A)** shows porewater sulfate, sulfide, and alkalinity, and **(B)** the temporal progression of modeled AOM rates from 10 years ago to up to 2 years into the future. **(C)** indicates percent abundances of dominant bacterial and archaeal classes, and dominant sulfate-reducing bacterial (SRB) and anaerobic methanotrophic archaeal (ANME) genera. **(D)** shows copy numbers of *mcrA* and *dsrAB* genes per gram bulk sediment.

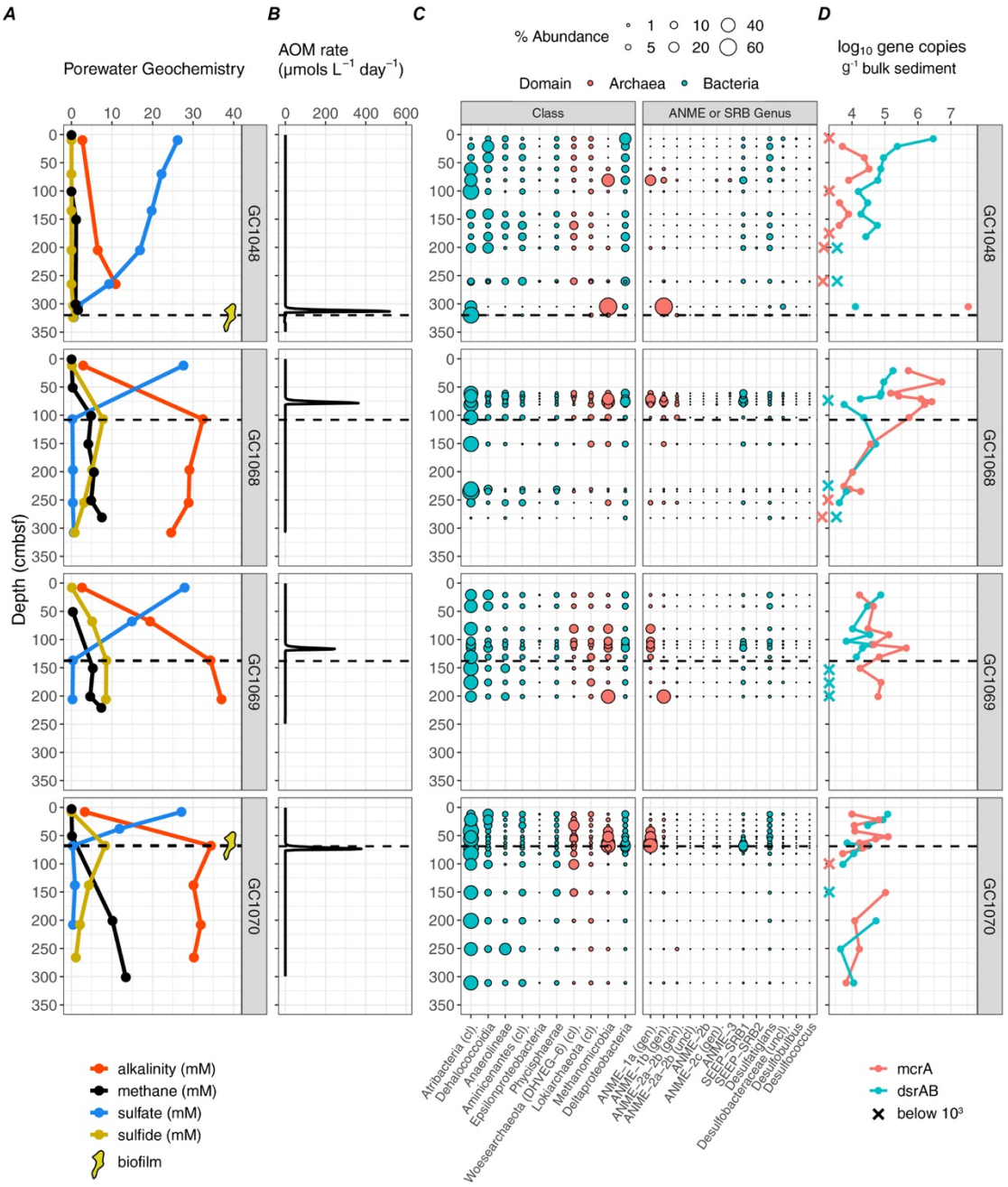

Figure 2.5. Geochemical, numerical, microbial community, and gene abundance data from four sites showing steady-state sulfate-methane dynamics. GC1068–1070 are from GHM5, and reference core GC1048 is located to the west of GHM5. Sulfate-methane transition depths are indicated by dashed lines. **(A)** shows porewater sulfate, sulfide, and alkalinity, and **(B)** present-day modeled AOM rates. **(C)** indicates percent abundances of dominant bacterial and archaeal classes, and dominant sulfate-reducing bacterial (SRB) and anaerobic methanotrophic archaeal (ANME) genera. **(D)** shows copy numbers of *mcrA* and *dsrAB* genes per gram bulk sediment, with values below the detectable limit (10^3 g^{-1}) indicated by X's. Macroscopic translucent-to-yellow biofilms, shown as yellow symbols in panel **(A)**, were observed at SMT depths in two cores (symbol size not to scale with depth axis).

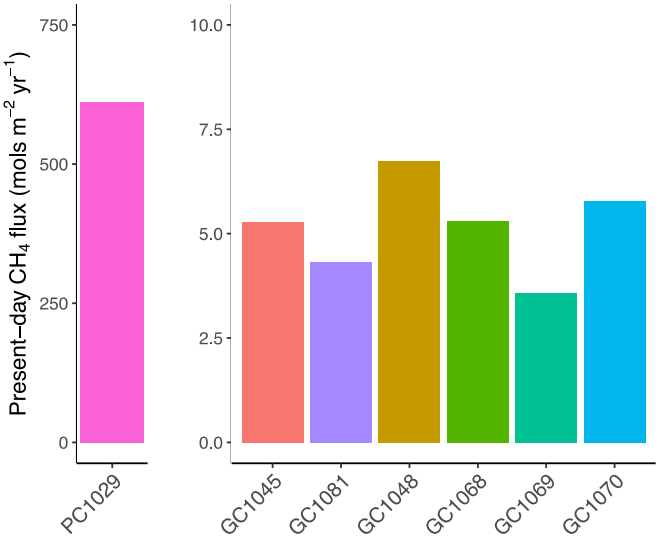

Figure 2.6. Present-day upwards methane flux integrated from modeled AOM rates in all cores. Because sulfate did not drop to 0 mM in PC1029, the flux shown in this core may be even higher.

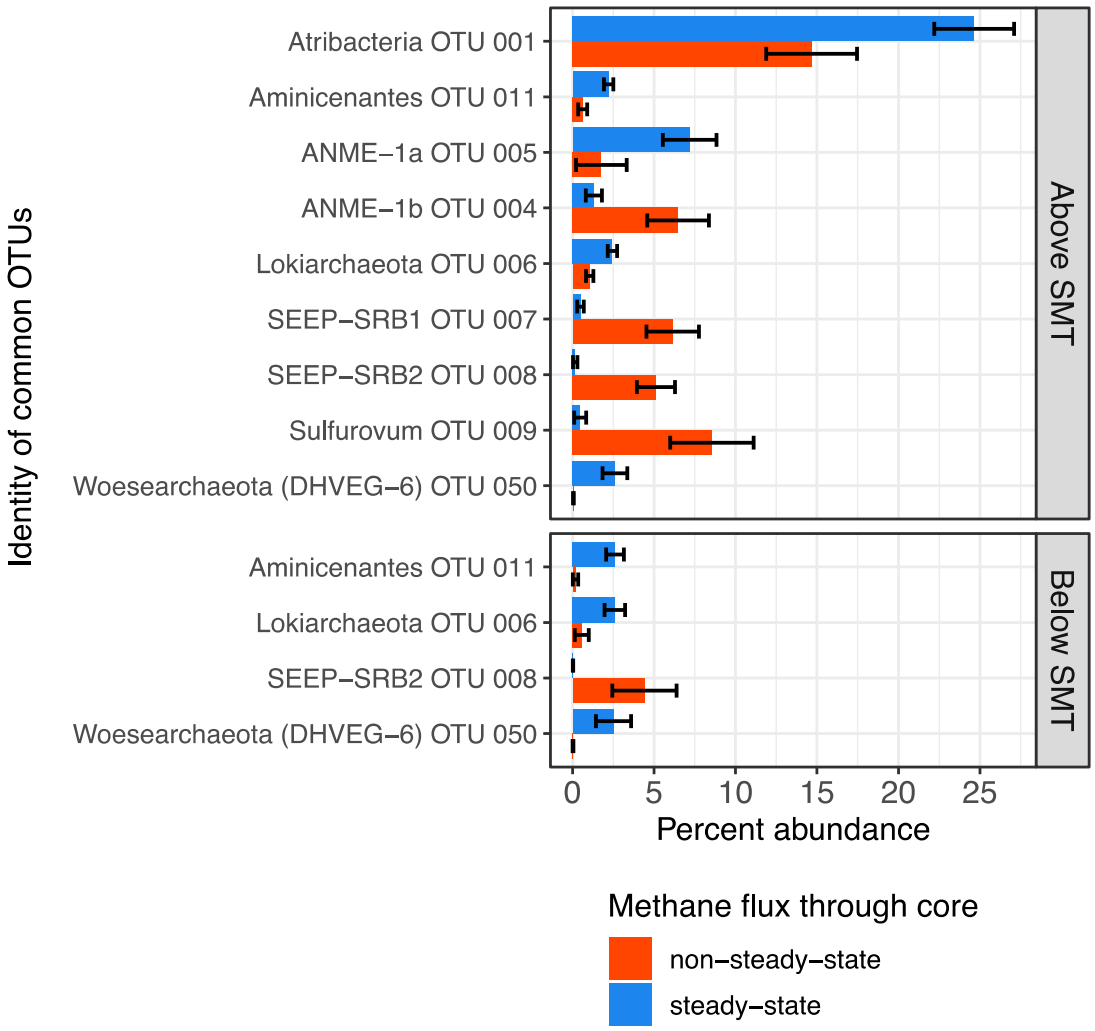

Figure 2.7. Percent abundance of all common OTUs (each comprising > 1% of sequences in the total dataset) that are differentially abundant between cores where methane flux is increasing (red) and cores at geochemical steady-state (blue) at the α=0.05 level, separated into above or below the SMT. The most specific taxonomic identity is shown for each OTU. Error bars depict standard error.

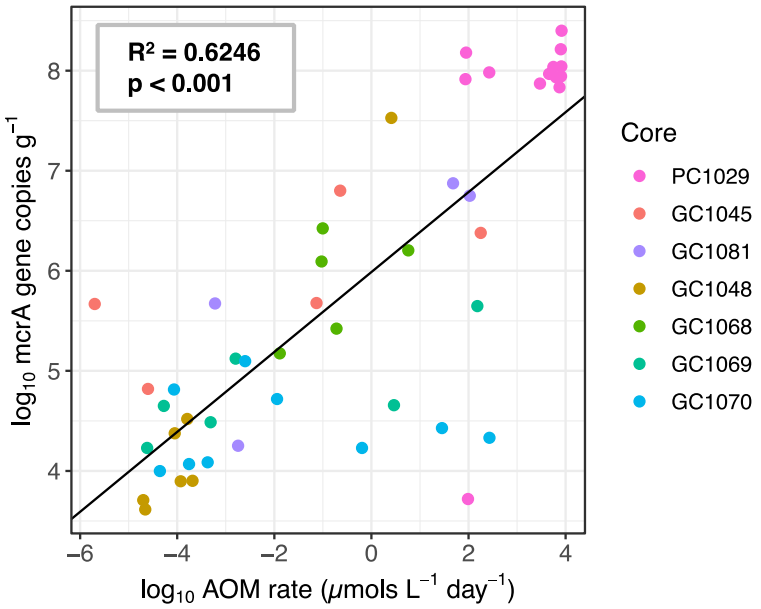

Figure 2.8. Regression of *mcrA* gene copy numbers (per gram bulk sediment) to modeled AOM rates shows a linear relationship across samples from all cores (log-log transformation). Samples that did not contain detectable *mcrA* were not included.

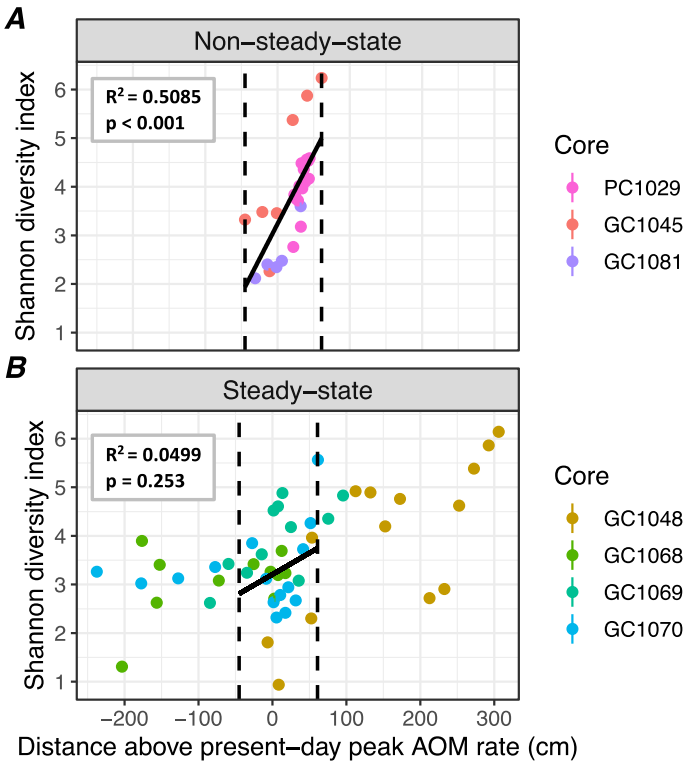

Figure 2.9. Microbial community diversity patterns across peak modeled AOM depths. Shannon-Weiner diversity indices of microbial communities for individual samples plotted by their distance above (positive) or below (negative) the depths corresponding to present-day maximum AOM rates across all cores. Cores are divided by panel based on whether sulfate-methane dynamics are **(A)** non-steady-state,

or **(B)** at steady-state. Dotted horizontal lines show the distance interval corresponding to samples from non-steady-state cores. Multiple R^2 and slope p-values are shown for linear regressions of points within these intervals. These analyses suggest microbial community diversity correlates better with the peak AOM depth in non-steady-state cores than in the others.

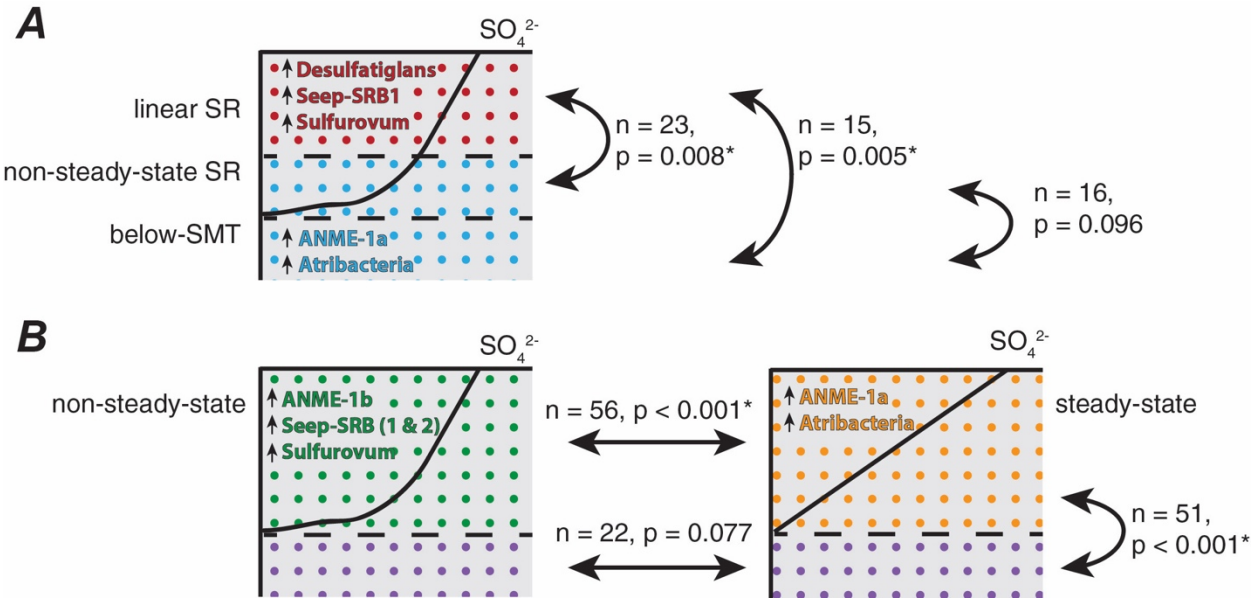

Figure 2.10. Differences in microbial community structure by geochemical zone or methane-sulfate dynamics. Analysis of molecular variance (AMOVA) tests comparing communities classified into **(A)** discrete geochemical zones based on the shape of the porewater sulfate profile and **(B)** by sulfate-methane dynamics above and below the SMT. Arrows indicate pairwise comparisons, and statistically different community structures are shown by zones with differently colored background dots. The number of communities compared for each test is indicated, and p-values with asterisks represent significance at the α=0.05 level. Taxonomic affiliations of common OTUs (>1% of the dataset) characteristic of certain zones are included.

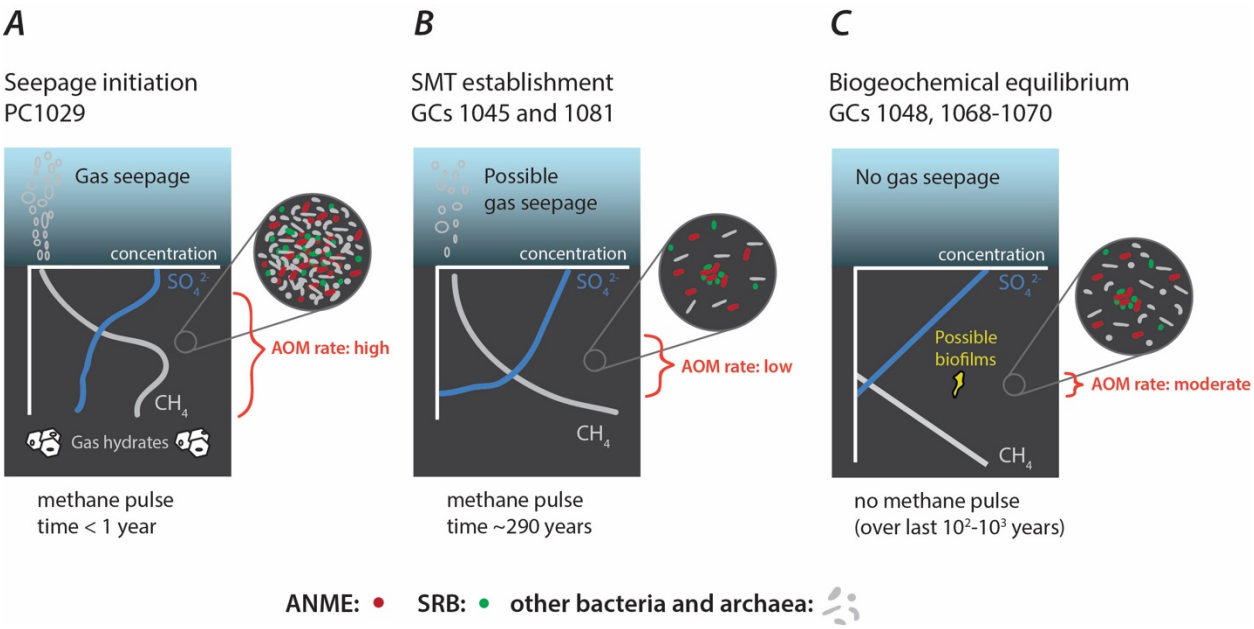

Figure 2.11. Conceptual depiction of microbial community changes concurrent with evolving methane supply at Storfjordrenna GHMs. Methane and sulfate profiles are shown in gray and blue lines, respectively, with microbial community changes indicated by blowup circles. ANME and SRB represent red and green circles, with all other bacteria and archaea in gray (cell shapes represent diversity of other taxa). **(A)** Gas hydrates at the upper limit of stability dissociate and aqueous methane diffuses upwards, stimulating AOM and drawing down sulfate while some of the methane escapes as bubbles of free gas. **(B)** Once sulfate drops below 1 mM, microbial diversity, rates of AOM, and the thickness of the AOM zone decrease. Non-steady-state conditions are still observed in sulfate-methane dynamics. **(C)** By the time a steady-state sulfate profile is reached, methane flux is no longer increasing. Gas seepage has stopped, microbial diversity rebounds, and the AOM zone is constrained to a thinner depth, but peak AOM rates are higher and can support the growth of macroscopic biofilms.

Tables

Table 2.1. Latitude, longitude, water depth, core recovery, and sulfate-methane transition depth of all cores analyzed in this study.

core	latitude	longitude	water depth (m)	core recovery (cm)	SMT depth (cm)
PC1029	76 06.398	15 58.151	381	27	NA
GC1045	76 06.347	15 57.959	387	130	82
GC1081	76 07.022	16 02.593	369	102	56
GC1048	76 06.737	15 59.845	387	335	320
GC1068	76 06.739	16 00.311	384	295	108
GC1069	76 06.719	16 00.334	383	227	138
GC1070	76 06.703	16 00.162	385	326	69

Table 2.2. Increases in methane flux over the past two decades for cores GC1045 and GC1081 and corresponding depths of modeled peak AOM rates. Fluxes are integrated from AOM rate data, using cell widths of 2.5 cm. (Peak AOM depths also at 2.5 cm resolution).

core	year before present	CH_4 flux (mols m^{-2} yr^{-1})	peak AOM depth (cm)
GC1045	21	3.674	280
GC1045	20	3.744	270
GC1045	19	3.808	257.5
GC1045	18	3.874	247.5
GC1045	17	3.944	237.5
GC1045	16	4.021	227.5
GC1045	15	4.101	217.5
GC1045	14	4.184	207.5
GC1045	13	4.268	197.5
GC1045	12	4.351	187.5
GC1045	11	4.433	177.5
GC1045	10	4.514	167.5
GC1045	9	4.593	157.5
GC1045	8	4.671	147.5
GC1045	7	4.749	137.5
GC1045	6	4.826	127.5
GC1045	5	4.902	117.5
GC1045	4	4.978	107.5
GC1045	3	5.054	97.5
GC1045	0	5.279	67.5
GC1081	22	2.93	275

GC1081	17	3.253	225
GC1081	12	3.589	175
GC1081	7	3.899	125
GC1081	2	4.207	75
GC1081	1	4.267	65
GC1081	0	4.325	55
GC1081	-1	4.379	45
GC1081	-2	4.43	35

Chapter 3

Microbial community changes in marine sediments across redox gradients during *ex situ* stimulation of anaerobic methane oxidation

Scott A. Klasek[1], Marta E. Torres[2], Douglas H. Bartlett[3], Madeline Tyler[1], Wei-Li Hong[4], Frederick S. Colwell[1,2]

1 Department of Microbiology, Oregon State University, Corvallis, OR, USA

2 College of Earth, Ocean, and Atmospheric Sciences, Oregon State University, Corvallis, OR, USA

3 Marine Biology Research Division, Scripps Institution of Oceanography, University of California, San Diego, CA, 92093-0202, USA

4 Centre for Arctic Gas Hydrate, Environment and Climate (CAGE), Department of Geosciences, UiT The Arctic University of Norway, N-9037 Tromsø, Norway

Abstract

Anaerobic methanotrophic archaea consume methane produced in marine sediments, limiting its release to the water column, yet their response to changes in methane and sulfate remains poorly constrained. To address how methane exposure affects rates of methanotrophy, microbial communities, and gene abundances in sediments from above, below, and within the sulfate-methane transition zone, we conducted time-series incubations at *in situ* temperature and pressure of Arctic marine sediments collected at and near sites of active seepage. Sediments from sulfate-reduction and methanogenic zones saw rapid increases in sulfur-cycling taxa, but failed to consume methane after nearly eight months of incubation. Seep sediments began consuming methane after two to four months, at which point anaerobic methanotrophs became more active within communities. Though we noted proliferation of taxa that were rare in natural communities, *ex situ* incubations can constrain time-dependent microbial responses to methane addition, providing important insight into microbial dynamics in environmentally sensitive regions where *in situ* time observations are difficult to achieve.

Introduction

Globally, marine sediments are sources and sinks of tens to hundreds of teragrams of methane per year (Valentine, 2002). Anaerobic methane oxidation (AOM) acts as a biofilter that prevents up to 90% of this methane from reaching into the hydrosphere (Boetius and Wenzhöfer, 2013; Reeburgh, 2007). This process is mediated by several clades of anaerobic methanotrophic archaea (ANME) and distributed in marine sediments worldwide using sulfate as an electron acceptor:

$CH_4 + SO_4^{2-} \rightarrow HCO_3^- + HS^- + H_2O$ (Equation 3.1)

ANME often associate with sulfate-reducing bacteria (SRB) at sulfate-methane transition zones (SMTs), sediment horizons where sulfate reduction (SR) and AOM remove these constituents from porewaters (Knittel and Boetius, 2009). Their global ubiquity and distribution within methane-rich sediments (Nunoura et al., 2008; Ruff et al., 2015) shapes microbial community structures in these zones (Harrison et al., 2009), and *in situ* observations suggest that these methanotrophic communities develop on timescales of years (Ruff et al., 2018). Sediment processes that could alter methane and/or sulfate supply to the SMT, such as changes in subseafloor methane flux (Hong et al., 2016), emission of mud breccia flows through mud volcanism (Ruff et al., 2018), and sediment gravity flows (Hensen et al., 2003), all presumably impact AOM rates, ANME/SRB populations, and microbial community structure. However, the temporal linkage between AOM-SR biomass and microbial community composition during establishment of AOM remains uncertain.

Seafloor methane leakage along continental margins, particularly in the Arctic (Mau et al., 2017; Shakhova et al., 2010), has triggered concerns that warming bottom waters will destabilize gas hydrates, increasing methane influx into the water column or even the atmosphere (Westbrook et al., 2009). Though there is no evidence that this is presently occurring (Berndt et al., 2014; Hong et al., 2017), methane production, consumption, and transport in Arctic seabed environments is complex and spatiotemporally variable. How ANME and other microbial community members respond to changes in methane fluxes remains unclear, and is a critical knowledge gap for understanding how a large-scale seafloor methane release could be mitigated in high-latitude regions (Dale et al., 2008).

Though ANME have not been isolated in pure culture (Wegener et al., 2016), enrichment studies have characterized their doubling times on the order of months (Nauhaus et al., 2007). Incubations at elevated pressure, which increases methane solubility in the aqueous phase, have successfully stimulated AOM in a methane-dependent manner (Deusner et al., 2010; Nauhaus et al., 2002), enriched microbial biomass (Girguis et al., 2005), and allowed characterization of transcriptional activity (Wang et al., 2014) and physical conditions for growth (Bhattarai et al., 2018b; Nauhaus et al., 2005; Timmers et al., 2015).

To directly determine how methane structures AOM-SR rates and how microbial communities would respond to changing methane fluxes in Arctic marine sediments, we collected marine sediments from Storfjordrenna, offshore Svalbard. The Storfjordrenna trough mouth fan hosts several seafloor gas hydrate-bearing mounds (GHMs) that emit methane into the overlying water and lie at depths corresponding to the upper limits of gas hydrate stability (Serov et al., 2017). Sediment samples were amended with methane at different concentrations, incubated at *in situ* temperature and pressure, and monitored for up to eight months during which geochemical changes, community composition, and abundances of marker genes were analyzed.

We hypothesized that 1) AOM-SR rates would be dependent on methane concentration and take longer to establish in sediments from above or below SMTs than those from a site of active seepage replete with both methane and sulfate; 2) highest community change would be observed in above- or below- SMT sediments as microbes adjusted to redox changes; and 3) correlations would be seen between AOM-SR rates and ANME/SRB marker gene abundances. We found that over several months, methane increased AOM-SR rates and methanotroph

abundances only in sediments from an active seep site, yet community composition of the other two sediment types changed more overall.

Methods

Fieldwork and sample collection

Sediment samples were collected aboard the RV Helmer Hanssen on cruise CAGE16-5, from June 16th to July 4th, 2016, at the mouth of the Storfjordrenna trough fan, offshore Svalbard (Fig. 3.1a) with gravity cores or push cores. Gravity core (GC) 1045 was recovered from the south slope of GHM3, while GC1036 was collected several km east of GHM3 in 394 m water depth. Once cores were recovered, their plastic liners were removed from the core barrel, sectioned into 1 m segments, labeled, and split in half with a table saw to obtain working and archive halves. Core halves were stored horizontally at 4˚C for up to two hours while alkalinity measurements were taken. Replicate PVC push cores (PC1029) for geochemical and microbiological sampling were collected approximately 30 cm from observed bubble seepage at GHM3 using a Sperre Subfighter 30k remotely operated vehicle (ROV) from the Centre for Autonomous Marine Operations and Systems (AMOS) equipped with a video camera and a raptor arm. Cores were extruded and subsampled using PVC tubing.

Sample selection for microbiology targeted discrete sediment horizons above, below, and within sulfate-methane transitions, hereby referred to as A_T, B_T, and T, respectively. This was guided by onboard porewater alkalinity titrations from the three cores (Fig. 3.1b-d). The low-alkalinity above-transition (A_T) sample was collected from GC1036 at 20-35 cm below seafloor, and the below-transition (B_T) sample was taken from GC1045 at 80-90 cm depth, just below the

porewater alkalinity increase corresponding to the SMT. The transition (T) sample, at 30-40 cm from PC1029, was chosen because it lay below an alkalinity increase but above gas hydrates recovered at 45 cm (Fig. 3.1b).

Using ethanol-sanitized spatulas to scrape away the outer few mm of sediment from the working core half, sediment samples were placed into Gaspak anaerobic pouches with oxygen-scavenging catalysts (BD Biosciences), and stored in a nitrogen-filled bag at 4˚C until the cruise ended, then transported to Oregon State University on ice. Unincubated subsamples were frozen immediately after collection. Samples were stored in anaerobic pouches in a cold room for 100 to 242 days until incubations began.

Incubation

A manual pressure pump generator (High Pressure Equipment Co. part 87-6-5) was used to hydrostatically pressurize standard or customized pressure vessels to 4.0 MPa, approximating *in situ* pressure (Fig. 3.2a). At this pressure, and at an incubation medium salinity of 35 ppt, hydrate can form between 3.0 and 3.1˚C, provided sufficient methane concentration (Sun and Duan, 2007). In an anaerobic glove bag, sediment samples were homogenized, and 2 g sediment and 8.0 ml anoxic artificial seawater medium were added to cutoff Hungate tubes (Fig. 3.2b), similar to (Bowles et al., 2011). The medium, modified from Widdel & Bak (Widdel and Bak, 1992), contained 2 mM HCO_3^-, 1.5 mM HS^-, and 10 mM SO_4^{2-}. Methane gas (99.7% pure) was sampled into a gastight ALTEF polypropylene bag (Restek) and transferred to glass cutoff Hungate incubation tubes (Bellco) using gastight syringes. Once fully dissolved, medium methane concentrations were 0, 1.5, or 5 mM for the different treatments. Tubes were placed

upside-down in vessels, pressurized to allow methane to dissolve completely and instantaneously, and incubated at 4˚C for 30, 118, or 222 days. Incubation microcosms were conducted in triplicate. 222-day incubations were started in October 2016, while 30- and 118-day incubations began in February 2017. The cold room temperature fluctuated between 4-6˚C during storage and incubation, with a single excursion to 8˚C for several days in January 2017. During each week of incubation, pressure vessels were gently shaken to resuspend sediment slurries and repressurized to 4.0 MPa as necessary.

Medium from 118-day incubations was sampled once (at 61 days), and medium for 222-day incubations was sampled twice (at 101 and 188 days). After letting sediment settle, as much of the remaining methane gas and medium as possible was removed (4.5 to 7 ml) before replenishing with fresh methane and medium. Medium was sampled from incubation tubes with a needle and syringe and passed through a 0.2 μm filter. Samples for sulfate measurements were frozen at -20˚C in Eppendorf tubes. Medium for sulfide measurements was preserved using a saturated zinc acetate solution, centrifuged, and stored at 4˚C. Medium for dissolved inorganic carbon measurements was poisoned with a saturated mercuric chloride solution. Sediment slurries were transferred to 15 ml falcon tubes, centrifuged, remaining supernatant poured off, and pellets frozen at -80˚C.

Geochemistry

Sediment porewater was collected using rhizon samplers spaced 10-25 cm through the sediment column (or every 1-2 cm for PC1029). Total porewater alkalinity (TA) was titrated onboard. Depending on the expected TA, we used 0.1 to 0.5 ml of porewater for titration in an

open beaker with constant stirring. pH was manually recorded with every addition of 0.0012M HCl. Seven to ten measurements were performed for every sample. TA was calculated from the recorded pH, and the amount of acid was added using the Gran function. Details of the calculation were reported previously in (Latour et al., 2018). Increases in porewater alkalinity determined by onboard titrations were used to roughly constrain the SMT depths (within 30 cm) for sampling purposes. Total sulfide (ΣHS) concentrations from porewaters were measured spectrophotometrically using the method of (Cline, 1969). Samples were preserved onboard with a 23.8 mM zinc acetate solution onboard less than 30 minutes after the syringes were disconnected from rhizons, and then kept frozen until shore-based analysis. Dissolved iron (II) was determined spectrophotometrically at 595 nm onboard with a ferrospectral complex in 1% ascorbic acid. Details of sulfide and iron (II) analyses are also available in (Latour et al., 2018). Porewater sulfate was analyzed with a Dionex ICS1100 ion chromatograph (IC) at the Geological Survey of Norway (NGU). An IonPac AS23 column was equipped on the IC with the eluent (4.5 mM $NaCO_3$ and 0.8 mM $NaHCO_3$) flow set to be 1 mL/min.

Sulfide from incubation medium was analyzed by the USEPA methylene blue method (Association et al., 1989) using commercial reagents (Hach) and a Hach 4000 UV/Vis spectrophotometer set to 690 nm after calibration with a sulfide standard (Sigma). Sulfate from incubation medium was measured on an Integrion HPIC RFIC Ion Chromatograph (Thermo Fisher Scientific) using a Dionex IonPac AS18 Analytical Column 4X250mm column. A KOH buffer was used as an eluent, and ranged from 22 to 40 mM throughout the 20-minute run. Sulfate eluted at 10.5 min. Calibrations were prepared with five laboratory standards (Dionex), and replicate IC measurements varied on average by 0.6%. To obtain concentrations and $\delta^{13}C$

isotopic signatures, dissolved inorganic carbon (DIC) samples were added to Exetainer vials (Labco), purged with helium, mixed with orthophosphoric acid to release CO_2, equilibrated for 10 h, and measured using a GasBench-DeltaV system as explained in (Torres et al., 2005). $\delta^{13}C$ values are expressed in ‰ relative to PDB. Sulfate reduction, sulfide production, and DIC production rates were calculated by taking the difference of the medium concentrations of these constituents across incubation intervals and dividing by the mass of bulk sediment and time interval incubated. For each interval, the amounts of sulfate reduced and methane added were compared stoichiometrically to determine the percentage of methane oxidized by sulfate. $\delta^{13}C\text{-}CH_4$ was measured using a MAT 253 isotope ratio mass spectrometer outfitted with a ConFlo IV interface (all components Thermo Fisher Scientific Inc.) at MARUM, University of Bremen, Germany and determined to be -35‰ VPDB (T. Pape, personal communication). A $\delta^{13}C\text{-}CH_4$ of -35‰ was used for all ε calculations because methane of the same isotopic signature was resupplied during incubation stages. Kinetic isotope effects (notated here as ε, epsilon) were determined by subtracting $\delta^{13}C\text{-}CH_4$ from $\delta^{13}C$-DIC measured after separate incubation intervals, and then corrected for the temperature-dependent carbon isotope fractionation between DIC and CO_2 at 4˚C (Zeebe and Wolf-Gladrow, 2001) to allow comparison with previously determined ε values (Whiticar, 1999):

$$\varepsilon = (\delta^{13}C\text{-DIC}) - (\delta^{13}C\text{-}CH_4) + 7 \qquad \text{(Equation 3.2)}$$

DNA Extraction, Amplification, Sequencing, and Analysis

DNA was extracted from sediments in a clean laminar flow hood using a Qiagen DNeasy PowerSoil kit (Hilden, Germany) following the manufacturer's protocol. The Earth Microbiome

Project 16S Illumina protocol was used to prepare amplicons for sequencing. Briefly, V4 regions of bacterial and archaeal 16S rRNA genes were amplified in triplicate 25 ul reactions using universal 515-forward and 806-reverse primers (Caporaso et al., 2011) modified with dual-indexed Illumina sequencing adapters (Kozich et al., 2013). The thermal cycling protocol of Caporaso et al. 2011 (Caporaso et al., 2011) was followed without modifications. After confirming amplification with agarose gel electrophoresis, triplicate PCR products were pooled and purified with a Qiagen QIAquick PCR purification kit. Amplicon concentrations were quantified with a Qubit fluorometer using the Qubit dsDNA high sensitivity assay kit and pooled in equimolar amounts. Illumina MiSeq V2 paired-end 250 bp sequencing was performed by technicians at Oregon State University's Center for Genome Research and Biocomputing (CGRB). A sediment-free DNA extraction blank was amplified and included in the sequencing run. 16S gene sequences were processed with mothur v. 1.39.3 (Schloss et al., 2009) following an established pipeline (Kozich et al., 2013). Reads were clustered into operational taxonomic units (OTUs) at a 97% similarity level and taxonomically classified using the SILVA database (v. 128) (Quast et al., 2013). We manually examined sequences known to be contaminants in DNA extraction kits and in subsurface ecosystems (Salter et al., 2014; Sheik et al., 2018). *Comamonas* represented the only suspicious genus, and because it was only present in an extraction blank and at low abundance, no contaminant sequences were removed from the dataset. After removal of singleton OTUs, communities were rarefied to 4,738 reads and relative abundances were calculated. Alpha diversity metrics (number of OTUs and Chao1, Shannon, and Simpson indices) were then determined. To compare beta diversity, a tree file containing the most common individual sequence from each OTU was constructed using clearcut (Evans et al.,

2006). Weighted Unifrac (Lozupone et al., 2007) distances were calculated from the untransformed OTU table to obtain coordinates for non-metric multidimensional scaling (NMDS) ordination. ANOSIM (Clarke, 1993) was used to test for differences in community structure between incubation treatments relating to time or methane addition. Metastats (White et al., 2009) was used to determine whether individual OTUs were differentially abundant between communities corresponding to these treatments.

Because microbial community composition can change appreciably during storage at these temperatures and on these timescales (Mills et al., 2012), unincubated sediments were subsampled and frozen at several times during storage to determine whether changes were brought about by incubation conditions specifically (Fig. 3.3). OTUs belonging to genera that changed by more than 1% in abundance during sediment sample storage were omitted from results that reported changes in OTU percent abundances.

Droplet Digital PCR

Droplet digital PCR (ddPCR) was used to quantify abundances of functional genes *dsrAB* and *mcrA* using primer pairs described by (Kondo et al., 2004) and (Luton et al., 2002), respectively. Reactions of 22 ul volume were prepared in a clean PCR hood in 96-well plates using 1x Bio-Rad QX200 ddPCR EvaGreen Supermix, 200 nM primers, and 0.88 ul of tenfold-diluted genomic DNA. Droplets were generated on a QX200 AutoDG Droplet Generator using automated droplet generation oil for EvaGreen Supermix (Bio-Rad). Thermal cycling was performed immediately afterwards on a Veriti 96-well thermal cycler. Protocols began with a single initialization step at 95˚C for 5 min and then proceeded to 40 cycles of denaturation at 95˚C for 30 sec, annealing for

1 min (at a temperature of 53˚C for *mcrA* and 58˚C for *dsrAB*), and for *mcrA* only, an extension at 72˚C for 75 sec. Signal stabilization steps (4˚C for 5 minutes, then 90˚C for 5 minutes) were then performed before maintaining a 4˚C hold. To ensure uniform heating of all droplets, the ramp rate for all amplification cycles was set to 2˚C/minute. Reactions were held at 4˚C overnight and read with the Bio-Rad QX200 Droplet Reader after 12 h. Droplet generation and reading were performed at OSU's CGRB core facility. Normalization was performed by inspecting fluorescence distributions using Quantasoft software (Bio-Rad). Threshold fluorescence values were manually imposed by visually inspecting distributions of DNA extraction blank and no-template-added control samples. Amplicon copy numbers per well were then converted to copies per gram bulk sediment.

Results

We conducted a timeseries of microcosm incubations on sediments from environments with different redox regimes to investigate how methane concentrations (0, 1.5, and 5 mM) structure microbial communities and control AOM-SR rates. We consider *in situ* geochemical distinctions between all sediment types before discussing geochemical changes during incubations. Microbial community and gene abundance data follow similarly.

Three sediments recovered from the Storfjordrenna GHM area (Fig. 3.1a) represent distinct geochemical regimes. A sample from an active seep site (core PC1029 at GHM3) was collected just below an incomplete decrease in porewater sulfate (Fig. 3.1b). An abundance of methane, as evidenced by observed seepage and gas hydrate nodules recovered further downcore, suggests this horizon corresponds with a geochemical transition capable of supporting AOM.

We classify this sample as “transition” (T), for future reference. The next sample, from GC1045 at the southern slope of GHM3, contained elevated alkalinity and a near-depletion in sulfate (Fig. 3.1c). We interpreted this depth to be below the transition and thus refer to it as “B_T”. Sulfide was not detected and porewater alkalinity was only slightly above seawater values in the sample from GC1036, which we interpret as a methane-naïve reference from above the transition, “A_T” (Fig. 3.1d). Downcore, sulfate decreased slightly and iron (II) peaked at 19.7 µM within the depth range of this sample, indicating sulfate and iron (III) reduction within this horizon.

When the T sediments were incubated, a methane-dependent increase in media sulfide and a concomitant decrease in sulfate were observed after 118 days, with even stronger changes shown in the later stages of the 222-day incubation (Figs. 3.4 & 3.5). Incubations amended with methane showed similar increases in media DIC (Fig. 3.6). These observations indicate that porewater chemistry changes due to stimulation of AOM occurred sometime between two and four months after incubations began. Sulfate reduction (SR) rates estimated from the drawdown of media sulfate were used to approximate AOM rates. SR rates for intervals of 118- and 222-day incubations increased with time and added methane, and exceeded rates measured in other sediment incubations (Fig. 3.7). Stoichiometrically, sulfate consumed an average of 98% of the added methane in the T incubations, far more than in other sediment types, but percentages of $SO_4^{2-}{}_{\text{consumed}}/CH_{4\ \text{added}}$ ranged from less than zero (in incubation stages where sulfate did not decrease) to over 200% in one instance (233% at 1.5 mM CH_4, from 30-101 days). Thus, SR was also coupled to oxidative breakdown of organic matter. A more salient interpretation is that a baseline amount of SR occurred regardless of the amount of

methane added: incubations without added methane serve as a reference (Fig. 3.7). SR rates exceeded sulfide production rates in incubations with added methane, which may reflect precipitation of sulfide minerals. During AOM-SR, the $\delta^{13}C$–DIC pool became more depleted due to preferential selection of ^{12}C-CH_4 by methanotrophs (Borowski et al., 1997). As methane was anaerobically oxidized to DIC during incubations, the kinetic isotope fractionation effect (ε) decreased from 42‰ to as low as 19‰, again in a methane-dependent manner (Fig. 3.8). Values of ε below 30 are generally indicative of AOM (Whiticar, 1999).

In contrast to the T incubations, the A_T and B_T sediment microcosms showed little to no sulfide buildup or sulfate consumption (Figs. 3.4 & 3.5, Table 3.1) and no evidence of methane-dependent SR at any point during the timeseries (Fig. 3.7). Values of ε did not reliably decrease when amended with 5 mM methane (Fig. 3.8, Table 3.1). Together these data show that AOM did not occur in the A_T and B_T sediment incubations.

Microbial communities from the three sediment types were different before incubations began (Table 3.2a). The T sediment communities consisted of mainly Epsilonproteobacteria and ANME (within class Methanomicrobia), while the A_T was dominated by Deltaproteobacteria and the B_T by Atribacteria (Fig. 3.9). ANMEs constituted 5% of the B_T sediment communities, and were not detected in the A_T sediments. Nevertheless, many overlapping classes were common to all three communities. Highest richness was seen in the A_T sediment community (Fig. 3.3). During sample storage at 4˚C after collection, A_T and B_T sediment communities showed reduced alpha diversity and increases in percent abundances of *Deltaproteobacteria,* but the T community did not change appreciably over nearly a year (Fig. 3.3).

Sediment microbial communities, particularly the A_T and B_T, shifted noticeably after only 30 days of incubation (Fig. 3.10). These changes first included increased percent abundances of Deltaproteobacteria, while eventually Clostridia and Bacteroidia became more dominant in longer incubations (Fig. 3.9). Longer incubations saw continued community changes in all but one instance (B_T sediments between 118 and 222 days, Fig. 3.10). During incubation, the A_T sediment communities changed the most over time, and the T communities the least (Table 3.1). Though A_T and B_T communities incubated for 222 days appear on the right side of the NMDS plot (Fig. 3.10), they still show discrete clustering by sediment type. Thus, across all incubations, we observe little evidence of convergence towards a common community structure.

Surprisingly, addition of methane did not alter community structure for any sediment type or incubation length (Table 3.2b). Methane addition significantly (α=0.05) increased percent abundances of only three OTUs that comprised over 1% of their communities. These included *Desulfuromonas* in the B_T, and a *Draconibacterium* and a *Desulforhopalus* in the T sediment communities.

At a finer-scale taxonomic resolution, percent abundances of twenty highly abundant OTUs across all sediment types changed when incubated for different times (Fig. 3.11). Many of these dynamic OTUs belong to the class *Deltaproteobacteria* and are implicated in sulfur cycling in anoxic marine sediments. Some (unclassified *Desulfuromonadales*) increased or decreased depending on the sediment type, while in other instances, different OTUs within the same genus (*Desulfocapsa* OTUs 4 and 5) show different concurrent responses within the same community. ANME percent abundances showed time-dependent changes, with ANME-1b

increasing in the T sediment communities between 30 and 118 days, and ANME-2a-2b decreasing in the B_T communities from 118 to 222 days.

Percent abundances of some taxa, particularly *Deltaproteobacteria*, increased as samples were stored at 4˚C and atmospheric pressure prior to incubation (Fig. 3.3), and these largely concurred with the community shifts seen in the first month of incubations (Fig. 3.9). Two genera from the B_T communities, *Desulfuromonas* and *Lutibacter*, increased significantly during storage. This made it appear that they had decreased over the final several months of incubations, so OTUs belonging to these groups were removed from Fig. 3.11.

The genes *mcrA* and *dsrAB* were quantified to represent abundances of anaerobic methanotrophs (Hallam et al., 2003; Luton et al., 2002) and dissimilatory sulfate reducers (Leloup et al., 2004), respectively. Before incubation, *mcrA* concentrations across the three sediment types differed by several orders of magnitude, with the A_T sediments showing the lowest, and the T sediments showing the highest levels of this functional gene (Fig. 3.12a, Table 3.3). Differences in *dsrAB* genes were less notable, but lowest concentrations were seen in the B_T sediments (Fig. 3.13a, Table 3.3). These patterns generally reflect biogeochemical processes particular to the zones from which the sediments were collected.

During incubation, *mcrA* gene abundances only increased with incubation time and methane concentration in the B_T sediments (Fig. 3.12a, Table 3.1). Changes in *dsrAB* abundances were more dynamic; A_T incubations showed time-dependent increases, while the B_T incubations showed increases over the first 30 days followed by a slight decline at 222 days (Fig. S3.13a). Though the T communities did not show significant changes in *mcrA* or *dsrAB* numbers throughout all incubation times and methane concentrations, percent abundances of ANME-1

OTUs increased in a methane-dependent manner after 222 days, while those belonging to ANME-2 showed little change (Fig. 3.12b). In contrast, A_T and B_T incubations showed negligible changes in ANME (<0.1% abundance) in incubations amended with methane. ANME-3 were either of insignificant abundance or not detected across the entire dataset. A positive correlation was observed between SR rates and *mcrA* gene abundances in the T samples incubated for 118 or 222 days (Fig. 3.12c). Interestingly, we found no correlation between SR rates and *dsrAB* gene abundances (Fig. 3.13b). Rather, the methane concentrations supplied to these incubations appeared to limit SR rates to a greater extent than the levels of either gene.

Discussion

Anaerobic methanotrophic archaea consume methane produced in marine sediments, limiting its release to the water column, yet their response to changes in methane and sulfate remain poorly constrained. To better understand how methane concentrations influence AOM rates and microbial community structure under *in situ* conditions, we incubated representative sediments at *in situ* pressure and added methane levels on months-long timescales. Sediments chosen for incubations represented different redox zones across the SMT (Fig. 3.1), and showed community differences characteristic of this transition (Parkes et al., 2014; Starnawski et al., 2017). We open the discussion by considering how changes in methane supply over time influence incubation geochemistry and AOM-SR rates, and then how they alter microbial community dynamics. We subsequently consider how this information derived from an *ex situ* laboratory incubation study can be applied to analyze AOM dynamics and microbial communities in seafloor environments.

Incubation geochemistry

As ^{12}C-methane is preferentially oxidized to DIC by microbes in marine sediments, the residual methane pool becomes isotopically heavier, resulting in a kinetic isotope effect (ε) ranging from 4-30‰. In contrast, acetoclastic methanogenesis produces ε values ranging from 35 to 55‰ (Whiticar, 1999). The T incubations that showed high SR rates and a decrease in ^{13}C in the DIC pool suggest anaerobic methane oxidation, with ε values ranging from around 37‰ to as low as 19‰ in the late-term incubations amended with 5 mM methane (Fig. 3.8). In the B_T incubations, the decrease in ε seen after 60 days may signal a slight shift towards AOM, but without any observation of methane-dependent SR, organoclastic SR may be more likely. Other incubations of microbial consortia mediating AOM-SR resulted in depletion of δ^{13}C-CH_4, which was attributed to co-occurring methanogenesis (Seifert et al., 2006) and/or carbon isotope equilibration during sulfate limitation (Yoshinaga et al., 2014).

Because methane solubility in seawater increases with pressure, prior incubations of methane-rich seafloor sediments have shown that AOM rates increase with methane partial pressures over a broad timescale, ranging from days to months (Deusner et al., 2010; Meulepas et al., 2009; Nauhaus et al., 2002; Zhang et al., 2010). In most cases, no lag times were observed before AOM was stimulated, though sulfate reduction coupled to organic matter breakdown may delay the onset of AOM during enrichment (Meulepas et al., 2009). This lag is evident in initial stages of 222-day incubations of T sediments, though in most other cases we observed minimal sulfate reduction without methane addition (Fig. 3.7).

In contrast to what we observed in our A_T sediment incubations, AOM has been stimulated in previously oxic, non-seep sediments amended with methane after 24 weeks of continuous-flow incubation (Girguis et al., 2003). Enrichment studies have yielded maximum AOM-SR rates that vary by several orders of magnitude, from 0.1 to 286 µmol g dry weight^{-1} day^{-1} (Meulepas et al., 2009). Assuming a sediment porosity of 0.5 and a density of 2.6 g/ml, our maximum measured rate of 0.91 µmol g dry weight^{-1} day^{-1} appears on the low end of this spectrum, but comparable to other long-term incubations where ANME were enriched (Bhattarai et al., 2018a). AOM-SR rates from our incubations are comparable to, or even an order of magnitude higher than, the numerically-derived rates from Vestnesa Ridge, west of Svalbard (Hong et al., 2016) despite the fact that methane concentrations in our incubations remained far below saturation. This may reflect different flow regimes at these sites, particularly between the T samples collected from an active seep and the Vestnesa SMTs that have lower fluxes of sulfate and methane. Other discrepancies in incubation rate measurements may be attributed to different methods used in sediment storage and rate calculation (Krüger et al., 2008), variations in methane and/or sulfate supply between batch and flow-through incubations (Zhang et al., 2010), physical parameters including pressure and temperature (Nauhaus et al., 2002), and variability in microbial community composition.

Methane-associated microbial community changes

We observed a limited effect of methane on microbial community structure across timescales of months. In the T sediment communities, the proliferation of an ANME-1b OTU between 30 and 118 days (Fig. 3.11) coincides with, and may account for, the increase in AOM-SR rate (Fig.

3.7). Total percent abundances of ANME-affiliated reads increased from 8% to 15-20% in the T communities amended with methane, but differences were not apparent until 222 days (Fig. 3.12b, Table 3.4). After several months of high-pressure incubations targeting AOM, similar studies reported increases in ANME 16S genes (Girguis et al., 2005), cells and aggregates (Zhang et al., 2014), and percent abundances in archaeal communities from <1% to up to 50-60% (Aoki et al., 2014; Bhattarai et al.). Years of enrichment with methane and sulfate were required for ANME and SRB to attain near-dominance of archaeal and bacterial communities (Wegener et al., 2016). Earlier studies that enriched ANME noted doubling times varying from 1.1 to 7.5 months (Zhang et al., 2011, and references therein). The T incubations that exhibited highest AOM-SR rates showed increases in *mcrA*; assuming one copy of *mcrA* per ANME genome (Haroon et al., 2013) these increases translate to doubling times of 7.6 months. In contrast to (Zhang et al., 2014), who saw bacterial alpha diversity increase after incubations, we observed no such diversity changes associated with incubation (data not shown) and even saw a decrease in alpha diversity associated with storage time in A_T and B_T samples (Fig. 3.3).

In the T sediment communities, *Draconibacterium* and *Desulforhopalus* OTUs proliferated most rapidly in response to methane addition, and support a model where organoclastic sulfate reduction is established before, or alongside, AOM. *Draconibacterium* is a recently-described genus of facultative anaerobes from marine environments capable of fermenting polysaccharides (Du et al., 2014; Li et al., 2016). Members of *Desulforhopalus* reduce sulfate with lactate, propionate, or alcohols, and include the SEEP-SRB4 clade of SRB commonly found in methane-rich sediments (Isaksen and Teske, 1996; Knittel et al., 2003). In B_T incubations, a *Desulfuromonas* OTU most similar to *Desulfuromonas svalbardensis* decreased drastically when

methane was added. *D. svalbardensis* is a psychrophile that couples acetate oxidation to Fe (III) reduction (Vandieken, 2006). This OTU, however, was barely present in the original B_T sediment community, and proliferated upon storage and incubation without methane. This suggests that methane addition (or other conditions associated with incubation) may suppress reduction of Fe (III) instead of coupling it to AOM (Beal et al., 2009).

Temporal community changes

Microbial community structure in all sediment types changed with the length of time they were incubated (Fig. 3.10) and not with the amount of methane they were amended with (Table 3.2). Nevertheless, shifts in microbial community structure mirrored redox changes associated with incubations mimicking SMT conditions: A_T sediments were introduced to sulfide in seawater media, while B_T sediments were re-exposed to sulfate. Sulfide never accumulated over 3 mM in media from A_T or B_T incubations (Fig. 3.4), so microbial communities likely did not experience sulfide toxicity, which has been noted to occur around 5 mM or more (Maillacheruvu and Parkin, 1996). Increases in *dsrAB* among A_T and B_T 30-day incubations (Fig. 3.13) probably reflect the proliferation of sulfate-reducing clades of Deltaproteobacteria (Fig. 3.9), but they apparently mediate different cycles or do not reduce sulfate until later stages of incubation. Alpha- and Gammaproteobacteria, which possess oxidative types of *dsrAB* (Müller et al., 2015), could also partially account for the increase in *dsrAB*. Because no sulfate reduction was observed at 30 days, high abundances of sulfur-cycling taxa may reflect other processes such as sulfide oxidation with organic matter (Heitmann and Blodau, 2006). Though *mcrA* abundances increased most quickly in B_T incubations amended with highest amounts of methane (Fig.

3.12a), ANME percent abundances did not change appreciably (Table 1). Instead, this increase could reflect growth of methanogens, which can be active even in methane concentrations of several mM (Lazar et al., 2012). OTUs belonging to the methanogenic clade *Methanococcoides* increased very slightly, from 0.04% to 0.21% after 222 days. *Methanococcoides* also increased up to 0.4% in A_T communities, where ANMEs were only sporadically detected. In addition, some of the *mcrA* detected could reflect non-Euryarchaeotal lineages (Evans et al., 2015; Vanwonterghem et al., 2016).

The A_T communities saw growth of OTUs belonging to *Geopsychrobacter* and *Desulfuromonas* (Fig. 3.11). These genera are capable of using acetate and a variety of other organic compounds derived from fermenters as electron donors, and Fe (III), Mn (IV), or S_0 as electron acceptors (Holmes et al., 2004; Pfennig and Biebl, 1976; Roden and Lovley, 1993). Since Fe (II) concentration peaked at over 19 µM within the A_T sediment depth, this Fe (II) produced through iron reduction could precipitate sulfide as iron sulfide minerals and account for the lack of sulfide accumulation observed in corresponding incubations (Fig. 3.4).

The T communities changed over time, but to a lesser degree than reported in a five-year enrichment with methane at ambient pressure (Aoki et al., 2014). No changes in *mcrA* or *dsrAB* abundance were observed in these incubations. This suggests that communities were already acclimated for AOM, and also that approximately eight months of incubation did not stimulate much ANME/SRB growth at the methane concentrations and conditions provided. However, a positive relationship between AOM-SR rate and *mcrA* abundance appears dependent on methane addition (Fig. 3.12c). In two outliers, *mcrA* exceeded 10^8 copies g^{-1}, suggesting growth

of ANME or other methanotrophic taxa that contain this gene. However, in the other incubations AOM-SR instead appeared to be driven by an increase in ANME activity.

Context for use of ex situ incubations

Several factors need to be considered when interpreting incubation studies to infer *in situ* microbial community function and dynamics. Dilutions and "bottle effects" (Hammes et al., 2010) can alter bacterial community activity (Stewart et al., 2012) and population dynamics of grazers (Agis et al., 2007), possibly due to organic matter flocculation (Pernthaler and Amann, 2005). Proliferation of Bacteroidia and Clostridia in our incubations was not expected, considering each class comprised around 0.01% of sequences from cores collected *in situ* at the same GHM area (data not shown). *Methanococcoides*, *Geopsychrobacter* and *Draconibacterium* were also barely detected *in situ*, which suggests that conditions pertaining to incubation, potentially related to organic carbon turnover, may influence community composition. In this study, media was replaced during batch incubations to limit sulfide accumulation. Continuous-flow high pressure enrichment strategies can accomplish this while supplying more environmentally realistic methane fluxes to incubated samples and minimizing shear forces that could potentially disrupt microbial consortia (Zhang et al., 2010). An integrated high-pressure coring and flow-through incubation technique has been used to further characterize the interplay between rates of biogeochemical processes and microbial community dynamics in seep environments (Case et al., 2017). Field studies have combined community analysis with seafloor observatory data across recent eruptions at a seafloor mud volcano and found that AOM communities develop on timescales of several years (Ruff et al., 2018).

Fundamentally, it can be quite challenging to conduct controlled long-term experiments in the field. And these experiments may also be subject to some bias. By using laboratory experimentation to study microbial communities under defined conditions, some insight can be gained into the causal relationships among biogeochemical processes that exist in nature. Estuarine sediments amended with high amounts of organic matter showed increased denitrification rates and denitrifier community diversity (Babbin et al., 2016), while incubations of lake sediment cores at temperatures anticipated by climate warming suggested that methanotrophy could balance, or even exceed, increased rates of methanogenesis (Fuchs et al., 2016). Ideally, both controlled laboratory incubations and careful experiments performed at field sites can function together as complementary approaches to resolve difficult microbial ecology issues.

After several months of exposure to methane, sediments from an active seep showed increases in AOM-SR rates that corresponded with higher abundances of *mcrA* genes and percent abundances of ANME. Although AOM-SR was not stimulated in A_T or B_T sediments after several months, redox-associated changes in communities and *dsrAB* gene abundances could represent a stage that precedes AOM establishment. Therefore, questions of how the activity or efficiency of the subseafloor microbial methane filter is predicted to change, possibly from increasing subseafloor methane fluxes (Boetius and Wenzhöfer, 2013; Dale et al., 2008), should consider realistic timescales for microbial community responses within particular sediment horizons. This work provides an approach for cross-validating complementary field-based studies, and for determining causative relationships between characteristics of microbial community structure and biogeochemical function.

Acknowledgements

We express gratitude to the officers and crew of R/V Helmer Hanssen on the CAGE cruise 16-5, cruise leader Michael Carroll, chief engineers Bjørn Runar Olsen, Pedro De La Torre, Frode Volden, and researcher Stein Nornæs from the Centre for Autonomous Marine Operations and Systems (AMOS) for helping with sample acquisition and ROV operation. We also thank Stefan Bünz for providing bathymetric data, and Alexey Portnov for mapping the study area. Benjamin Russell at the Oregon State University (OSU) College of Earth, Ocean, and Atmospheric Science (CEOAS) Machine and Technical Development Facility designed parts for the Benthos pressure vessel. We also thank Mark Dasenko, Anne-Marie Girard Pohjanpelto, and Jessica Nixon at the OSU Center for Genome Resources and Biocomputing (CGRB) for support with DNA sequencing and droplet digital PCR. Andy Ross ran carbon isotope measurements at the OSU stable isotope laboratory, and Thomas Pape aided with methane isotope measurements. Iria Giménez provided instruction in measuring sulfate. Logan Peoples (Scripps Institute of Oceanography) provided assistance with incubation setup, and Yasaman Jaladat (UCSD) provided additional help with sample storage. This work is supported by the Research Council of Norway (RCN) through its Centres of Excellence funding scheme project no. 223259, and also by the U.S. Department of Energy (DE-FE0013531) and the Deep Carbon Observatory's Deep Life Cultivation Internship (supported through the Sloan Foundation).

Figures

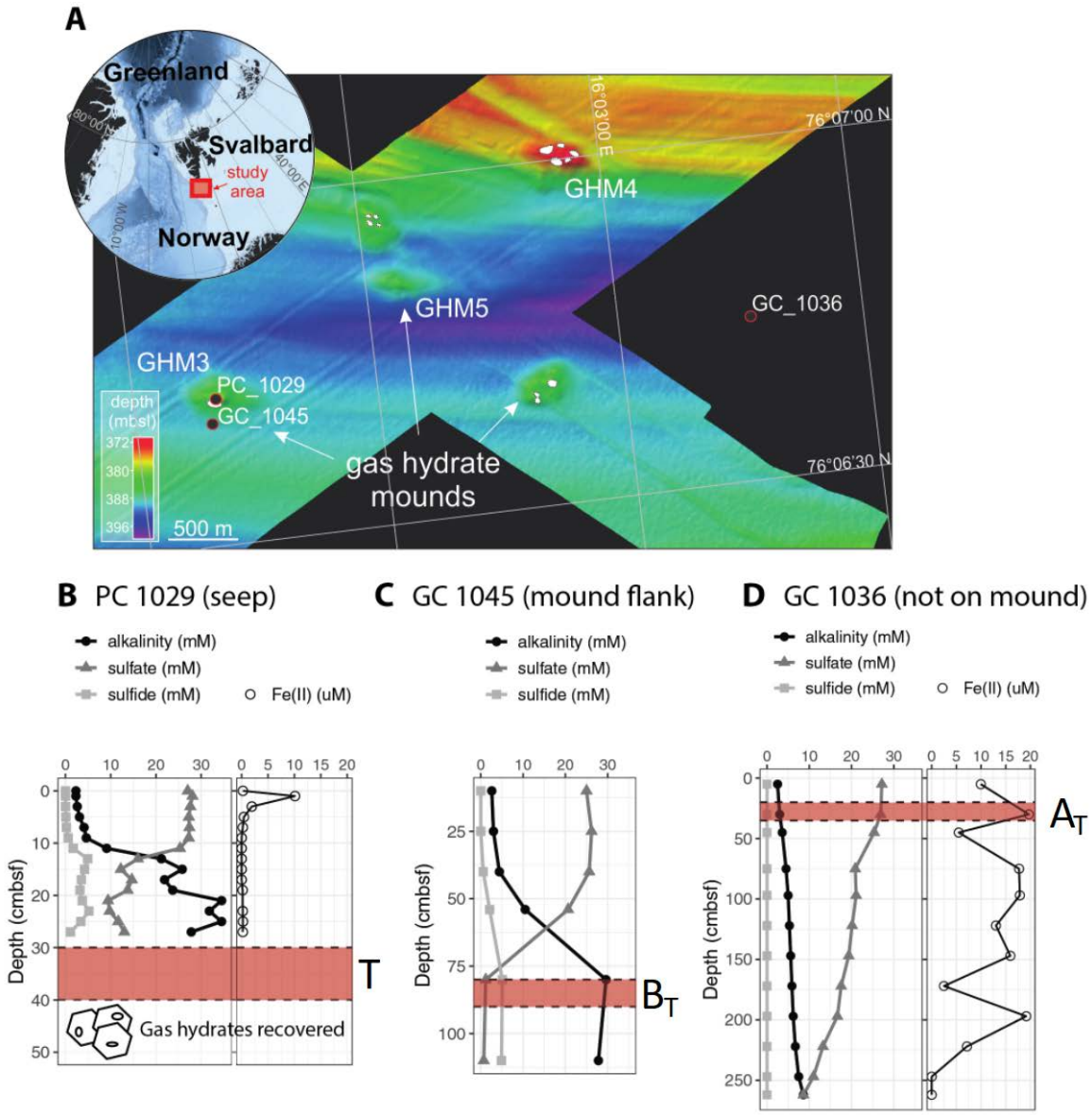

Figure 3.1. Map of the Storfjordrenna trough mouth fan, south of Svalbard, showing locations of the three cores taken. White polygons indicate areas of methane seepage observed during sampling (A). Sulfate, sulfide, alkalinity, and iron (II) porewater profiles are shown successively in (B-D): PC1029, a push core from a seep at GHM 3; GC1045, a gravity core from the flank of the same GHM, and GC1036, a reference core near the mounds. Red bands within dotted lines indicate sediment sample depths collected for incubations. Sediment sample names correspond to the sulfate-methane transition: transition (T), below transition (B_T), and above transition (A_T).

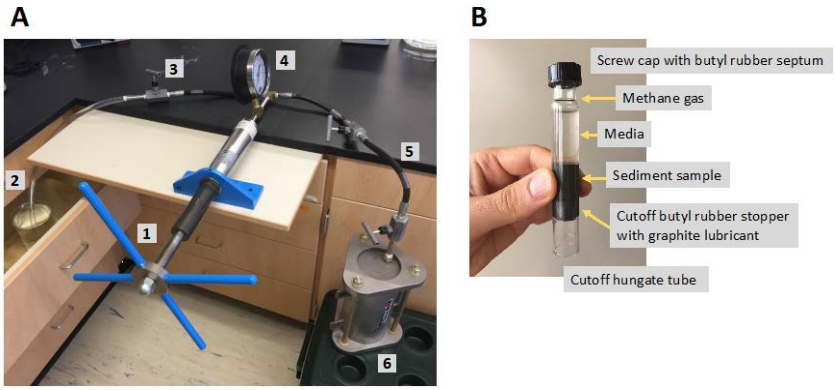

Figure 3.2. Laboratory high pressure incubation setup (A) and incubation tubes (B). In the incubation setup (A), a hand pump (1) draws water (2) into its barrel. A valve (3) is tightened, and clockwise turning of the hand pump forces hydrostatic pressure into the vessel, where it measured by a gauge (4). Additional tubing and valves (5) can be used to control pressure entering the Benthos (6) or other pressure vessels. Glass cutoff Hungate tubes (B) are placed upside-down in the vessel. Shown right-side up, they contain a slurry of sediment, anoxic seawater media, and methane gas. Butyl rubber stoppers allow anoxic transfer of methane gas and sampling of media. Pressurization of the vessel pushes the cutoff butyl stoppers inwards, fully and immediately dissolving methane gas into the slurry.

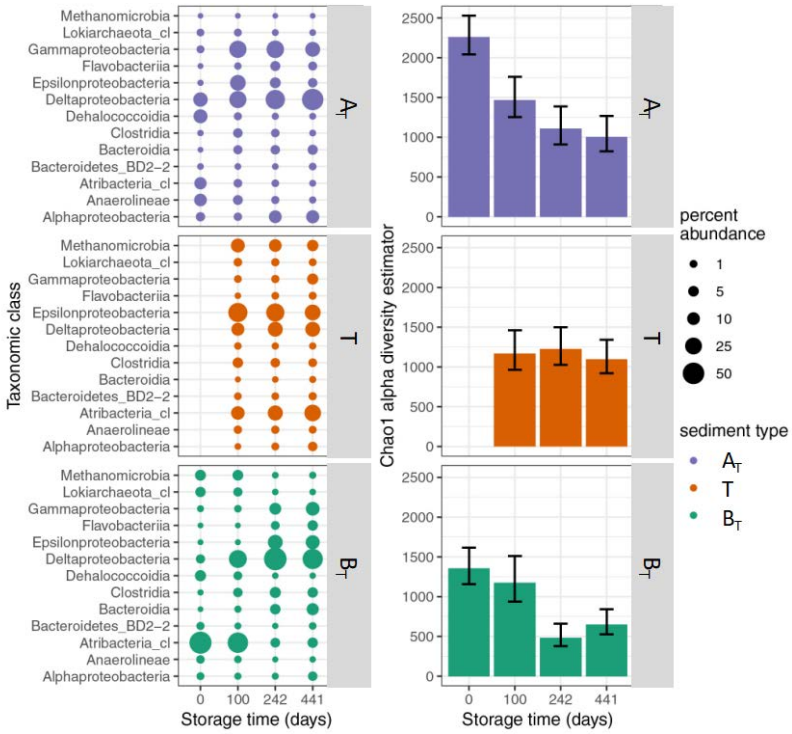

Figure 3.3. Community composition and diversity of stored sediment samples. Percent abundances of taxonomic classes among sediment samples collected and stored (anoxically, at 4˚C and atmospheric pressure) for different lengths of time (left panel). These classes constitute 85% of the reads from these communities. Chao1 alpha diversity estimates of these

communities are shown in the right panel with 95% confidence intervals assuming lognormal variance distribution.

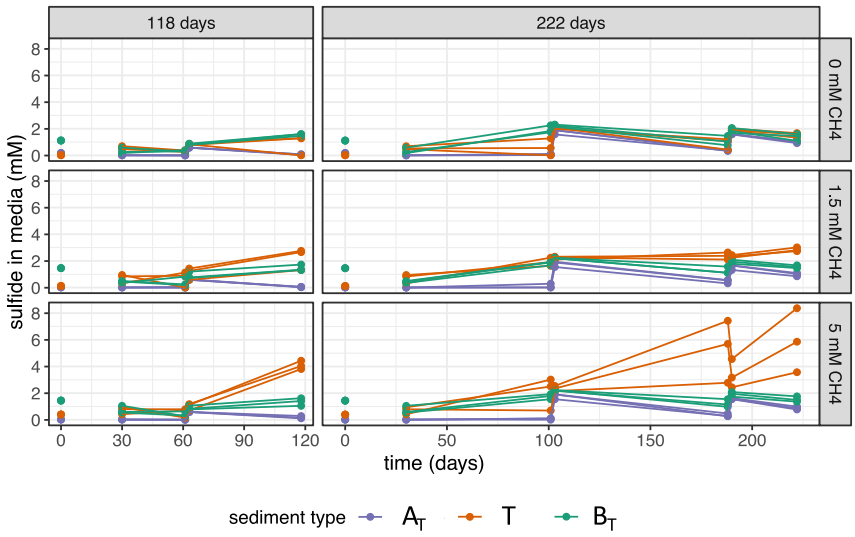

Figure 3.4. Sulfide concentrations measured in incubated sediment-media slurries. Panels are separated by total incubation time (118 or 222 days) and by added methane concentration. Sediment types are designated by color, and triplicate incubations shown. Lines are connected between points where rate measurements were determined.

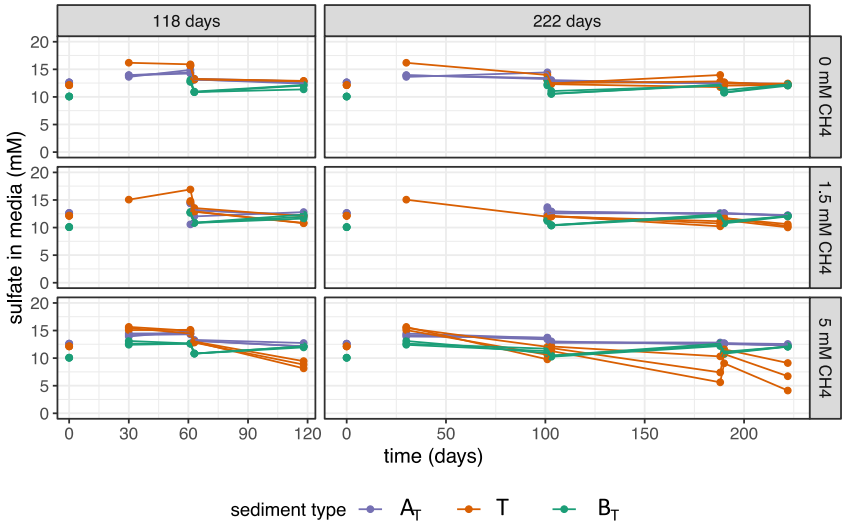

Figure 3.5. Sulfate concentrations measured in incubated sediment-media slurries. Panels are separated by total incubation time (118 or 222 days) and by added methane concentration. Sediment types are designated by color, and triplicate incubations shown. Lines are connected between points where rate measurements were determined.

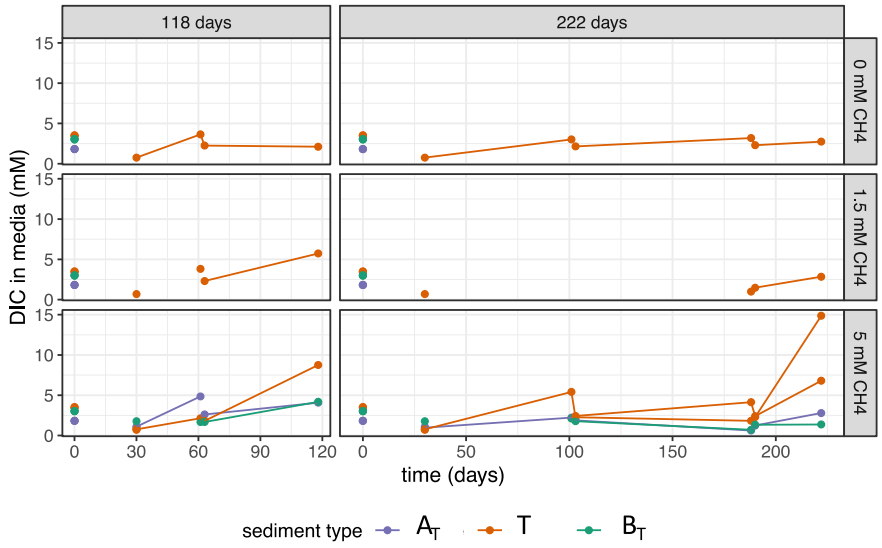

Figure 3.6. Dissolved inorganic carbon (DIC) concentrations measured in incubated sediment-media slurries. Panels are separated by total incubation time (118 or 222 days) and by added methane concentration. Sediment types are designated by color.

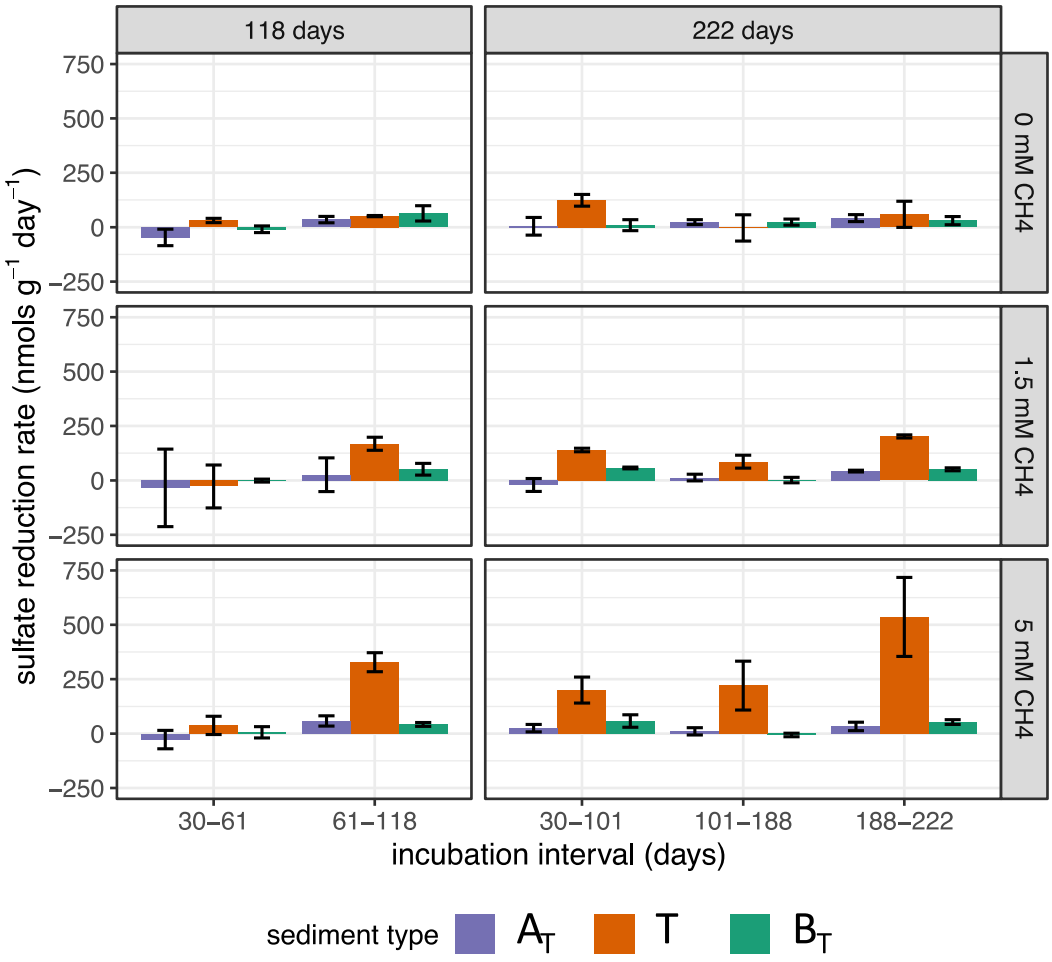

Figure 3.7. Sulfate reduction rates measured across incubation intervals. Panels are separated by horizontally by total incubation time (118 or 222 days) and vertically by added methane concentrations. Colors designate sediment types, and error bars represent 95% confidence intervals from triplicate measurements. Methane-dependent SR was only observed in the T sediments collected from an area of active seepage.

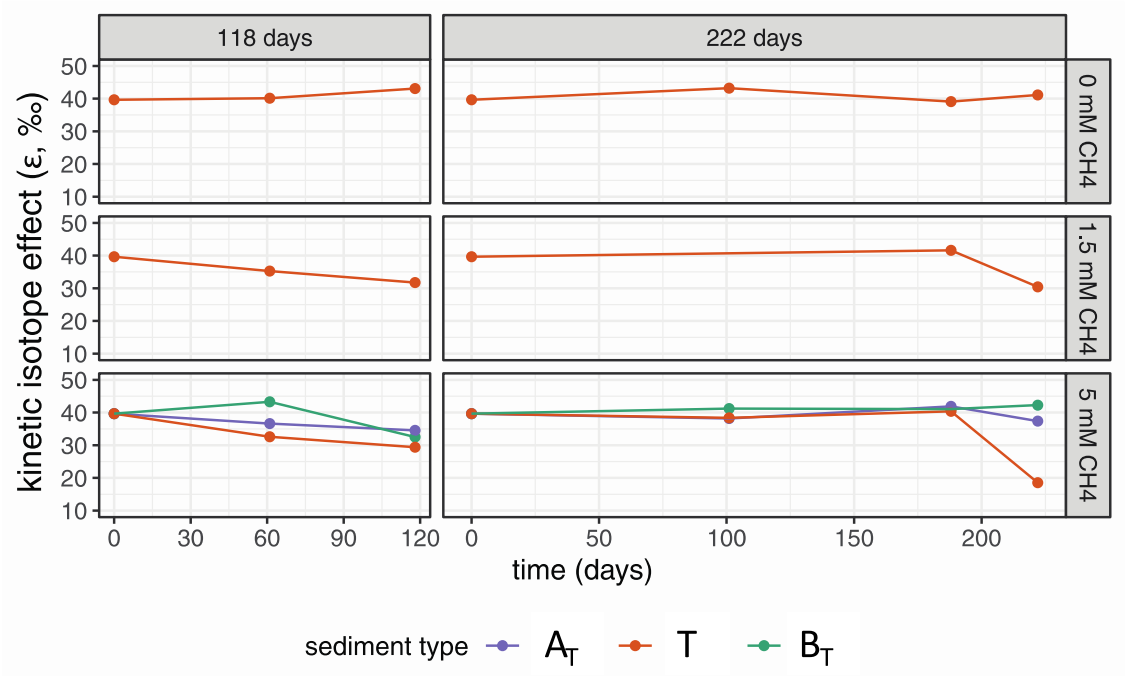

Figure 3.8. Changes in ε, the kinetic isotope fractionation during anaerobic oxidation of methane to DIC, over incubation time. The decreasing values of ε during incubations of T sediment samples indicate a more prominent influence from AOM. Panels are separated horizontally by total incubation lengths (118 or 222 days) and vertically by added methane concentrations, and colors designate sediment types.

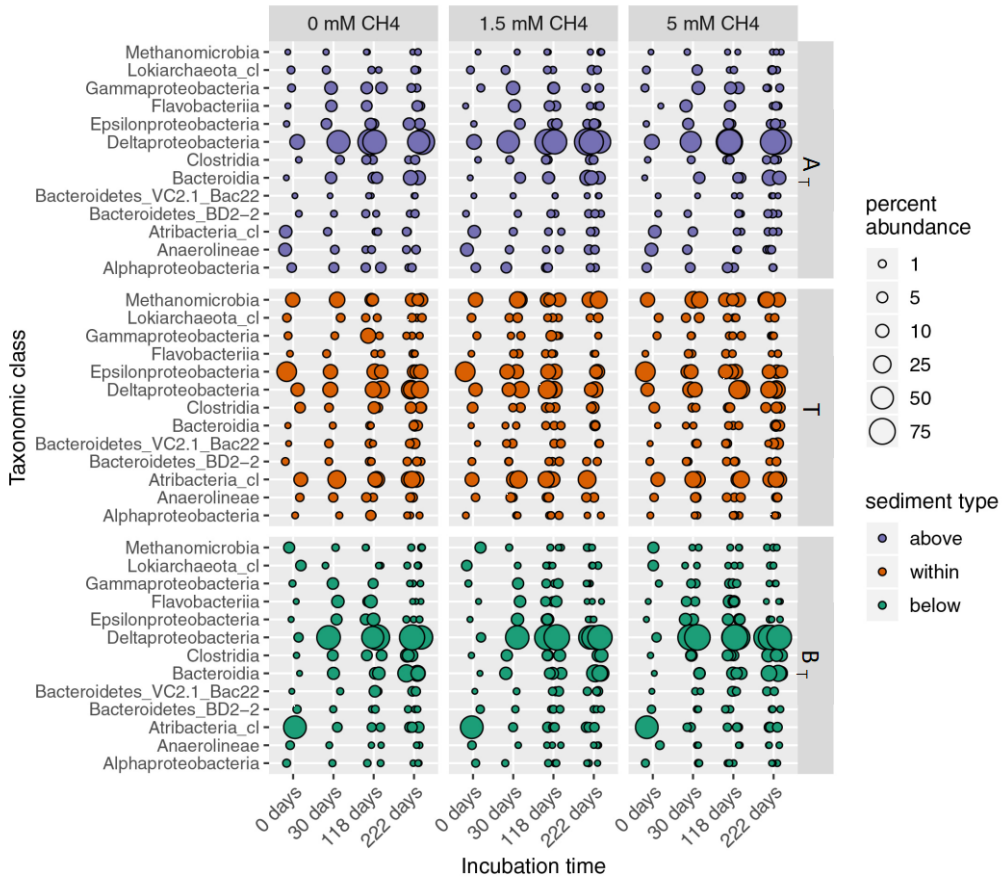

Figure 3.9. Percent abundances of class-level taxonomic divisions across all sediment types, times incubated, and initial methane concentrations. These sequences constitute >90% of the dataset. Where relevant, duplicates or triplicates are shown as offset points to convey the extent of variation between microbial communities incubated under the same conditions.

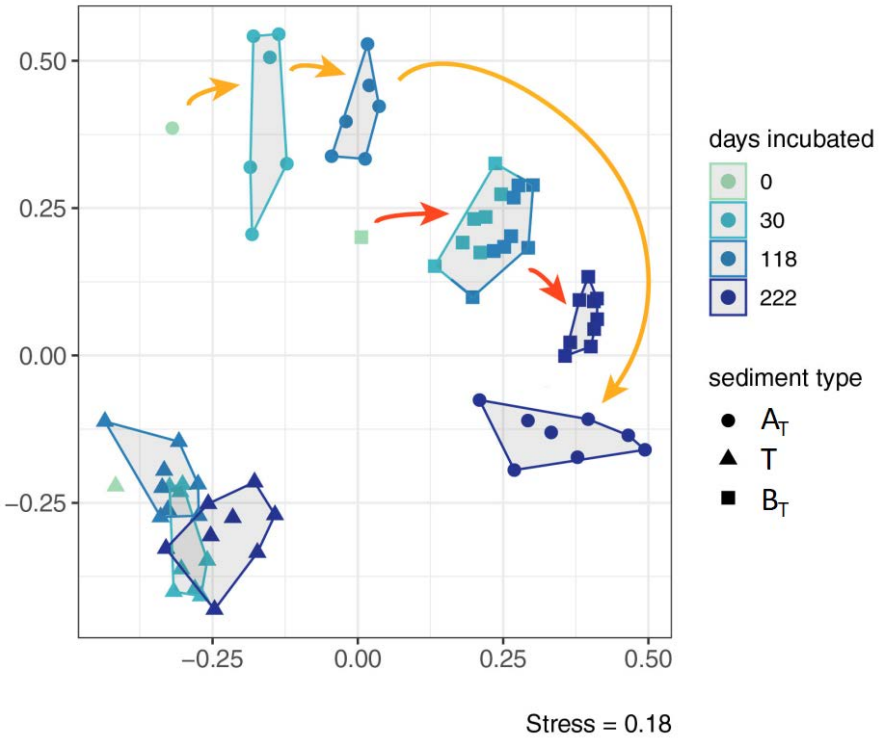

Figure 3.10. NMDS ordination of weighted Unifrac distances between communities. Symbols are colored according to incubation length, and shaped according to sediment type. Polygons indicate sample groups with different community structures as determined by ANOSIM using α=0.05 with a Bonferroni correction for multiple comparisons (For details, see Table S1). All sediment types changed over time during incubation, but A_T the most drastically.

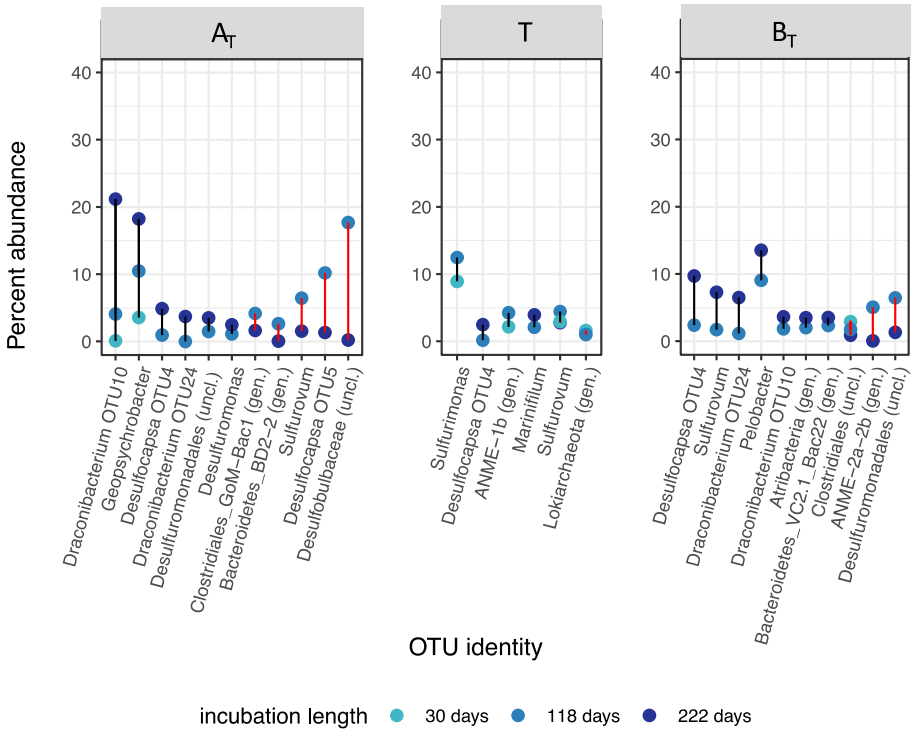

Figure 3.11. Percent abundance and taxonomic identity of the most common OTUs (each >1% of their communities) whose abundances changed significantly (α=0.05) when incubated for different lengths of time. Blue dots represent incubations of different lengths, and are connected by black or red vertical lines that respectively show increases or decreases in OTU percent abundance over the corresponding interval. Where multiple OTUs share taxonomic identity, OTU numbers are included.

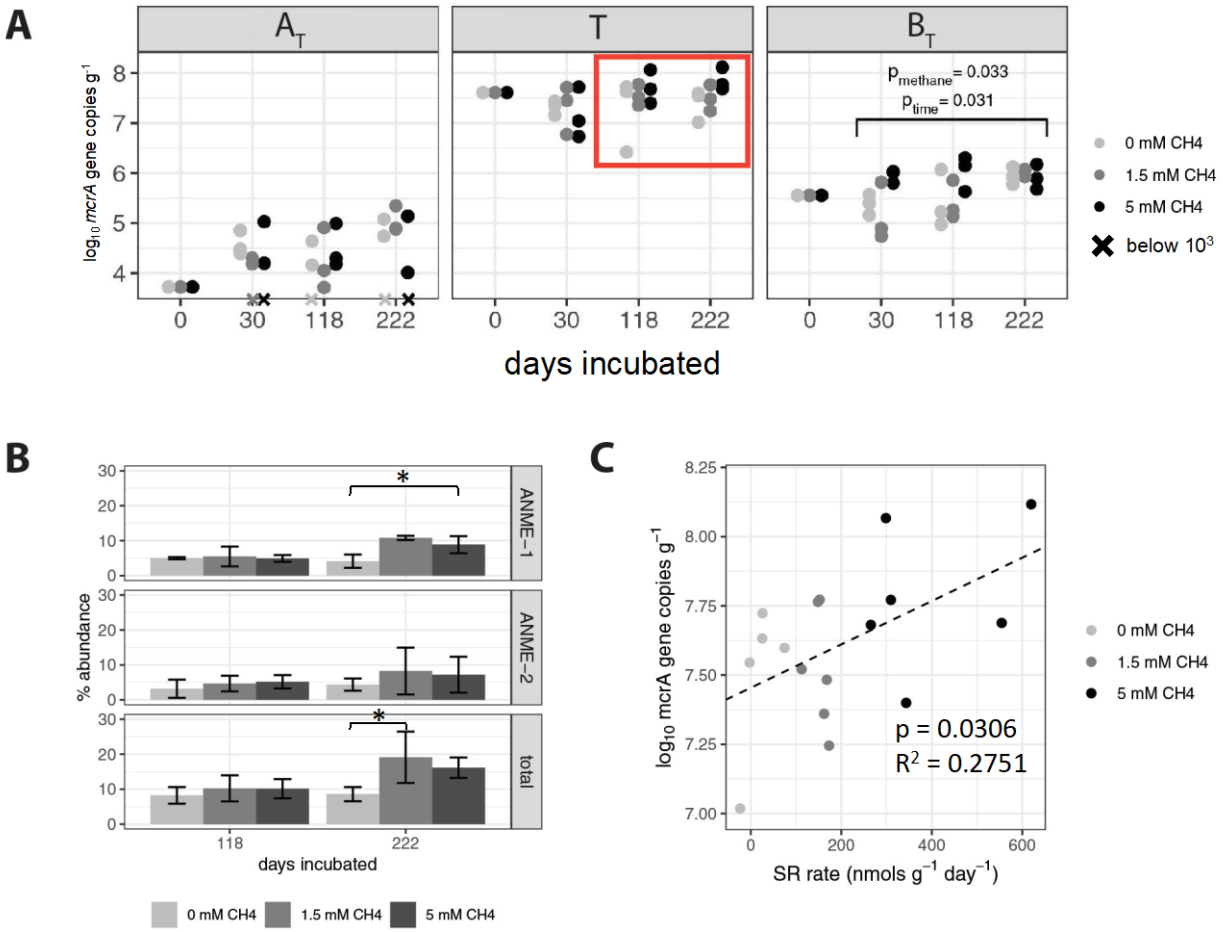

Figure 3.12. *mcrA* concentrations, ANME percent abundances, and relationships to SR rates in select incubations. Log-normalized abundances of *mcrA* genes (per gram bulk sediment) in incubated samples, enumerated by ddPCR (A). Points are shaded by initial methane concentrations, and X denotes readings below detection (10^3). One measurement was taken for preincubated (day 0) samples. Significant differences in gene abundances across incubation times and methane concentrations, excluding day 0 samples, are shown as brackets with corresponding p-values (two-way factorial ANOVA, α=0.05). Table 3.3 gives additional information on these tests. Orange box shows a subset of transition (T) sediments incubated for 118 or 222 days. Of this subset, Panel (B) shows changes in percent abundances of ANME clades, with 95% confidence intervals shown for three replicates and brackets denoting significance among close comparisons. (C) relates sulfate reduction rates and *mcrA* gene abundances of the same subset through a linear regression.

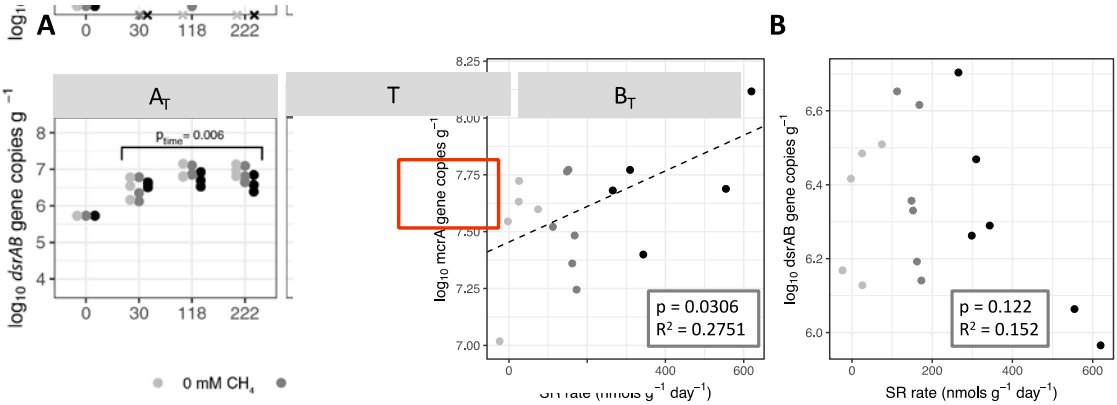

Figure 3.13. *dsrAB* concentrations and relationships to SR rates in select incubations. Changes in *dsrAB* gene abundance (log-normalized, per gram bulk sediment) in incubated samples, enumerated by ddPCR (A). Points are shaded by initial methane concentrations. One measurement was conducted for preincubated (day 0) samples. Significant differences in gene abundances across incubation times and methane concentrations, excluding day 0 samples, are shown as brackets with corresponding p-values (two-way factorial ANOVA, α=0.05, see Table S3). Orange box shows a subset of transition (T) sediments incubated for 118 or 222 days. Of this subset, panel (B) plots *dsrAB* gene abundances against sulfate reduction rates, showing no distinct linear relationship.

Tables

Table 3.1. Summary of key geochemical and microbiological measurements across all incubated sediment types that changed significantly based on added methane concentration [CH_4], incubation time, or both. ND: not detected. Because all methane-dependent changes observed were also time-dependent, methane concentration alone is not listed as a variable.

	SR and solute conc.	**ε**	**Microbial community**	***mcrA***	***dsrAB***	**ANME % abundance**
	[CH_4] & time	*[CH_4] & time*	*time*	*[CH_4] & time*	*time*	*[CH_4] & time*
A_T	ND	ND	Shifts the most	ND	↑	ND
T	↓ in SO_4^{2-} ↑ in HS^-	↓	Shifts slightly	ND	ND	↑
B_T	ND	ND	Shifts significantly	↑	↑	ND
	Fig. 3.3.2	*Fig. 3.3*	*Fig. 3.4*	*Fig. 3.6a*	*Fig. S3.7*	*Fig. 3.6b*

Table 3.2. ANOSIM test statistics indicating whether microbial community structure varied by A) sediment type, B) methane concentration added, and C) incubation time. Asterisks indicate statistical significance (experiment-wise error rate: 0.05, pairwise Bonferroni error rate: 0.01667).

A. Sediment type

comparison	R-value	P-value
above-within-below	0.805102	<0.001*
above-within	0.908417	<0.001*
above-below	0.536665	<0.001*
within-below	0.88227	<0.001*

B. Initial methane concentration

sediment type	comparison	R-value	P-value
above	0 mM – 1.5 mM – 5 mM	-0.130722	0.996
within	0 mM – 1.5 mM – 5 mM	-0.0341854	0.668
below	0 mM – 1.5 mM – 5 mM	-0.044287	0.696

C. Incubation time

sediment type	comparison (days incubated)	R-value	P-value
A_T (above transition)	222-118-30	0.823145	<0.001*
A_T	222-118	0.987403	<0.001*
A_T	222-30	0.971899	<0.001*
A_T	118-30	0.407407	0.011*

T (transition)	222-118-30	0.385789	<0.001*
T	222-118	0.339844	0.002*
T	222-30	0.416295	0.006*
T	118-30	0.425781	0.004*
B_T (below transition)	222-118-30	0.795504	<0.001*
B_T	222-118	0.955295	<0.001*
B_T	222-30	0.993317	<0.001*
B_T	118-30	0.182216	0.05

Table 3.3. ANOVA test statistics for functional gene quantification. To determine whether time- or methane-related differences in *mcrA* and *dsrAB* abundances were observed across incubations, we conducted two-way factorial ANOVAs for both genes and each sediment type (including all sediment types). Tests were conducted omitting or including preincubated samples (time zeros). Factors were bolded if significant for a particular test.

gene	sediment type	time zeros included	factor* (bold if p < 0.05)	Df	Sum Sq.	Mean Sq.	F value	Pr(>F)
mcrA	all	no	time	2	1.81	0.9065	0.47	0.627
			initial [CH4]	2	0.59	0.2941	0.152	0.859
			both	4	1.19	0.2981	0.155	0.96
			residuals	72	138.89	1.929		
mcrA	A_T	no	time	2	0.565	0.2824	0.989	0.391
			initial [CH4]	2	0.032	0.0159	0.056	0.946
			both	4	1.456	0.3641	1.275	0.316
			residuals	18	5.138	0.2855		
mcrA	within	no	time	2	0.4936	0.2468	1.568	0.236
			initial [CH4]	2	0.3039	0.1519	0.965	0.4
			both	4	0.427	0.1067	0.678	0.616
			residuals	18	2.8327	0.1574		
mcrA	B_T	no	**time**	2	1.0429	0.5214	4.252	0.0307
			initial [CH4]	2	1.0186	0.5093	4.154	0.0329
			both	4	0.7568	0.1892	1.543	0.2322
			residuals	18	2.2072	0.1226		
mcrA	all	yes	time	3	12.13	4.045	2.059	0.111
			initial [CH4]	2	0.47	0.234	0.119	0.888
			both	6	1.31	0.219	0.111	0.995
			residuals	90	176.76	1.964		
mcrA	A_T	yes	**time**	3	3.733	1.2443	5.812	0.00392
			initial [CH4]	2	0.024	0.0119	0.056	0.94605
			both	6	1.464	0.244	1.14	0.37005
			residuals	24	5.138	0.2141		
mcrA	within	yes	time	3	0.5624	0.18748	1.191	0.341
			initial [CH4]	2	0.2735	0.13674	0.869	0.436

			both	6	0.4574	0.07623	0.484	0.811
			residuals	18	2.8327	0.15737		
mcrA	B_T	yes	**time**	3	1.167	0.3892	4.232	0.0155
			initial [CH4]	2	0.764	0.382	4.154	0.0282
			both	6	1.012	0.1686	1.833	0.1349
			residuals	24	2.207	0.092		
gene	**sediment type**	**time zeros included**	**factor**	**Df**	**Sum Sq.**	**Mean Sq.**	**F value**	**Pr(>F)**
dsrAB	all	no	**time**	2	0.955	0.4775	5.126	0.00829
			initial [CH4]	2	0.128	0.0639	0.686	0.50683
			both	4	0.177	0.0443	0.476	0.75352
			residuals	72	6.707	0.0931		
dsrAB	A_T	no	**time**	2	0.6781	0.3391	6.858	0.00611
			initial [CH4]	2	0.1219	0.0609	1.233	0.315
			both	4	0.2214	0.0553	1.12	0.37818
			residuals	18	0.8899	0.0494		
dsrAB	within	no	time	2	0.3197	0.15983	3.229	0.0633
			initial [CH4]	2	0.0254	0.01269	0.256	0.7766
			both	4	0.1378	0.03444	0.696	0.6047
			residuals	18	0.891	0.0495		
dsrAB	B_T	no	**time**	2	0.3629	0.18146	3.695	0.0452
			initial [CH4]	2	0.1582	0.07909	1.61	0.2273
			both	4	0.0378	0.00946	0.193	0.9391
			residuals	18	0.884	0.04911		
dsrAB	all	yes	**time**	3	22.599	7.533	50.22	<2e-16
			initial [CH4]	2	0.101	0.051	0.338	0.714
			both	6	0.204	0.034	0.226	0.967
			residuals	90	13.5	0.15		
dsrAB	A_T	yes	**time**	3	7.337	2.4457	65.958	9.81E-12
			initial [CH4]	2	0.091	0.0457	1.233	0.309
			both	6	0.252	0.042	1.132	0.374
			residuals	24	0.89	0.0371		

dsrAB	within	yes	**time**	3	0.4718	0.15725	3.177	0.0492
			initial [CH4]	2	0.0228	0.01142	0.231	0.7963
			both	6	0.1403	0.02338	0.472	0.8199
			residuals	18	0.891	0.0495		
dsrAB	B_T	yes	**time**	3	20.418	6.806	184.78	<2e-16
			initial [CH4]	2	0.119	0.059	1.61	0.221
			both	6	0.077	0.013	0.35	0.903
			residuals	24	0.884	0.037		

Table 3.4. ANOVA test statistics for percent abundances of ANMEs in incubations. (A) A one-way ANOVA was used to determine differences in percent abundance of ANMEs in communities from different sediment types. (B) Two-way factorial ANOVAs for each sediment type were conducted to assess whether time- or methane-related differences were observed across incubations.

A

	Df	Sum sq.	Mean sq.	F value	Pr(>F)	significance
sediment type	2	2670.7	1335.3	155.9	<2e-16	***
Residuals	65	556.6	8.6			

B

A_T sediment	Df	Sum sq.	Mean sq.	F value	Pr(>F)	
time	2	6.66E-05	3.33E-05	1.469	0.272	
ch4	2	8.17E-06	4.08E-06	0.18	0.837	
time:ch4	4	1.25E-05	3.11E-06	0.137	0.965	
Residuals	11	2.49E-04	2.27E-05			

T sediment	Df	Sum sq.	Mean sq.	F value	Pr(>F)	
time	2	162.32	81.16	5.588	0.0154	*
ch4	2	119.29	59.65	4.107	0.0378	*
time:ch4	4	56.92	14.23	0.98	0.4478	
Residuals	15	217.86	14.52			

B_T sediment	Df	Sum sq.	Mean sq.	F value	Pr(>F)	
time	2	0.05579	0.027894	5.039	0.0212	*
ch4	2	0.03478	0.017389	3.141	0.0725	
time:ch4	4	0.02265	0.005662	1.023	0.4271	
Residuals	15	0.08303	0.005536			

Chapter 4

Deep-sourced fluids from a convergent margin host distinct subseafloor microbial communities that change upon mud flow expulsion

Scott A. Klasek[1], Marta E. Torres[2], Markus Loher[3], Gerhard Bohrmann[3], Thomas Pape[3], Frederick S. Colwell[1,2*]

[1] Department of Microbiology, Oregon State University, Corvallis, OR, USA

[2] College of Earth, Ocean, and Atmospheric Sciences, Oregon State University, Corvallis, OR, USA

[3] MARUM–Center for Marine Environmental Sciences and Department of Geosciences at University of Bremen, Klagenfurter Str., 28359 Bremen, Germany

Abstract

Submarine mud volcanoes (MVs) along continental margins emit muds and hydrocarbon-rich fluids from the deep subsurface in significant amounts, and host distinct chemosynthetic communities of microbes and macrofauna. Venere MV lies at 1600 m water depth in the Ionian Sea offshore Italy and sits atop the forearc of the Calabrian accretionary prism. Recently-extruded mud breccia flowing from its west summit is comparatively fresh (10 PSU), high in Li^+ and B (up to 300 and 8000 µM, respectively), and strongly depleted in K^+ (<1 mM) at depths as shallow as 20 cm below seafloor. These properties document upward transport of fluids sourced from >3 km below seafloor. 16S rRNA gene and metagenomic sequencing were used to characterize microbial community composition and gene content within deep-sourced mud breccia flows as they become exposed to seawater along a downslope transect of Venere MV. Summit samples showed consistency in microbial community composition. However, beta-diversity increased markedly in communities from downslope cores, which were dominated by methyl- and methanotrophic genera of *Gammaproteobacteria*. Sulfate and chloride concentrations were minor but significant contributors to variation in community composition. Metagenomic analyses revealed differences in relative abundances of predicted protein categories between Venere MV and other subsurface microbial communities, characterizing mud volcanoes as windows into distinct deep biosphere habitats.

Introduction

Seafloor mud volcanoes (MVs) release tens of teragrams of methane annually into the overlying ocean, as well as muds containing rock fragments (mud breccias) and fluids sourced from

kilometers below the seafloor (Kopf, 2003; Mazzini and Etiope, 2017; Milkov et al., 2004; Sauter et al., 2006). This methane forms the basis of chemosynthetic ecosystems, and is fixed aerobically or anaerobically through microbially-mediated oxidation (Hanson and Hanson, 1996; Knittel and Boetius, 2009; Van Dover et al., 2003). High fluxes of methane and other fluids from active seafloor MVs can restrict the movement of relevant electron acceptors, such as oxygen or sulfate, into sediments, and as a result, limit their capacity for methane oxidation (Boetius and Wenzhöfer, 2013; Niemann et al., 2006b). Anaerobic methanotrophs, or ANME, which are the dominant methane sink in sediments (Reeburgh, 2007), take years to establish in situ (Ruff et al., 2018). This additional limitation on biological methane removal underlies the importance of MVs as potent sources of methane emission to the hydrosphere or even the atmosphere (Etiope and Milkov, 2004).

The impacts of active mud volcanism, particularly how the deposition of fresh muds and fluids drive biogeochemical cycles and structure microbial communities, is only beginning to be recognized (Lin et al., 2018; Ruff et al., 2018). How tectonically-derived, deep-sourced MV fluids impact microbial communities is even less clear. A recent study from within a serpentinite MV identified an energetically favorable regime for microbial habitation and recovered methanogens, but methane from the fluids likely formed abiotically (Kawagucci et al., 2018). Considering the numerous challenges associated with such drilling-based studies, microbial characterizations of deep subsurface systems are often limited to sites of fluid discharge into shallower horizons, often referred to as “windows to the deep biosphere” (Deming and Baross, 1993; Hoshino et al., 2017; Krauze et al., 2017; Lee et al., 2015; Woycheese et al., 2015).

Venere MV, in the central Mediterranean, sits atop the Crotone forearc basin on the Calabrian Accretionary Prism outside of Messinian-derived evaporites (Ceramicola et al., 2014; Panieri et al., 2013). Its active status is apparent through methane seepage along its caldera rim and freshly-extruded mud breccia flows without hemipelagic cover that extend 1.6 km downslope from the summit (Loher et al., 2018a, 2018c). Thermogenic hydrocarbons emitted from a site of seepage near the summit and chloride depletions consistent with smectite-illite clay dehydrations corroborate a fluid origin between 3.5 to 7.5 km below the seafloor (Loher et al., 2018c), which may still be within the 5-7 km sediment column (Ferrucci et al., 1991; Voogd et al., 1992).

Using a suite of geochemical, 16S amplicon, and metagenomic sequence data, we sought to characterize microbial communities inhabiting deep-sourced mud breccias at Venere MV and document their changes as flows were extruded from the summit and began to entrain seawater. We hypothesized that 1) both deep-sourced fluids and seawater-derived electron acceptors such as sulfate would exert a notable influence on microbial community structure; 2) methanotrophic taxa would be found with increasing distance downslope of the Venere MV summit; and 3) gene content from MVs would be distinct from that of microbial communities inhabiting other subsurface environments.

Materials and Methods

Sample collection

Sediment samples were collected from Venere MV (Fig. 4.1) using gravity cores, minicores, or ROV-guided push cores onboard the R/V METEOR during MARUM cruise M112, from November

29th to December 10th, 2014. The barrel of the gravity corer was lined with plastic foil, which enabled rapid access to the cored material while sampling for pore water, gas composition and microbial analyses on deck. Minicores and push cores were transferred to the ship's laboratory and sampled in selected intervals by extruding the sediments from the plastic tube with a piston. Samples for DNA extractions and methane concentrations were collected from the same minicores and pushcores, while porewater sampling was done on parallel cores.

Whole round core samples for DNA extraction were sliced using an ethanol-sanitized spatula, transferred to Whirlpak bags (VWR, Radnor, PA, USA) before flash freezing in liquid nitrogen and storing at -80˚C. To determine porewater methane concentrations, 3 ml bulk sediment was transferred to a 20 ml glass vial filled with 5 ml NaOH, leaving 12 ml headspace. Rhizons (Seeberg-Elverfeldt et al., 2005) were used to draw porewater samples into acid-washed syringes over a period of 10 h at room temperature, because bottom waters were 18˚C. Porewater samples for cation measurements were transferred to 1.5 ml acid-washed tubes and acidified with 20 ul ultrapure concentrated (65%) HNO_3.

Geochemistry

Shipboard salinity was measured with a salinometer (Krüss Optronic, Hamburg, Germany) with a ± 0.1 PSU precision, and calibrated daily against dilution of IAPSO with salinities of 9.989, 29.968, 34.993, and 38.022 PSU. Shipboard alkalinity was determined by diluting a 0.5 ml sample with 9.5 ml distilled water and stirring constantly in an open beaker while titrating with aliquots of a 0.01 M HCl standard until pH decreased below 4, normally between 3.9 and 3.5.

The pH electrode (Hanna Instruments, Woonsocket, RI, USA) was calibrated with buffers of pH 4, 7, and 10. Alkalinity was calculated using the equation:

$$\text{Alkalinity (mol/L)} = [(v_{HCl}*c_{HCl})-10^{-pH_{final}}*(v_0+v_{HCl})/f_{H^+}+10^{-pH_{start}}*v_0/f_{H^+}]/v_0 \quad \text{(Equation 4.1)}$$

where v_{HCl} is the volume (in ml) of HCl added to final pH; C_{HCl} is the molar concentration of HCl; pH_{start} and pH_{final} are the initial and final pH readings, respectively; v_o is the initial sample volume in ml and f_H is the activity coefficient of H^+ in seawater, taken as 0.79 (Culberson and Pytkowicz, 1973).

Dissolved methane in bulk sediment was analyzed onboard using an Agilent 6890N gas chromatograph (Agilent Technologies, Santa Clara, CA, USA) equipped with a capillary column connected with a flame ionization detector as previously described (Pape et al., 2010). Reported concentrations of dissolved methane are *ex situ* concentrations uncorrected for sediment porosity and Bunsen coefficient.

Sulfate and chloride concentrations were measured by ion chromatography using a Metrohm 882 Compact IC plus (Metrohm, Herisau, Switzerland) on a Metrosep A Supp 5 column. Analytical errors below 0.4% were reported for both ions. Linear interpolation was used to determine chloride, sulfate, and alkalinity concentrations at depths where samples for microbiology were taken.

Lithium and boron samples were diluted 1:50, and potassium diluted 1:100, with 1% quartz-distilled nitric acid and run on a Leeman Labs Prodigy ICP-OES ion chromatograph using a radial viewing mode. IAPSO seawater and in-house solution standards were run every eleven samples and used to evaluate instrumental accuracy and precision. Detection limits were determined according to EPA method 200.7 (Environmental Monitoring Systems Laboratory, 1996). The

limit of detection for potassium was 1.0 mM, and the high standards for lithium and boron were 10.2 µM and 327 µM, respectively.

DNA extraction for amplicon sequencing

DNA was extracted using a modified sodium dodecyl sulfate (SDS)-based DNA extraction protocol (Zhou et al., 1996). Other DNA extraction methods, such as MoBio PowerSoil kits (Qiagen, Hilden, Germany), or those detailed in (Lever et al., 2015) produced much lower yields of genomic DNA that amplified less consistently. DNA extraction buffer was prepared as in Zhou et al., (1996) and filtered through a 0.2 µm syringe filter. In a clean laminar flow hood, 0.3 g sediment, 550 µl extraction buffer, and 50 µl 20% 0.2 µl filtered-SDS were placed into autoclaved 1.5 ml internally-threaded cryogenic vials (VWR, Radnor, PA, USA). Upon thawing, vials were bead-beaten using a vortex adaptor (Qiagen, Hilden, Germany) at high speed for 5 min. Vials were sonicated at in a room-temperature water bath sonicator at 40 kHz (Thermo Fisher Scientific, Waltham, MA, USA) in two pulses of 30 s each, separated by 90 s, and then incubated in a 65˚C water bath for 1 h, inverting to resuspend flocculated sediment every 15-20 min. Vials were then centrifuged at 10,000 g for 5 min to pellet sediment. Supernatants were combined with equal volumes of phenol-chloroform-isoamyl alcohol (25:24:1) in 2 ml heavy phase lock gel tubes (Quantabio, Beverly, MA, USA) and continuously inverted for 4 min. Tubes were spun down at 14,000 g for 5 min, and aqueous layers carefully transferred to clean tubes with 2.5x the aqueous volume of ethanol and 1 µl glycoblue coprecipitant (Thermo Fisher Scientific, Waltham, MA, USA). DNA was precipitated at -20˚C for 2 h. DNA was pelleted by centrifuging at 14,000 g for 30 min at 4˚C. Supernatant was carefully removed by pipetting and

residual liquid was left to evaporate for 10-15 min. A subsequent salt wash was performed by adding 500 µl cold 70% ethanol and then centrifuging and removing the supernatant as before. Tubes were then placed in a Savant vacuum concentrator (Thermo Fisher Scientific, Waltham, MA, USA) at 55˚C for up to 10 min to evaporate any remaining liquid. DNA pellets were resuspended in 50 µl nuclease-free water and stored at -20˚C. Two DNA extraction blanks were conducted: one without any added sediment, and another with sediment that had been baked in an oven at 175˚C for two h. DNA was measured with a Qubit Fluorometer and High Sensitivity Assay Kit (Thermo Fisher Scientific, Waltham, MA, USA) after extraction.

16S library amplification and sequencing

16S amplicons were prepared following the Earth Microbiome Project Illumina protocol. V4 regions of bacterial and archaeal 16S rRNA genes were amplified in triplicate 25 µl reactions using universal 515-forward and 806-reverse primers (Caporaso et al., 2011) modified with dual-indexed Illumina sequencing adapters (Kozich et al., 2013). The thermal cycling protocol of Caporaso et al. (2011) was followed without modifications. After confirming amplification with agarose gel electrophoresis, triplicate PCR products were pooled and purified with a QIAquick PCR purification kit (Qiagen, Hilden, Germany). In addition to the DNA extraction blanks, a sample without any added template DNA was amplified and purified as a PCR negative control. Amplicon concentrations were quantified with a Qubit fluorometer (Thermo Fisher Scientific, Waltham, MA, USA) using the Qubit dsDNA high sensitivity assay kit and pooled in equimolar amounts. Illumina MiSeq V2 paired-end 250 bp sequencing was performed at the Oregon State University Center for Genome Research and Biocomputing (CGRB).

16S amplicon sequence analysis

16S amplicon sequences were processed with version 1.39.3 of mothur (Schloss et al., 2009) following an established pipeline (Kozich et al., 2013). Reads were clustered into operational taxonomic units (OTUs) at a 97% similarity level and taxonomically classified using version 128 of the SILVA database (Quast et al., 2013). Singleton OTUs and contaminant genera were removed (for details on potential contaminants, see Results). Communities were rarefied to 356 reads, and relative abundances and metrics of alpha diversity (richness and Chao1, Shannon, and Simpson indices) were then calculated.

To compare beta diversity, a tree file containing the most abundant sequence from each of the 11,572 OTUs was constructed with Clearcut (Evans et al., 2006). A dissimilarity matrix was then calculated using weighted Unifrac distances (Lozupone et al., 2007). Principal coordinates analysis (PCO) was conducted in PRIMER7 (Clarke and Warwick, 2001) from the community dissimilarity matrix and a Euclidean-normalized environmental data matrix containing porewater chloride and sulfate concentrations corresponding to all samples. Distance-based linear modeling was used to evaluate the influence of these variables on community structure. Differences in community structure among sites and cores were evaluated using ANOSIM (Clarke, 1993). Metastats (White et al., 2009) was used to determine whether individual OTUs showed patterns of differential abundance between communities based on sulfate and chloride concentrations and summit mud flow ages.

DNA extraction for metagenome sequencing

Metagenomic DNA from samples was extracted using the procedure described above, with modifications to account for the increased sediment volumes. 8.4 g from sample 19242-15 at 2-3 cm, 4.8 g from sample 19263-1 at 48-52 cm, and 31.2 g from sample 19263-1 at 267-270 cm were used. Volumes of extraction reagents were scaled up according to sediment masses. Samples were placed in 15 or 50 ml conical tubes, and centrifuging steps were carried out at 4,500 g for 10 min when pelleting sediment and 1,500 g for 5 min when extracting with phenol-chloroform-isoamyl alcohol. Samples were precipitated at 4˚C for 12 h with 0.6 volume isopropanol and 0.1 volume sodium acetate in 2 ml tubes. Pellets were pooled, desalted with ethanol as described previously, resuspended in nuclease-free water, and DNA was then purified with a Norgen CleanAll DNA/RNA clean-up and concentration kit (Norgen Biotek, Thorold, Ontario, Canada) according to manufacturer's instructions for genomic DNA (>10,000 bp).

Metagenomic library preparation, sequencing, and analysis

Metagenomic library construction and sequencing was conducted at the Josephine Bay Paul Center Marine Biological Laboratory (MBL), Woods Hole, MA, using an established protocol available online (https://vamps.mbl.edu/resources/faq.php#methods). To add to the three samples described here, fastq files from seven additional metagenomes derived from recent mud flows of the Håkon Mosby Mud Volcano (Ruff et al., 2018) were downloaded from NCBI and analyzed in parallel. The ends of low-quality fastq sequences were removed using version 1.0-r72-dirty of the seqtk trimfq tool (https://github.com/lh3/seqtk). Paired reads were assembled with Megahit v1.1.1-2-g02102e1 (Li et al., 2015) and annotated in ShotMAP v1.1

(Nayfach et al., 2015) against the clusters of orthologous group (COG) protein family database (Galperin et al., 2015) using a classification threshold score of 42.8 and a coverage-based abundance calculation strategy. This classification method was more accurate than other pre-2018 pipelines in quantifying gene family abundances using the COG database (Franzosa et al., 2018). Alpha diversity statistics were obtained across all ten mud volcano metagenomes using the ShotMAP script compare_shotmap_samples.pl. Percent abundances of reads annotated to each COG functional category were summed across samples. Reads annotated to multiple COG categories were omitted and percent abundances re-normalized to allow for comparison against other publicly available metagenomes from subsurface ecosystems annotated using the COG database. This information was obtained from the MG-RAST and IMG/M metagenome databases (Keegan et al., 2016; Markowitz et al., 2014).

Results

To investigate microbial community changes as fresh mud breccia flows are extruded from the marine subsurface and begin to entrain seawater, we collected samples for geochemical and microbial analyses from Venere Mud Volcano offshore Calabria, Italy (Fig. 4.1a). We describe sampling locations, then results of DNA extractions/quality controls, geochemical and microbial community characteristics, and finally we compare gene content from Venere MV metagenomes with that reported for other marine subsurface environments.

Site and core descriptions

At the western summit of Venere MV (Fig. 4.1b), freshly exposed mud flows extending up to 1.6 km downslope were visually inferred during multiple ROV dives. Areas of gas seepage were also detected near the western summit and at several locations around the caldera rim (Fig. 4.1b). The freshest mud flow from the summit showed a distinct plated texture, in contrast to previously deposited flows which were characterized by a smoother texture and a yellowish color. Sedimentological interpretation of cores from recent and older flows identified the material from both flows as mud breccia without any noticeable hemipelagic cover (Loher et al., 2018a). Given that sedimentation rates at Venere MV and the nearby Spartivento forearc basin range from 0.17–0.26 mm/yr (Ceramicola et al., 2014; Loher et al., 2018a), the maximum ages of these freshly extruded flows are likely only a few years. The spatial extent of the flows are shown in Fig. 4.1c and previously characterized in (Loher et al., 2018a, 2018c).

For this study we targeted sites from the summit, where the fresh mud is extruded. We analyzed a gravity core (GeoB19245-1), and a series of ROV guided push cores along the mud flow track. These cores are compared with a gravity core from gas seep site 1 (Fig. 4.1b), located on the caldera rim where methane discharge is evidenced in hydroacoustic data and chemosynthetic communities typical of cold seep sites were observed (Loher et al., 2018b). This core (GeoB 19236-1) consists of mud breccia covered by 2 cm of fine sandy sediment. In addition, a reference core (GeoB 19279-3) retrieved southeast of the mud flow area (Fig. 4.1b) served as a background control; this core consisted of only fine sand and hemipelagic sediment.

Yield and controls for DNA and 16S amplicon sequence analysis

DNA extraction yields from summit mud breccia flows ranged several orders of magnitude, from < 0.12 to 145 ng per g bulk sediment. Yields were lowest in deep samples within the

summit gravity core, and higher in shallower samples (2-3 cm below seafloor) and in gravity core 19263 near seep site 3. Extractions of mud breccia samples with added *E. coli* genomic DNA recovered only 8.3% of the DNA as extractions with gDNA and no mud breccia. Therefore, in addition to the evident low biomass within these samples, sorption of DNA to clayey materials also likely reduced recovery. Faint amplification was observed in one DNA extraction blank, but not in another with baked sediment added to it. In addition, several samples intended for 16S amplicon sequencing failed to amplify.

The low amounts of extracted DNA recovered from Venere MV samples necessitated extra scrutiny in identifying and removing potential contaminant sequences. Nineteen genera present at higher abundances in the three blanks than in 68 samples (α=0.05), were removed, in addition to four genera previously identified as common laboratory or reagent contaminants in low-biomass samples (Salter et al., 2014). The removed genera comprised six bacterial phyla and 81% of the sequences identified in blanks but only 2.7% of sample communities (Table 4.1). Bacterial and Archaeal genera that were plotted in figures include the thirteen genera that comprised > 1% of all sequences in the dataset, and an additional six genera that were each over 0.3% of all sequences and were over 10% of any particular community. Altogether, these nineteen genera made up 72.5% of all sequences in the dataset.

Fluid composition and microbial community diversity at the various sites investigated

We organized the results according to sampling areas: Venere MV summit and mud flow gravity cores, summit and mud flow push cores, methane seep site 1 uninfluenced by mud volcanism, and then a reference site uninfluenced by mud volcanism or methane. A comparison of microbial diversity and variation with porewater geochemistry is presented next.

Summit and flow gravity cores

Gravity core GeoB19245-1 collected at the summit show elevated concentrations of lithium and boron, and a depletion in potassium less than a meter below seafloor (Fig. 4.2). A marked decrease in dissolved chloride is highest at the summit, where fluids show 80% freshening relative to bottom seawater values. These data clearly point to a deep fluid source, likely originating from clay dehydration reactions at depth (Loher et al., 2018c). Freshening is observed in cores GeoB 19263-1 and GeoB 19276-1, collected 80 and 150 m downslope along the mud flow (Fig. 4.3a). The deep-sourced fluids are highly alkaline (40 to 60 mM), depleted in sulfate, and have methane concentrations ranging from 2 to 4 mM (Figs. 4.3b, c). Microbial communities at all depths of the summit gravity core show consistent relative abundances of Atribacteria, anaerobic methanotrophs (ANME)-1b, and Anaerolinaceae, suggesting these taxa dominate in depths of the sediment column that are mobilized upwards through mud volcanism (Fig. 4.3d). Other methanotrophs are present in two cores several meters downslope of the summit: ANME-2a-2b in 19263, and several genera of Gammaproteobacteria at 24 cmbsf in 19276. Higher abundances of Clostridia and Desulfobacteraceae may reflect proliferation in response to changes in physical conditions (such as changes in temperature and pressure), geochemical conditions (presence and nature of electron acceptors) or time after mud flow expulsion from the center conduit.

Summit and flow push cores

ROV-guided push cores taken from Venere MV summit and downslope from the mud breccia flows also show significant freshening in porewater with chloride values of 200 mM measured only a few cm below seafloor (Fig. 4.4a). As observed in the gravity core, lithium, boron, and potassium profiles all document the presence of deep, fresh fluids within mud flow push cores (Fig. 4.2). Sulfate concentrations decrease and alkalinity increases with depth (Fig. 4.4b). Methane concentrations were higher in cores closer to the summit, but still exceeded 1 mM at 150 meters downslope (Fig. 4.4c).

Porewater chloride and sulfate concentrations at the Venere MV summit show a positive linear relationship, suggesting that most samples lie between deep-sourced and seawater-influenced end-members (Fig. 4.5). Mud flow gravity core samples downslope from the summit show anomalously low sulfate, suggestive of biological sulfate reduction.

As in the gravity cores, push core communities contained high abundances of Atribacteria and ANME-1b, particularly in core GeoB 19242-12 near the summit (Fig. 4.4d). However, methylotrophic Gammaproteobacteria were the most dominant community members in cores from the older mudflow sequence downslope of the summit. The top four OTUs from this group matched most closely to the genus *Methylomonas*, which are obligately aerobic group 1 methanotrophs capable of fixing nitrogen (Lidstrom, 2006). High abundances of an OTU belonging to *Ammonifex* and most similar to *Thermodesulfitimonas autotrophica*, an anaerobic chemolithoautotroph (Slobodkina et al., 2017), were present at similar or slightly deeper depths. The most abundant OTU, a marine group 1 methanotroph, is most closely related to *Methylomonas methanica* (Boden et al., 2011).

Seep site 1 and reference

In contrast with samples retrieved from the mud flow, core GeoB 19236-1 from Seep site 1 (Fig. 1b) shows no evidence of porewater freshening even though sediments are comprised of mud breccia (Fig. 4.6a). Lithium, boron, and potassium concentrations in porewaters at seep site 1 also match those of overlying seawater (Fig. 4.2). Here, the decrease in sulfate with depth and corresponding increases in alkalinity and methane (Fig. 4.6b, c) appear to be driven by microbial sulfate reduction and anaerobic oxidation of methane (AOM). This is supported by high abundances of several ANME clades throughout the core (Fig. 4.6d). Sulfate-reducing bacteria (SRB) SEEP-SRB1, which often associate with ANME to mediate anaerobic methane oxidation (Knittel et al., 2003), are also present in high abundances.

The reference minicore GeoB 19279-3, located away from mud flows and sites of methane seepage (Fig. 4.1b), showed no evidence of freshening, sulfate reduction, or increasing alkalinity (Fig. 4.7a, b). Methane was detected in porewater in nanomolar amounts (Fig. 4.7c). Bacterial and archaeal genera present in high abundance at other cores were not present in shallow sediments at this reference site, which instead contained high abundances of Marine Group I Thaumarchaeota (Fig. 4.7d). However, these communities were characterized by much higher alpha diversity than those from all other cores, with Chao1 indices of 606-782 as compared to 153 or lower for mud breccia flow communities.

Community diversity and variation with porewater geochemistry

A principal coordinates analysis (PCO) ordination was used to examine patterns of beta diversity among Venere MV microbial communities and their relation to porewater

geochemical parameters (Fig. 4.8). Two principal coordinates captured 54.1% of the community variance. Communities from Venere MV summit flows showed highest beta-diversity, though a high degree of similarity was observed in summit gravity core communities. ANOSIM tests indicated differences in community structure between samples from older and younger summit mud flows, and between most cores (34 of 55). However, when summit gravity core communities were reclassified as a distinct group instead of as younger mud flows, this difference disappeared (Table 4.2). For this reason, and because they showed high similarity, summit gravity core communities were colored separately (Fig. 4.8). It is noteworthy that communities from the gas seep at site 1 and from a methane-naïve reference core were distinct from those inhabiting mud flows at or near the summit (Table 4.2), highlighting the unique nature of this deep biosphere habitat.

Porewater sulfate, methane, and chloride concentrations were all significant drivers of community structure ($p \leq 0.006$), and respectively accounted for 8.6%, 7.6%, and 6.4% of the difference in community structure (22.6% of the total). Methane and sulfate vectors point in opposite directions on the PCO (Fig. 4.8), reiterating contrasting observations of methane-rich, sulfate-depleted fluids in summit and site 1 gravity cores compared to shallower mud flows, which have begun to entrain sulfate-rich seawater (Figs. 4.3, 4.4). On the other hand, direct trends between porewater chloride and community composition are not conveyed in the ordination (Fig. 4.8), which is likely obscured by the high beta-diversity among summit flow communities.

Several abundant OTUs in Venere MV summit flows are present in communities at different abundances based on mud flow age, and methane or chloride concentrations (Fig. 4.9). One

aerobic methanotroph belonging to *Methyloccocales* was more dominant in older summit flow communities. Another, classified to Marine Methylotrophic Group 1, constituted nearly a quarter of the communities where methane was below 0.5 mM, suggesting it was active in removing methane from pore fluids. Atribacteria dominated methane-rich sediments, and two OTUs belonging to *Desulfobacteraceae* were more abundant in older flows where methane concentrations exceeded 2 mM. ANME-1b was the only genus showing a preference for deep fluids with low chlorinity (Fig. 4.9c). These anaerobic methanotrophs were presumably dead, dormant, or outcompeted by other populations as mud breccias were emitted from the Venere MV summit and exposed to a more oxidizing environment.

Metagenomes from Venere and other MVs

Metagenomes were analyzed from three samples at Venere MV: a surface mud flow near the Venere MV summit, and two samples at 50 and 267 cm below seafloor from gravity core GeoB 19263-1, 80 m downslope of the summit. COG category abundances from Venere MV metagenomes were similar to those of six others from Håkon Mosby MV, off Norway in the Barents Sea (Ruff et al., 2018), and diversity of COGs among all MV metagenomes did not vary significantly. However, these two mud volcanoes together showed a distinctly different composition of COG categories than metagenomes belonging to hydrothermal vent, basaltic crust, or sediment ecosystems (Fig. 4.10, Table 4.3). Table 4.4 contains additional information for other metagenomes compared, which either displayed COG category information in-text or online in MG-RAST or IMG/M databases. In particular, mud volcano metagenomes showed higher abundances of reads classified to defense mechanisms (to combat viral attack) than the

other three environments (Fig. 4.11). In addition, higher content in the categories of cell wall/membrane/envelope biogenesis, translation, and posttranslational modification came at the expense of energy production/conversion and amino acid transport and metabolism. These broad-level differences may hint at specialized adaptations that allow life to persist in a distinct deep subsurface environment.

Discussion

Despite hosting methane-oxidizing microbial communities, mud volcanoes emit large quantities of methane into the oceans and host fluids generated at depths from clay dewatering and convergent margin activity. To further understand linkages between methane, deep-sourced fluids, and the biosphere, we characterized microbial communities from freshly extruded mud breccia flows of Venere MV within a geochemical context as they were exposed onto the seafloor. We first consider the nature of the deep fluids, then follow with a discussion of microbial gene content and metabolic potential, and finally place microbial community changes within the context of this transitional environment.

Deep-sourced Fluids

As interpreted previously by (Loher et al., 2018c), the upward advection of deep-sourced muds is responsible for the decrease in porewater chloride at Venere MV summit and mud flows. These fresh fluids appear to be generated not from gas hydrate decomposition (Loher et al., 2018c), but by smectite-illite clay mineral dehydration reactions, which occur at temperatures between 60-150˚C (Kastner et al., 2014). The estimated regional heat flow gradient of

0.020˚C/m and the geothermal hydrocarbon signature from the summit of Venere MV points to a fluid source at depths of 3 to 7.5 km below the seafloor (Loher et al., 2018c).

Boron enrichment in porewaters results from desorption from clay particles during mineral dehydration reactions and leaching from basalts at high (>150˚C) temperatures (Kopf and Deyhle, 2002; Seyfried et al., 1984), often in fluids sourced from convergent margin subduction zones (You et al., 1993, 1995). Lithium is also released from sediments and basalts at high temperatures (You et al., 1995), which can be up to 200-300˚C, below smectite-illite transition depths (Nishio et al., 2015). At the Venere MV summit, porewater boron concentrations measured up to 13 mM, exceeding values from several other MVs worldwide (Kopf and Deyhle, 2002). Porewater lithium values of several hundred µM at Venere MV are comparable in magnitude to the MVs of the Barbados convergent margin (Martin et al., 1996), and exceed those of the Kumano MVs of the Nankai wedge (Nishio et al., 2015). Boron and lithium enrichments have also been noted to infer fluid mobilization depths of 4-6 km below seafloor in the active Carmen MV in the western Mediterranean (López-Rodríguez et al., 2019). Potassium concentrations below 1 mM in Venere MV pore fluids are without precedent, though values as low as 2.4 mM have been measured in MVs of the Barbados margin (Martin et al., 1996). Potassium is incorporated into illite structure, as has been documented in settings including the Ulleung basin (Kim et al., 2016) and Canadian Shield sedimentary deposits (Bottomley and Clark, 2004).

Below 1 m depth, porewater chloride (Fig. 4.3a), potassium, boron, and lithium (Fig. 4.2) in the Venere MV summit gravity core does not change appreciably, suggesting that below this horizon, there is no admixture with seawater; rather active upward advection of deep sourced

fluids maintain the highly altered fluid composition as shallow as 50 cmbsf. The nonlinear nature of these profiles (Fig. 4.3a, b) evinces a system out of steady-state conditions, wherein seawater has only begun to diffuse into depths of 50 cm or less.

Distinct microbial gene content at Venere compared with other MVs

To compare microbial communities with the nature of the fluid regime, we use low chlorinity (< 200 mM) in Venere MV summit and mud flows as a reliable proxy for deep-sourced fluids. Despite the considerable geochemical transition from deep-sourced to seawater-influenced fluids in Venere MV flows, chloride concentration only explained 6.4% of the difference among microbial communities. This would suggest communities in recently extruded mud breccia flows are affected only minimally by these deep fluids, or have not yet had the time to shift as they begin to mix with seawater and electron acceptors therein. Only one OTU, an ANME-1b, changed noticeably with chloride concentration (Fig. 4.9); it may thus be inactive or outcompeted by other taxa considering that doubling times for anaerobic methane oxidizers are over a month, and that years may be required before they become dominant within communities (Girguis et al., 2005; Ruff et al., 2018). Despite the minimal influence of deep fluids on community structure, clear patterns are noted in mud flows with increasing distance from its source. The increased percent abundances of methyl- and methanotrophic Gammaproteobacteria, Ammonifex, and Desulfobacteraceae (Figs. 4.3, 4.4) likely reflect new growth instead of a decline in actual numbers of competing taxa.

Microbial groups present in muds from the central conduit at Venere MV presumably have adaptations to high temperature environments, or are able to persist in a dormant state under

considerable energy limitation for extended timescales (Hoehler and Jørgensen, 2013). Atribacteria are understood to disperse through mud volcanism (Hoshino et al., 2017). Thermophilic ANME-1 clades have been described (Brazelton et al., 2006; Teske et al., 2002). Members of Anaerolineae are currently poorly understood, but are considered to be anaerobic fermenters that show evidence of cellulolytic activity (Xia et al., 2016). Additional investigation is needed to determine whether community members present in these deep-sourced mud breccias constitute live and potentially active populations.

Currently, only members of the bacterial phylum Firmicutes are understood to form endospores (Fritze, 2004), and Clostridia are the only class of these present in significant amounts at Venere MV communities. In particular, Thermoanaerobacteraceae and *Ammonifex* contain hyperthermophilic, chemolithotrophic members isolated from hot springs that employ hydrogen or formate as electron donors, and several sulfur compounds as acceptors (Miroshnichenko et al., 2008; Slobodkina et al., 2017). These groups are most prevalent in shallow push core sediments where sulfate is present (Fig. 4.4), yet the sulfate in these flows is consistent with a mixing ratio from deep-sourced fluids and seawater as end members, suggesting an absence of ongoing sulfate reduction (Fig. 4.5).

Microbial communities at MVs display high variability, though several keystone OTUs, particularly those relating to methane and sulfur metabolism, occur in these systems (Pachiadaki and Kormas, 2013). Methanotrophic communities at the center of the active Håkon Mosby MV are restricted to surface sediments, but anaerobic methanotrophs are active in peripheral zones with lower rates of deep fluid flow at sediment depths where sulfate permeates (Niemann et al., 2006b). Studies of recent flows at this location identified additional

populations similar to those found at Venere MV, including Atribacteria and Chloroflexi associated with the subsurface conduit, and sulfate reducers and sulfur oxidizers in surface-exposed mud flows (Ruff et al., 2018). In addition, high abundances of Methylococcales (up to 20%) characterized communities of active MVs compared to nearby inactive ones (Coelho et al., 2016). In contrast to active methanogens described at other MVs (Lazar et al., 2012) or deep biologically-sourced methane described at other accretionary margins (Ijiri et al., 2018), the low abundance of sequences belonging to canonical methanogens (0.7%) and thermogenic gas signature at the Venere MV summit suggest that microbial methane production is negligible. Based on preliminary comparisons with other marine subsurface ecosystems, the distinct gene content in MV metagenomes (Fig. 4.10) likely reflects functional adaptations in community members that may not be endemic to MVs, but are nevertheless highly abundant therein. Elevated percentages of defense mechanism COGs in MV metagenomes are suggestive of diversified adaptations against viral attack (Makarova et al., 2013), though viral diversity may select against certain defense elements (such as CRISPR-Cas systems) from the genome (Weinberger et al., 2012). Viruses are thought to outnumber bacterial and archaeal cells in subsurface environments (Engelhardt et al., 2014; Nigro et al., 2017), and as such, their influence on microbial community dynamics and evolution within MVs should be topics of future investigation.

Compared to basalts and hydrothermal environments, the higher percentages of COGs related to translation, ribosomal structure, and biogenesis in MVs suggests smaller average genome sizes (Konstantinidis and Tiedje, 2004). The gain, loss, or modification of cell membrane genes in populations of *Sulfurovum* have been implicated in adaptations to hydrothermal

environments (Anderson et al., 2017); these forces could also explain high percent abundances of COGs in MVs as well. With the exception of amino acids, the observation that most COGs were not differentially abundant among MVs could imply that metabolic gene content among subsurface environments is similar to a degree. Further analyses of MV metagenomes should consider characterizing metabolisms involved in biogeochemical cycles, and what specific adaptations to temperature, pressure, or the unique geochemistry of deep-sourced fluids these microbial genomes could hold.

Community changes upon mud flow expulsion on a transitional environment

Microbial community changes have been characterized across transitional environments in many settings. Increased diversity observed in aging basalt outcrops has been explained by geochemical changes, such as the accretion of organic matter and allochthonous minerals, that could support a wider variety of metabolisms (Lee et al., 2015). In contrast, (Woycheese et al., 2015) observed a decrease in diversity in serpentinizing seep fluids after they were exposed to the atmosphere and a select few genera became dominant. It took around two years for alpha diversity to increase in freshly exposed muds from Håkon Mosby MV, despite the availability of electron donors and acceptors (Ruff et al., 2018). Patterns of alpha diversity in Venere MV mud flows are not apparent, and thus may reflect a similar time dependency.

The observation that Venere MV mud flow microbial community composition was influenced by methane and sulfate availability is suggestive of energy limitation, which has also been found to structure communities in deep sediments of the South China Sea (Graw et al., 2018). Preliminary IODP data from Expedition 370 found that subsurface temperatures above 65˚C can

drastically restrict cell numbers (Heuer et al., 2017). Incomplete heat flow data from shallow Venere MV flows prevented us from determining whether temperature influenced community composition. Decreasing pressure as fluidized muds are transported upwards may represent another physical factor that may influence microbial community composition (Bartlett et al., 2007; Myka et al., 2017). Differences observed between communities from the Venere summit gravity core and nearby downslope flows may indicate additional geochemical or physical forces at play, though community assembly may be stochastic to some extent (Stegen et al., 2012).

Similar to microbial communities in extruded flows of the Håkon Mosby MV (Ruff et al., 2018), we observed increases in sulfate-reducing bacteria (*Desulfobacteraceae* and SEEP-SRB1) with time and distance from the MV summit, particularly in cores where chloride is high but sulfate is low, suggesting ongoing microbial sulfate reduction (Fig. 4.5). Populations of ANME do not change or increase in abundance, though ANME-2a-2b is one notable exception, present in downslope mud flow gravity cores and also at the more mature seep site 1. We postulate that mud flows closest to the summit (< 80 m) are too young for ANME populations to develop. If community successional patterns align with those described by (Ruff et al., 2018), these flows were likely extruded less than two years ago, and push core communities dominated by aerobic methanotrophs may be even less than a year old.

Nevertheless, the high abundances of aerobic methyl- and methanotrophic Gammaproteobacteria in recently exposed mud volcano surface sediments is somewhat unexpected. These groups are highly abundant > 20 cmbsf into the low-chloride and presumably oxygen-free mud flow fluids, and inhabit the same depths as obligate anaerobic

genera such as *Ammonifex*. Delivery of oxygen from bottom water into the mud flows, possibly via limited advection through the plated and fractured structure of the most recently extruded mud breccias may be possible; however, we have no oxygen measurements with which to address this question. Anaerobic methane oxidation by bacteria is not without precedent: *Methylomirabilis,* of the NC10 phylum, uses nitrite to generate oxygen and oxidize methane using a particulate methane monooxygenase homologous to those found in aerobic methanotrophic bacteria (Ettwig et al., 2010). Though the clayey composition of these mud breccias would limit diffusion rates, the low biomass in Venere MV summit mud flows may not consume oxygen very quickly. Fluid penetration into flows could also explain the delivery of methylotrophic Gammaproteobacteria into shallow mud breccia depths, as these groups normally persist in bottom waters (Tavormina et al., 2010) or at the sediment-water interface, and were not detected in deep sediments from the summit GC. Additional constraints on mud flow dynamics, pore fluid movement, and geochemical interfaces are needed to better understand how microbial communities respond to a highly dynamic environment.

The active Venere MV, atop the Calabrian accretionary prism offshore Italy, emits fluids and muds sourced from kilometer-scale depths within sediments that are depleted in sulfate and much fresher than seawater. Microbial communities inhabiting summit mud flows are distinct from those at reference and peripheral methane seepage sites. Downslope mud flow communities contain several clades of aerobic methyl- and methanotrophic Gammaproteobacteria, while anaerobic methanotrophs and sulfate-reducing bacteria develop in older flows further from the summit. Spatiotemporal succession patterns of similar

communities from another MV suggest that Venere MV flows may have been extruded less than two years ago. Microbial gene content from both of these MVs is distinct from that of other marine subsurface habitats, and likely reflects adaptations to a unique environment.

Acknowledgements

This study was possible though a collaboration with the MARUM team funded through the Deutsche Forschungsgemeinschaft (DFG) and the Research Center / Excellence Cluster "The Ocean in the Earth System". We thank the masters and crews of cruises RV METEOR M112 and the teams of the MARUM AUV SEAL 5000 and ROV QUEST 4000m for their assistance at sea. Marta Torres acknowledges support through a fellowship from the Hanse Wissenschaftskolleg. We also thank Jesse Muratli for porewater cation measurements, and Vengatesha Perumal and Heath Mills for DNA extraction suggestions. The Deep Carbon Observatory's Census of Deep Life supported metagenome sequencing which was performed at the Marine Biological Laboratory (Wood Hole, MA, USA). We are grateful for the assistance of Mitch Sogin, Joseph Vineis, Andrew Voorhis, and Hilary Morrison at MBL. We also appreciate Mark Dasenko for assisting with amplicon sequencing at the Oregon State University Center for Genome Research and Biocomputing (CGRB) and Tom Sharpton for assistance with metagenome annotation.

Figures

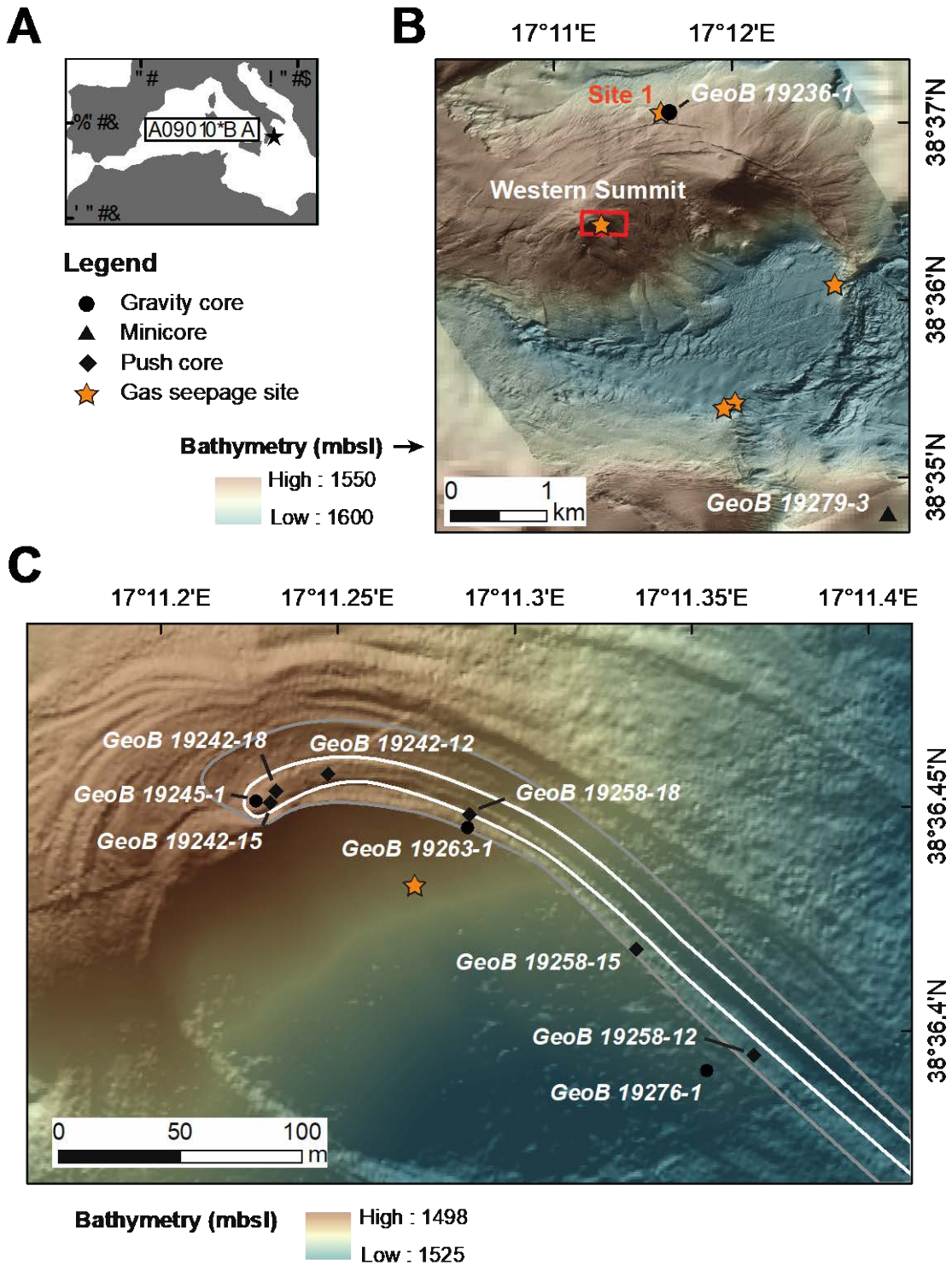

Figure 4.1. Venere Mud Volcano (MV) location, bathymetry, and sampling areas. (A) Venere MV lies offshore Calabria, Italy in the Mediterranean Sea. **(B)** AUV-derived bathymetry of Venere MV (1.6 m grid) showing Eastern and Western summits, ring faulting along the caldera

rim, five sites of observed gas seepage (orange stars), and locations of cores at seep site 1 and at a non-seep reference site to the southeast. Data from Loher et al., 2018a. **(C)** Zoomed-in view of the Venere MV western summit showing locations of gravity and push cores collected for microbiological sampling (circles and diamonds, respectively) and the extent of two recently-extruded mud breccia flows (older flow outlined in gray, younger in white). Maps modified from Loher et al., 2018a.

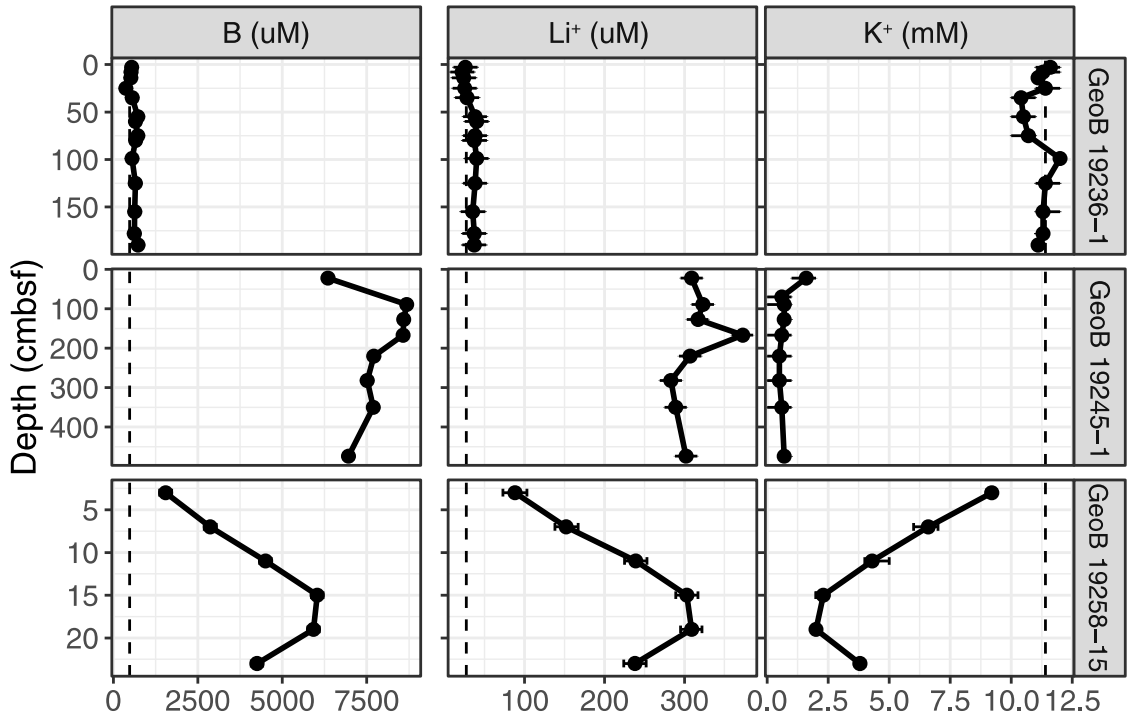

Figure 4.2. Lithium, boron, and potassium concentrations in porewater of freshly extruded Venere MV mud breccia flows. Cores include a gravity core from Seep Site 1 away from the fresh flows (GeoB 19236-1), a gravity core from the summit (GeoB19245-1), and a push core 110 m downslope (GeoB 19258-15). Dashed lines indicate seawater values, and confidence intervals represent standard deviations.

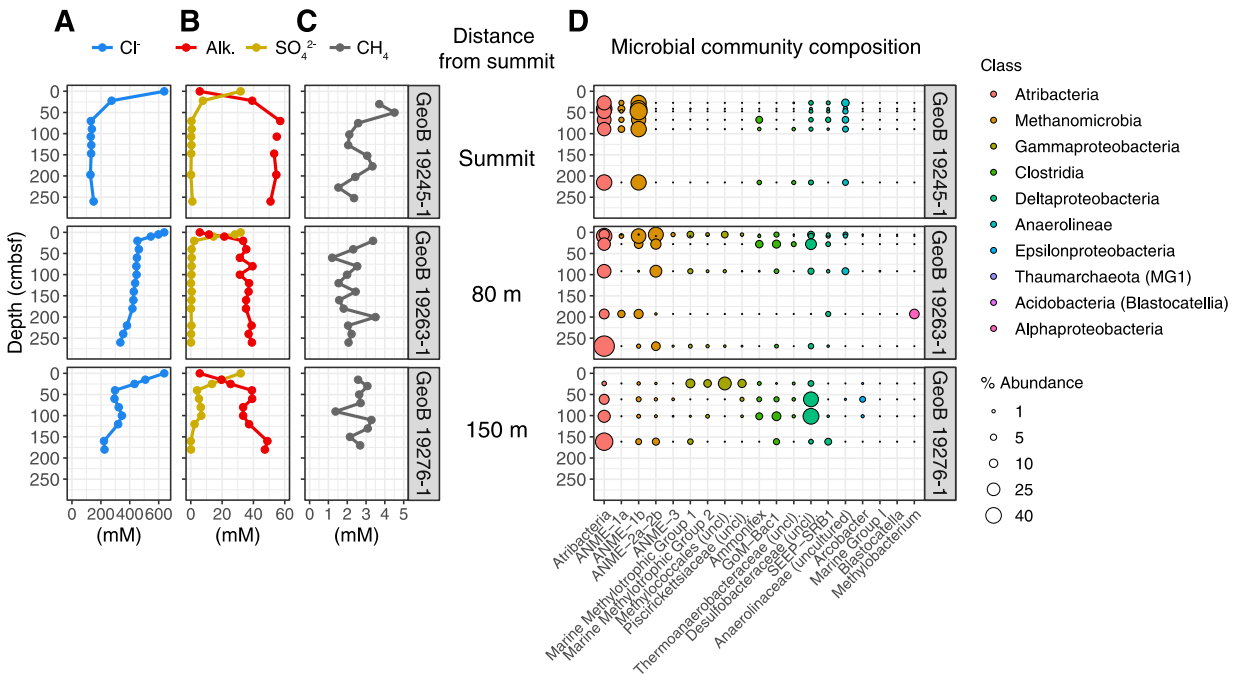

Figure 4.3. Geochemical and microbial community data from mud breccia flow gravity cores at the summit, 80 m downslope, and 150 m downslope, ordered from top to bottom. (A) Porewater chloride, **(B)** alkalinity and sulfate, and **(C)** methane concentrations. **(D)** Percent abundances of dominant bacterial and archaeal genera within microbial communities, colored by taxonomic classes to which they belong.

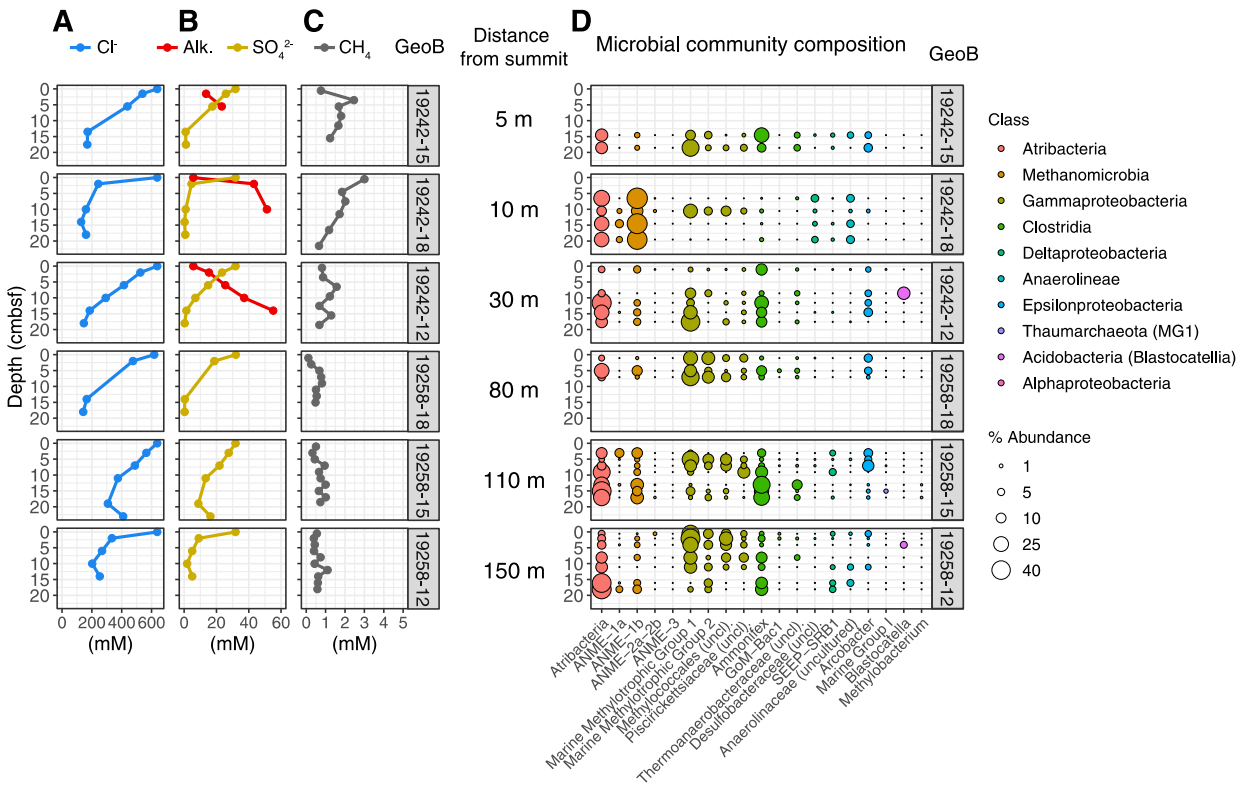

Figure 4.4. Geochemical and microbial community data from mud breccia flow push cores collected near the summit, ordered by increasing distance downslope from top to bottom. The first three cores are collected from within the younger flow at the summit and 5 m and 10 m downslope, and the last three from 80 m, 110 m, and 150 m downslope within the older flow. **(A)** Porewater chloride, **(B)** alkalinity and sulfate, and **(C)** methane concentrations. **(D)** Percent abundances of dominant bacterial and archaeal genera within microbial communities, colored by taxonomic classes to which they belong.

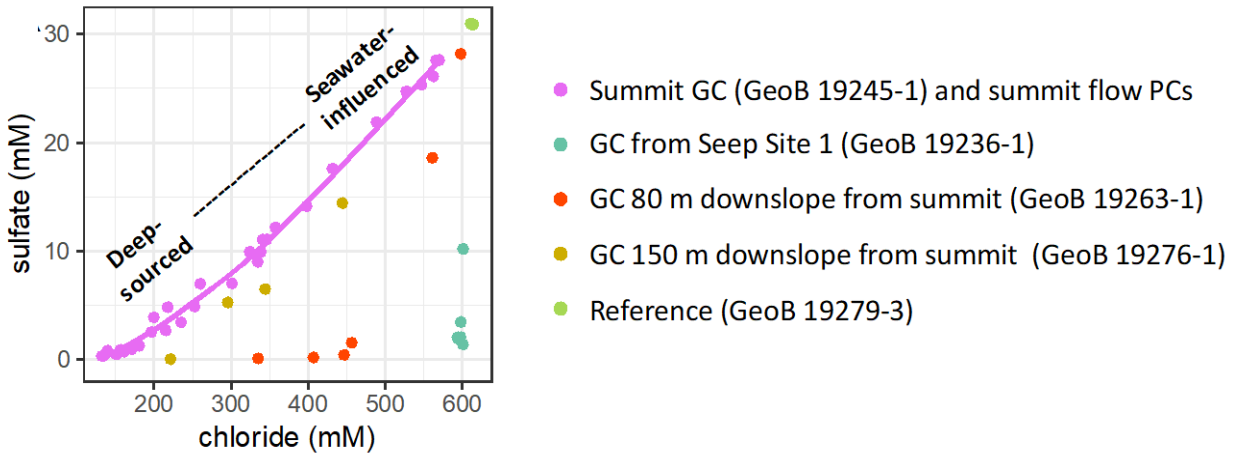

Figure 4.5. Biplot of porewater chloride and sulfate concentrations from Venere MV samples. Summit flows representing mixed fluids are colored purple, and downslope gravity cores (GCs) in gold and red. Cores located away from the summit flows are turquoise and green. The

shaded line around summit flow samples is a 95% confidence interval calculated by locally estimated scatterplot smoothing.

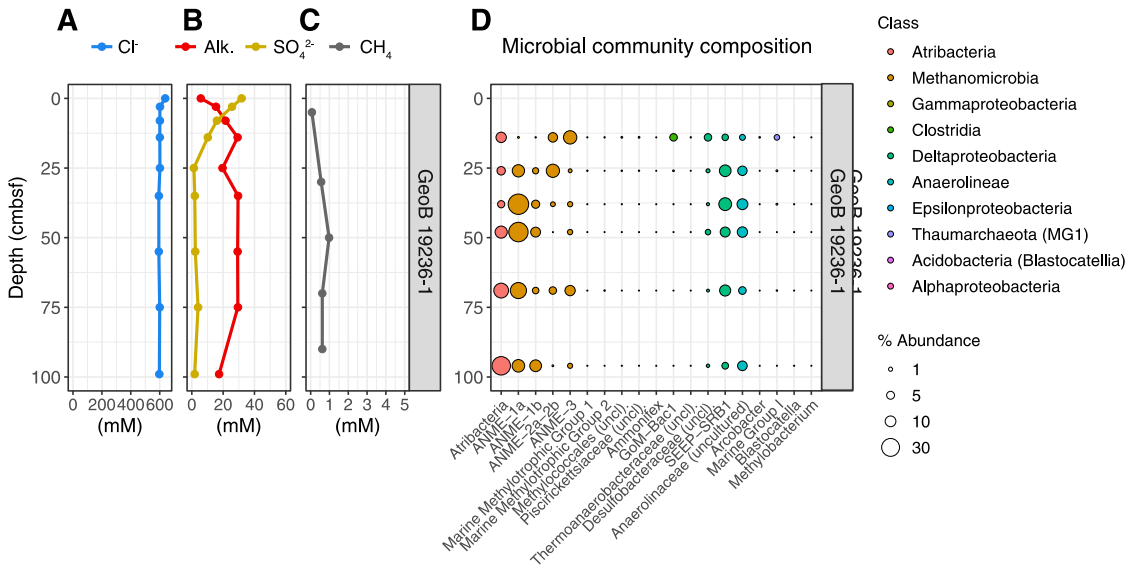

Figure 4.6. Geochemical and microbial community data from gravity core 19236-1 at seep site 1. (A) Porewater chloride, **(B)** alkalinity and sulfate, and **(C)** methane concentrations. **(D)** Percent abundances of dominant bacterial and archaeal genera, colored by taxonomic classes to which they belong.

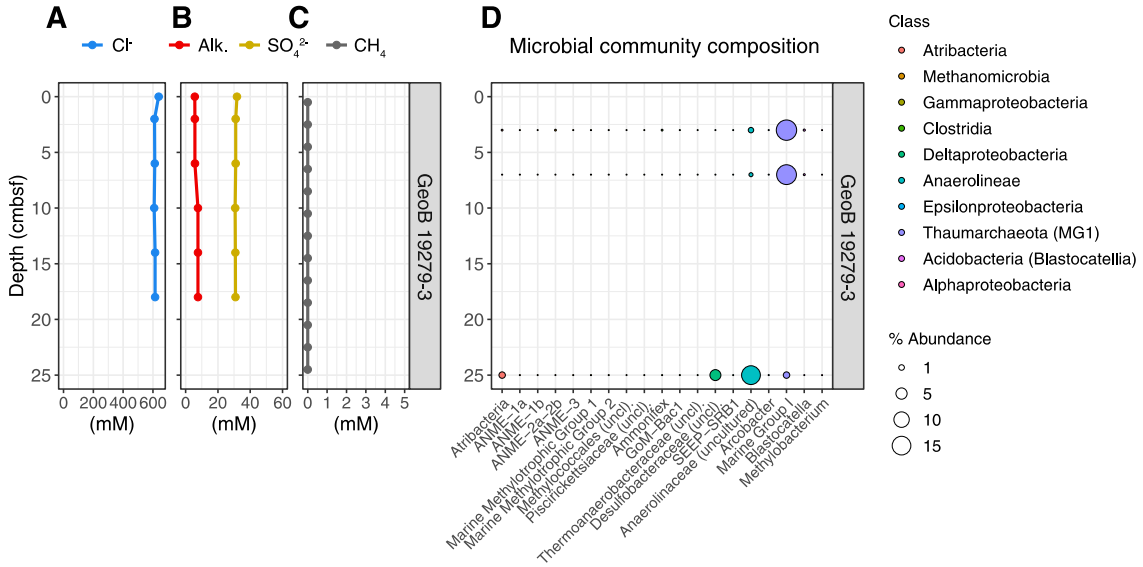

Figure 4.7. Geochemical and microbial community data from reference site minicore GeoB19279-3. (A) Porewater chloride, **(B)** alkalinity and sulfate, and **(C)** methane concentrations. **(D)** Percent abundances of dominant bacterial and archaeal genera across the entire dataset, colored by taxonomic classes they belong to.

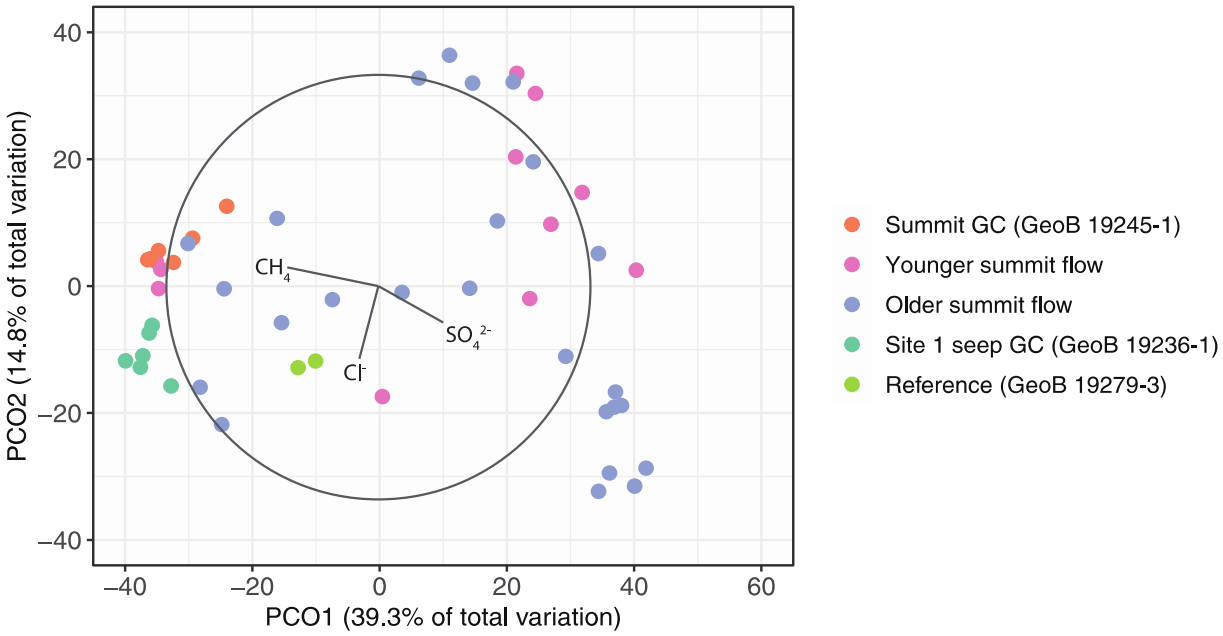

Figure 4.8. Principal coordinates analysis (PCO) plot of microbial communities from Venere MV summit flows, seep site 1, and a non-seep reference. Vectors represent porewater geochemical concentrations that correlate with differences among microbial communities.

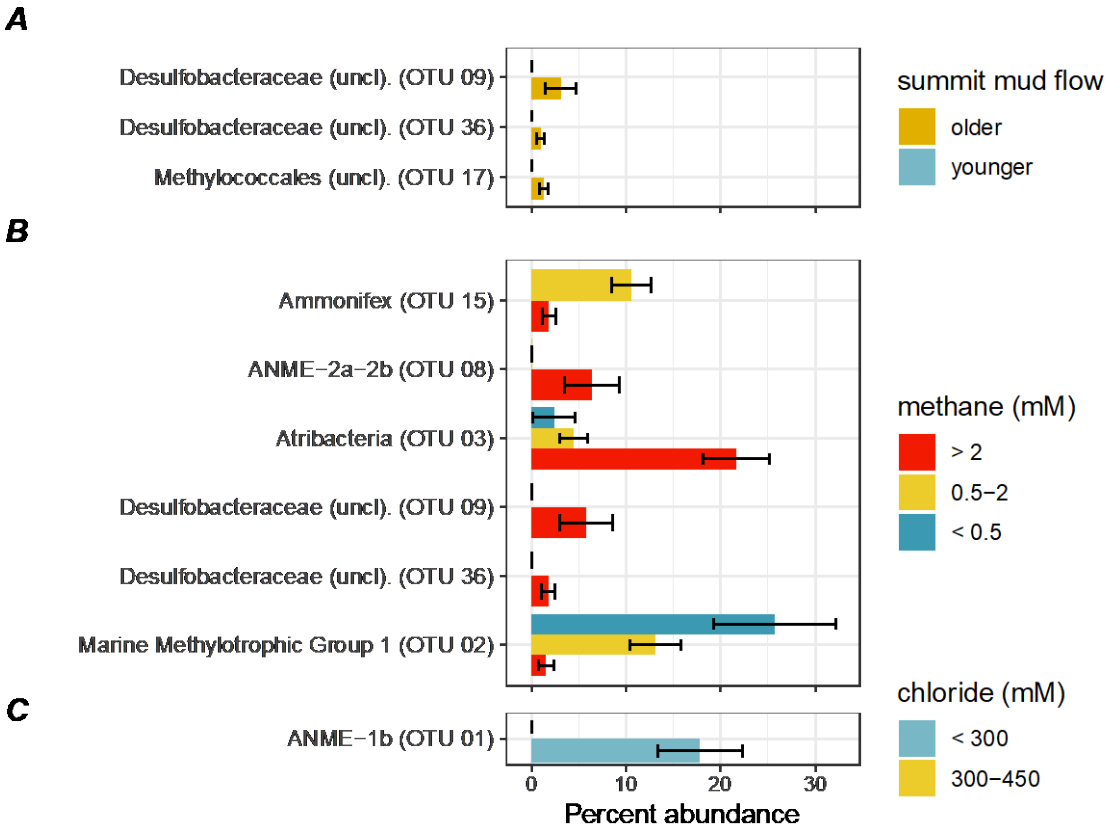

Figure 4.9. Percent abundances of OTUs in Venere MV summit samples that differed across (A) older or younger summit mud flows, (B) methane concentrations, and (C) chloride

concentrations. Only OTUs that were > 1% in abundance among groups being compared were considered. Significance was determined at the α=0.05 confidence level with a Bonferroni correction applied for the number of pairwise comparisons (23-26, depending on treatment). Error bars represent standard errors.

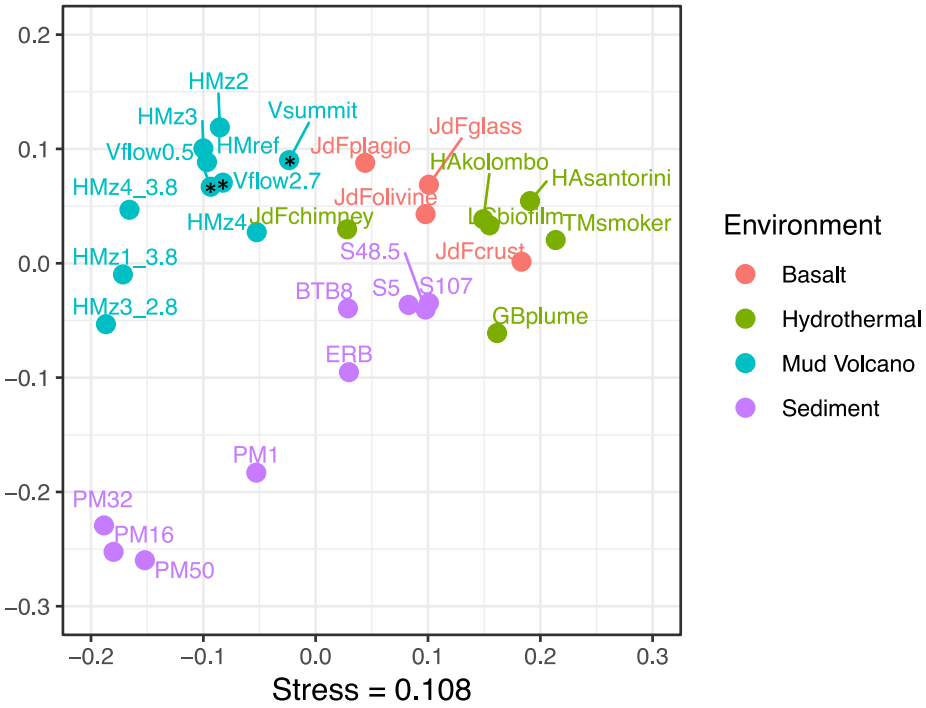

Figure 4.10. Non-metric multidimensional scaling (NMDS) ordination of COG functional category percent abundances among publicly available metagenomes from diverse marine subsurface environments. Venere MV samples are indicated by asterisks. Abbreviations: V, Venere; HM, Håkon Mosby; JdF, Juan de Fuca; HA, Hellenic Arc; TM, Tahi Moana; GB, Guaymas Basin; PM, Peru Margin, ERB, Eel River Basin. Where indicated, numbers at ends of labels represent depths below seafloor in meters. Additional information is supplied in Table 4.4.

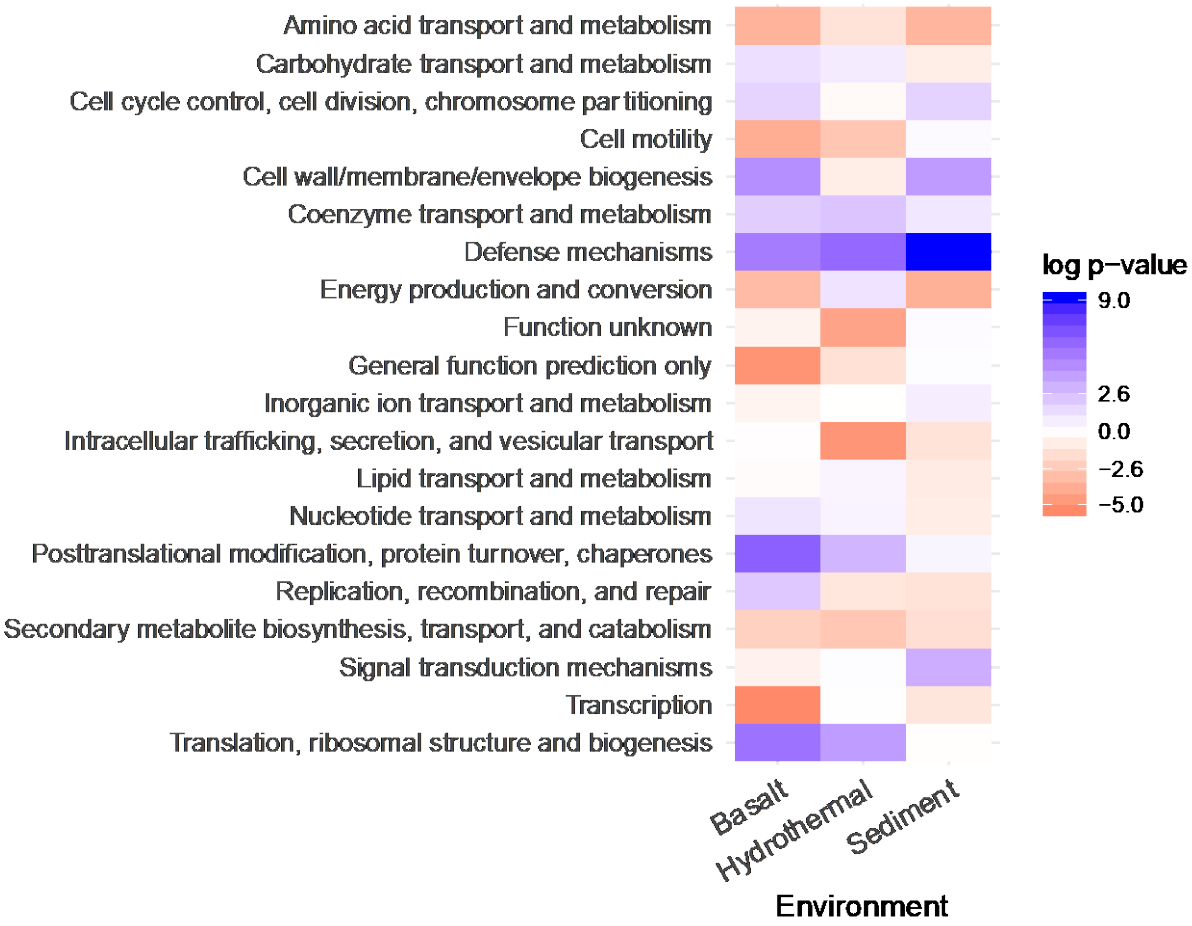

Figure 4.11. Heatmap of log-transformed p-values from COG category abundance comparisons between mud volcano metagenomes and those from other marine subsurface ecosystems. Values shaded in blue indicate higher abundances in mud volcanoes, while red values are higher in other ecosystems. Statistically significant comparisons are indicated by values over or under 2.6 (α=0.05 with Bonferroni correction for multiple pairwise comparisons).

Tables

Table 4.1. Genera identified as contaminants and removed from downstream community analysis. Highlighted genus names identify reagent-associated contaminants reported in Salter et al (2014). Highlighted p-values correspond to genera that are higher in percent abundance among the three blanks (two from DNA extraction, and one PCR blank) as compared to 68 samples.

taxon	avg % among samples	avg % among blanks	% higher in blanks	p-value of difference	max % in any non-blank	max % in any blank
Comamonadaceae (uncl).	0.621	15.566	14.945	1.019E-09	16.575	34.304
Neisseria (uncultured)	0.014	11.208	11.194	2.317E-07	0.275	33.623
Corynebacteriaceae (uncl).	0.177	9.709	9.532	4.695E-12	4.706	21.807
Enhydrobacter	0.136	8.499	8.363	5.396E-07	5.917	25.184
Truepera	0.228	5.169	4.941	5.140E-04	14.365	15.508
Halomonadaceae (uncl).	0.202	4.880	4.677	1.872E-05	6.071	14.639
Fibrobacterales FD035 (gen).	0.021	4.598	4.577	2.620E-07	0.621	13.793
Sulfurovum	0.410	3.762	3.352	4.717E-03	12.581	11.285
Phycisphaerae MSBL9 (gen).	0.185	3.553	3.368	5.471E-04	9.823	10.658
Pelagibius	0.003	1.672	1.669	2.379E-07	0.140	5.016
Dehalococcoidia MSBL5 (gen).	0.065	1.567	1.502	2.760E-06	1.059	4.702
Escherichia-Shigella	0.071	1.555	1.484	5.032E-06	1.429	4.665
Micrococcus	0.315	1.508	1.193	0.023	3.677	4.525
Paracoccus	0.066	1.438	1.372	1.870E-05	1.697	4.314
Sphingomonadales (uncl).	0.552	1.254	0.702	0.600	14.894	3.762
Alkanindiges	0.000	1.149	1.149	2.245E-07	0.000	3.448
Phreatobacter	0.028	0.927	0.899	6.331E-06	1.146	2.780
Sphingopyxis	0.000	0.836	0.836	2.245E-07	0.000	2.508
Bradyrhizobium	0.004	0.731	0.728	3.053E-07	0.239	2.194
Pseudomonas	0.435	0.627	0.192	0.775	6.378	1.881
Corynebacterium	0.279	0.418	0.139	0.801	6.591	1.254
Brevibacterium	0.110	0.348	0.238	0.584	5.882	1.043
Methyloversatilis	0.000	0.105	0.105	2.245E-07	0.000	0.314

Table 4.2. ANOSIM test statistics comparing Venere MV microbial communities separated by groups depicted in Figure 4.8. Note that the Venere MV summit center is located on the younger mud breccia flow. When summit center GC samples are included with other communities from the younger flow, they are distinct from older summit flow communities, but when they are removed, no such difference is seen.

Groups	R statistic	Significance level %	Possible permutations	Actual permutations	Number ≥ observed
All five groups	0.171	0.5	__	999	4
Pairwise tests					
site 1 seep GC, older summit flow	0.345	0.1	736281	999	0
site 1 seep GC, summit center GC	0.737	0.2	462	462	1
older summit flow, reference	0.499	0.3	351	351	1
site 1 seep GC, younger summit flow	0.416	0.8	18564	999	7
younger summit flow, reference	0.568	1.1	91	91	1
summit center GC, older summit flow	0.178	3.5	736281	999	34
site 1 seep GC, reference	1	3.6	28	28	1
summit center GC, reference	1	3.6	28	28	1
younger summit flow, summit center GC	0.148	7.2	18564	999	71
younger summit flow, older summit flow	-0.011	51.2	Very large	999	511
younger flow (including summit center GC) and older summit flow	0.08	3.4	Very large	999	33

Table 4.3. ANOSIM test statistics comparing COG category abundances (normalized by percent) across several subseafloor environments, using metagenomes depicted in Figure 4.10.

Groups	R statistic	Significance level %	Possible permutations	Actual permutations	Number ≥ observed
All four environments	0.559	0.1	__	999	0
Pairwise tests					
mud volcano, hydrothermal	0.841	0.1	8008	999	0
mud volcano, basalt	1	0.1	1001	999	0
mud volcano, sediment	0.611	0.1	92378	999	0
hydrothermal, basalt	0.397	1.4	210	210	3
hydrothermal, sediment	0.266	2.1	5005	999	20
basalt, sediment	0.168	9.2	715	715	66

Table 4.4. Metagenome samples shown in Figure 4.10 with references.

Name	Sample	Environment	Reference
JdFglass	Juan de Fuca glass minerals	Basalt	(Smith et al., 2016)
JdFolivine	Juan de Fuca olivine minerals	Basalt	(Smith et al., 2016)
JdFplagio	Juan de Fuca plagioclase minerals	Basalt	(Smith et al., 2016)
JdFcrust	Juan de Fuca basaltic crust	Basalt	(Stepanauskas, 2012)
TMsmoker	Tahi Moana black smoker plume	Hydrothermal	(Anantharaman et al., 2016)
LCbiofilm	Lost City biofilm	Hydrothermal	(Brazelton and Baross, 2009)
GBplume	Guaymas Basin vent plume	Hydrothermal	(Dick and Tebo, 2010)
HAkolombo	Hellenic Arc Kolombo caldera mats	Hydrothermal	(Oulas et al., 2016)
HAsantorini	Hellenic Arc Santorini caldera mats	Hydrothermal	(Oulas et al., 2016)
JdFchimney	Juan de Fuca black smoker chimney	Hydrothermal	(Xie et al., 2011)
HMref	Håkon Mosby MV background reference	Mud Volcano	(Ruff et al., 2018)
HMz1_3.8	Håkon Mosby MV flow, zone 1	Mud Volcano	(Ruff et al., 2018)
HMz2	Håkon Mosby MV flow, zone 2	Mud Volcano	(Ruff et al., 2018)
HMz3_2.8	Håkon Mosby MV flow, zone 3	Mud Volcano	(Ruff et al., 2018)
HMz3	Håkon Mosby MV flow, zone 3	Mud Volcano	(Ruff et al., 2018)
HMz4_3.8	Håkon Mosby MV flow, zone 4	Mud Volcano	(Ruff et al., 2018)
HMz4	Håkon Mosby MV flow, zone 4	Mud Volcano	(Ruff et al., 2018)
Vflow2.7	Venere MV flow, GC 19263-1	Mud Volcano	This study
Vflow0.5	Venere MV flow, GC 19263-1	Mud Volcano	This study
Vsummit	Venere MV flow, PC 19242-15	Mud Volcano	This study
PM1	Peru Margin	Sediment	(Biddle et al., 2008)
PM16	Peru Margin	Sediment	(Biddle et al., 2008)
PM32	Peru Margin	Sediment	(Biddle et al., 2008)
PM50	Peru Margin	Sediment	(Biddle et al., 2008)
BTB8	Brazos Trinity Basin	Sediment	(Biddle et al., 2011)
ERB	Eel River Basin	Sediment	(Hallam et al., 2004)
S107	Shimokita	Sediment	(Kawai et al., 2014)
S48.5	Shimokita	Sediment	(Kawai et al., 2014)
S5	Shimokita	Sediment	(Kawai et al., 2014)

Chapter 5

Conclusion

Over the past decade, the development of high-throughput DNA sequencing technology and computational analyses have allowed for routine characterization of complex microbial communities and inference of biogeochemical cycles they are capable of mediating (Zhou et al., 2015). Despite these impressive advancements, microbial community structure often does not add any predictive power in explaining rates of ecosystem processes such as carbon and nitrogen transformations, even when considering phylogenetically narrow groups capable of specific metabolisms (Bier et al., 2015; Graham et al., 2016). Of course, some of this disconnect may arise from the fact that DNA sequence data cannot determine whether cells are active or even alive. In marine sediments, for example, a majority of the DNA pool may be extracellular (Dell'Anno et al., 2002; Torti et al., 2015), though this has been argued to have a minimal effect on overall community composition (Ramírez et al., 2018). Nevertheless, assessing linkages between community structure and function must be seen within the spectrum of cell activity, dormancy, and death (Orsi et al., 2013; Wang et al., 2015), whether instigated by energy limitation (Bradley et al., 2019) or viral infection (Roux et al., 2016). Understanding these linkages are undoubtedly major foci of microbial ecology, and as we uncover more about the functional potential of microbial dark matter, questions of "who is there?" and "what are they doing?" must be placed in appropriate biogeochemical contexts (Solden et al., 2016).

In addition to understanding these questions of which microbes are present and what they are doing in marine sediments, the goals set forth in this dissertation focused on better understanding the development of anaerobic methane oxidation as a biological process. To

accomplish this, sediments were sampled across transitional gradients where we hypothesized the onset of AOM based on the mixing of methane- and sulfate-rich fluids, and also incubated in a timeseries of laboratory microcosms to stimulate AOM *ex situ*. The chapters presented here detail a dynamic interplay between methanotrophic activity and microbial community structure that is affected by time and energy.

In Chapter 2, sediment microbial communities and abundances of sulfate reducers and anaerobic methanotrophs were paired with reactive transport modeling of methane fluxes at Storfjordrenna gas hydrate mounds, offshore Svalbard. The impetus of this research was to understand how microbial communities and AOM rates within sediments are predicted to change as methane fluxes from subseafloor Arctic gas hydrate reservoirs increase. Recent influx of methane into shallower sediment horizons corresponded with increases in methanotrophs and sulfate reducers and a decline in microbial diversity. This effect was nearly erased after biogeochemical equilibria were established, suggesting a “boom-and-bust” community response to increases in methane flux. This study builds on others that merge microbial community dynamics with modeling of redox-associated biogeochemical cycles (Danczak et al., 2016; Esser et al., 2015; Reed et al., 2014; Stegen et al., 2016), but is currently the only one describing methane oxidation in sediments. In addition, it provides one of the first *in situ* doubling time estimates for ANME (Ruff et al., 2018). The growth and stimulation of ANME activity after a year or less of methane intrusion into a sediment horizon suggests that the considerably high fluxes measured at Storfjordrenna support an active and responsive microbial methane filter. Further studies should use these findings to predict maximum fluxes of methane that could be fully consumed within sediments, and continue to assess the physical,

geochemical, or ecological constraints of methanotrophy across seep sites and other ecosystems.

To complement this field-based approach, Chapter 3 detailed a three-way factorial incubation approach where Storfjordrenna sediments were collected across a sulfate-methane transition and incubated at *in situ* temperature and pressure. These were amended with varying amounts of methane over a timeseries to understand how communities and marker gene abundances develop in concordance with empirically-measured sulfate reduction-AOM rates after stimulation with methane and sulfate. Sediments from sulfate-reduction and methanogenic zones saw notable community changes and increases in sulfur-cycling taxa, but failed to consume methane. Rates of methanotrophy and ANME abundances were highest in sediments from a site of active gas seepage that had been exposed to highest concentrations of methane for the longest times. Similar incubation approaches have been used to examine the effects of methane partial pressures on AOM (Deusner et al., 2010), characterize growth kinetics and metabolic potential of ANME (Girguis et al., 2005; Nauhaus et al., 2007; Wegener et al., 2016), and examined community changes (Bhattarai et al.; Zhang et al., 2011), but the study presented here is so far the only one linking community and rate changes across a timeseries. Observations of stark community changes without concurrent changes in rates (and vice versa) suggest that ANME may operate independently from the dynamics of the microbial community more broadly. The experimental approach we employed allowed us to determine that methane concentration did not affect communities on the timescales tested. However, further studies could carry similarly integrated experimental designs across longer timescales to more powerfully assess relationships between environmental parameters (such as methane or

temperature) and microbial community structure and function. Another implicit hypothesis in this experimental approach was that communities and rates in microcosms would resemble those *in situ*, though we observed significant proliferation of OTUs that were not dominant in native sediments. Researchers may choose field-based or laboratory methodologies to better understand linkages between subseafloor microbial communities and the biogeochemical cycles they drive, but the decision of which approach to use should depend on the specific questions being asked of the system. For example, if it is more important to characterize communities in a natural environment, it may be well worth designing and implementing a field experiment despite using logistically challenging and/or expensive instrumentation and ship time. However, if the ability to manipulate conditions and run adequate controls outweighs this, then laboratory experiments may be a better strategy.

Chapter 4 investigated microbial community diversity and changes associated with the expulsion of a fresh mud flow hosting deep-sourced fluids from the active Venere mud volcano (MV) offshore Italy. Communities from the mud flow changed as sulfate-rich seawater began to enter deep-sourced fluids, which were rich in methane and low in chloride. Sulfate and methane concentrations explained more of the differences in community structure than did chloride, indicating that energy, rather than fluid source, appears to be the dominant driver of community structure. Several clades of aerobic methanotrophic Gammaproteobacteria dominated flow communities, but ANME did not appear to become established in the samples. Using the findings of (Ruff et al., 2018) as a guide, Venere flows may have been less than two years old at the time of sampling, and thus too young to allow large ANME populations to develop. Though the two MVs inhabit different thermal regimes and are fed by fluids mobilized

at different subsurface depths (Loher et al., 2018c; Perez-Garcia et al., 2009), their similarities in methane- and sulfur-cycling populations relative to other marine subsurface environments suggests MVs select for a distinct ecosystem. Going forward, it may be important to consider how dynamic methanotrophic populations at MV flows modulate methane emissions from these high-flux point sources into the ocean (Kopf, 2003), or in the case of terrestrial MVs, the atmosphere (Cheng et al., 2012; Mazzini and Etiope, 2017). Further microbiology research at MVs should also continue to investigate the metabolic and adaptive diversity to the physical or geochemical conditions encountered in the deep biosphere (Colwell and D'Hondt, 2013; Orcutt et al., 2013).

Each chapter discusses or infers microbial community activity and responses to perturbances in methane-sulfate gradients encountered in marine sediments. These perturbances, whether caused by mud volcanism or increases in the flux of methane, change the redox potential of these environments. This affects the favorability of certain metabolisms, which drives microbial community dynamics in sediments, soils, estuarine waters, and other environments where shifts in redox potentials occur (Crump et al., 2007; D'Hondt et al., 2004; Orcutt et al., 2013; Pett-Ridge et al., 2006). This theme of energetics is seen across all chapters: highest concentrations of *mcrA* genes and AOM rates were seen at methane-sulfate interfaces in Storfjordrenna gas hydrate mounds, methane concentrations increased SR-AOM rates and percent abundances of ANME from corresponding incubations, and methane and sulfate were dominant drivers of microbial community diversity in fresh mud breccia flows from Venere MV. Energy is often thought to be the driving force explaining the distribution and activity of microbial communities in the marine subsurface (Bradley et al., 2019; Graw et al., 2018;

Hoehler and Jørgensen, 2013; Starnawski et al., 2017). The extent to which mineralogical variability (Smith et al., 2016), or organic carbon composition (Nunoura et al., 2009) factor into energy limitations remain topics of study. Mechanical or geometric limitations on microbial habitability and activity in the deep subsurface have additionally been suggested (Fredrickson et al., 1997; Rebata-Landa and Santamarina, 2006). Combined effects of energetic and physical drivers on community composition and activity warrant further investigation within the field of subsurface microbiology.

All chapters also temporally constrained community responses to these transitional environments. Storfjordrenna gas hydrate mounds showed clear successional patterns linking geochemistry with microbial diversity and composition at areas of increasing methane flux, and provided estimates of ANME doubling times *in situ*. The emergence of certain populations in Venere MV flows and in several microcosm incubations were less clearly associated with the onset of certain biogeochemical cycles, but provide helpful observations for future studies to test hypotheses of AOM community dynamics within a successional framework. Incubations of seep sediments were useful in showing simultaneous development of AOM and changes in ANME populations, but questions of theoretical limits of AOM rates (Hong et al., 2016), ANME population densities, and how long they would take to develop still remain unresolved. Studies like these provide better estimations of methane oxidation potential within the context of global carbon cycling, but are nevertheless constrained to marine sediments. AOM and ANME have also been described in euxinic water columns (Wakeham et al., 2004), hydrothermal systems (Biddle et al., 2012; Schouten et al., 2003), wetlands (Valenzuela et al., 2017), and in thawing permafrost (Winkel et al., 2018). Across these distinct systems, the

extent to which AOM is coupled to nitrite (Hu et al., 2014; Zhu et al., 2010), iron (Ettwig et al., 2016; Wankel et al., 2012), manganese (Beal et al., 2009), or other electron donors (Caldwell et al., 2008), is still being understood. To further complicate this, the recent discovery of methyl-coenzyme M reductase genes in non-Euryarchaeotal lineages (Boyd et al., 2019; Evans et al., 2015) suggest that methane consumption or production is ancient, present in several Archaeal phyla (Mondav et al., 2014; Vanwonterghem et al., 2016). In addition, how viruses impact microbial ecology in methane-rich ecosystems is beginning to be understood (Corinaldesi et al., 2012; Emerson et al., 2018).

This dissertation presents novel findings on how the most globally significant methanotrophs, their activities, and microbial communities are linked together and develop over time. Microbes have shaped Earth's climate going back billions of years. Their contributions to global carbon cycling are particularly relevant today within the context of anthropogenic climate change. More research is needed to further elucidate links between these processes, though it should be coupled with education and outreach to build broader understanding among our own communities.

References

Agis, M., Granda, A., and Dolan, J. R. (2007). A cautionary note: Examples of possible microbial community dynamics in dilution grazing experiments. *Journal of Experimental Marine Biology and Ecology* 341, 176–183. doi:10.1016/j.jembe.2006.09.002.

Anantharaman, K., Breier, J. A., and Dick, G. J. (2016). Metagenomic resolution of microbial functions in deep-sea hydrothermal plumes across the Eastern Lau Spreading Center. *The ISME Journal* 10, 225–239. doi:10.1038/ismej.2015.81.

Anderson, R. E., Reveillaud, J., Reddington, E., Delmont, T. O., Eren, A. M., McDermott, J. M., et al. (2017). Genomic variation in microbial populations inhabiting the marine subseafloor at deep-sea hydrothermal vents. *Nature Communications* 8, 1114. doi:10.1038/s41467-017-01228-6.

Andreassen, K., Hubbard, A., Winsborrow, M., Patton, H., Vadakkepuliyambatta, S., Plaza-Faverola, A., et al. (2017). Massive blow-out craters formed by hydrate-controlled methane expulsion from the Arctic seafloor. *Science* 356, 948–953. doi:10.1126/science.aal4500.

Aoki, M., Ehara, M., Saito, Y., Yoshioka, H., Miyazaki, M., Saito, Y., et al. (2014). A Long-Term Cultivation of an Anaerobic Methane-Oxidizing Microbial Community from Deep-Sea Methane-Seep Sediment Using a Continuous-Flow Bioreactor. *PLOS ONE* 9, e105356. doi:10.1371/journal.pone.0105356.

Association, A. P. H., Association, A. W. W., and Federation, W. P. C. (1989). *Standard methods for the examination of water and wastewater. 17th edition.* American Public Health Association Available at: https://tamug-ir.tdl.org/handle/1969.3/24401 [Accessed October 16, 2018].

Åström, E. K. L., Carroll, M. L., Ambrose, W. G., Sen, A., Silyakova, A., and Carroll, J. (2018). Methane cold seeps as biological oases in the high-Arctic deep sea: Cold seeps in the high-Arctic deep sea. *Limnology and Oceanography* 63, S209–S231. doi:10.1002/lno.10732.

Babbin, A. R., Jayakumar, A., and Ward, B. B. (2016). Organic Matter Loading Modifies the Microbial Community Responsible for Nitrogen Loss in Estuarine Sediments. *Microb Ecol* 71, 555–565. doi:10.1007/s00248-015-0693-5.

Bar-On, Y. M., Phillips, R., and Milo, R. (2018). The biomass distribution on Earth. *PNAS*, 201711842. doi:10.1073/pnas.1711842115.

Bartlett, D. H., Lauro, F. M., and Eloe, E. A. (2007). Microbial Adaptation to High Pressure. *Physiology and Biochemistry of Extremophiles*, 333–348. doi:10.1128/9781555815813.ch25.

Beal, E. J., House, C. H., and Orphan, V. J. (2009). Manganese- and Iron-Dependent Marine Methane Oxidation. *Science* 325, 184–187. doi:10.1126/science.1169984.

Berndt, C., Feseker, T., Treude, T., Krastel, S., Liebetrau, V., Niemann, H., et al. (2014). Temporal Constraints on Hydrate-Controlled Methane Seepage off Svalbard. *Science* 343, 284–287. doi:10.1126/science.1246298.

Berner, R. A., and Westrich, J. T. (1985). Bioturbation and the early diagenesis of carbon and sulfur. *Am. J. Sci.; (United States)* 285:3. doi:10.2475/ajs.285.3.193.

Bhattarai, S., Cassarini, C., Rene, E. R., Kümmel, S., Esposito, G., and Lens, P. N. L. (2018a). Enrichment of ANME-2 dominated anaerobic methanotrophy from cold seep sediment in an external ultrafiltration membrane bioreactor. *Engineering in Life Sciences* 18, 368–378. doi:10.1002/elsc.201700148.

Bhattarai, S., Cassarini, C., Rene, E. R., Zhang, Y., Esposito, G., and Lens, P. N. L. Enrichment of sulfate reducing anaerobic methane oxidizing community dominated by ANME-1 from Ginsburg Mud Volcano (Gulf of Cadiz) sediment in a biotrickling filter. *Bioresource Technology*. doi:10.1016/j.biortech.2018.03.018.

Bhattarai, S., Zhang, Y., and Lens, P. N. L. (2018b). Effect of pressure and temperature on anaerobic methanotrophic activities of a highly enriched ANME-2a community. *Environ Sci Pollut Res* 25, 30031–30043. doi:10.1007/s11356-018-2573-2.

Biastoch, A., Treude, T., Rüpke, L. H., Riebesell, U., Roth, C., Burwicz, E. B., et al. (2011). Rising Arctic Ocean temperatures cause gas hydrate destabilization and ocean acidification. *Geophys. Res. Lett.* 38, L08602. doi:10.1029/2011GL047222.

Biddle, J. F., Cardman, Z., Mendlovitz, H., Albert, D. B., Lloyd, K. G., Boetius, A., et al. (2012). Anaerobic oxidation of methane at different temperature regimes in Guaymas Basin hydrothermal sediments. *ISME J* 6, 1018–1031. doi:10.1038/ismej.2011.164.

Biddle, J. F., Fitz-Gibbon, S., Schuster, S. C., Brenchley, J. E., and House, C. H. (2008). Metagenomic signatures of the Peru Margin subseafloor biosphere show a genetically distinct environment. *PNAS* 105, 10583–10588. doi:10.1073/pnas.0709942105.

Biddle, J. F., Lipp, J. S., Lever, M. A., Lloyd, K. G., Sørensen, K. B., Anderson, R., et al. (2006). Heterotrophic Archaea dominate sedimentary subsurface ecosystems off Peru. *PNAS* 103, 3846–3851. doi:10.1073/pnas.0600035103.

Biddle, J. F., White, J. R., Teske, A. P., and House, C. H. (2011). Metagenomics of the subsurface Brazos-Trinity Basin (IODP site 1320): comparison with other sediment and pyrosequenced metagenomes. *ISME J* 5, 1038–1047. doi:10.1038/ismej.2010.199.

Bier, R. L., Bernhardt, E. S., Boot, C. M., Graham, E. B., Hall, E. K., Lennon, J. T., et al. (2015). Linking microbial community structure and microbial processes: an empirical and conceptual overview. *FEMS Microbiol Ecol* 91. doi:10.1093/femsec/fiv113.

Boden, R., Cunliffe, M., Scanlan, J., Moussard, H., Kits, K. D., Klotz, M. G., et al. (2011). Complete Genome Sequence of the Aerobic Marine Methanotroph Methylomonas methanica MC09. *Journal of Bacteriology* 193, 7001–7002. doi:10.1128/JB.06267-11.

Boetius, A., Ravenschlag, K., Schubert, C. J., Rickert, D., Widdel, F., Gieseke, A., et al. (2000). A marine microbial consortium apparently mediating anaerobic oxidation of methane. *Nature* 407, 623–626. doi:10.1038/35036572.

Boetius, A., and Suess, E. (2004). Hydrate Ridge: a natural laboratory for the study of microbial life fueled by methane from near-surface gas hydrates. *Chemical Geology* 205, 291–310. doi:10.1016/j.chemgeo.2003.12.034.

Boetius, A., and Wenzhöfer, F. (2013). Seafloor oxygen consumption fuelled by methane from cold seeps. *Nature Geoscience* 6, 725–734. doi:10.1038/ngeo1926.

Borowski, W. S., Paull, C. K., and Ussler, W. (1996). Marine pore-water sulfate profiles indicate in situ methane flux from underlying gas hydrate. *Geology* 24, 655–658. doi:10.1130/0091-7613(1996)024<0655:MPWSPI>2.3.CO;2.

Borowski, W. S., Paull, C. K., and Ussler, W. (1997). Carbon cycling within the upper methanogenic zone of continental rise sediments; An example from the methane-rich sediments overlying the Blake Ridge gas hydrate deposits. *Marine Chemistry* 57, 299–311. doi:10.1016/S0304-4203(97)00019-4.

Bottomley, D. J., and Clark, I. D. (2004). Potassium and boron co-depletion in Canadian Shield brines: evidence for diagenetic interactions between marine brines and basin sediments. *Chemical Geology* 203, 225–236. doi:10.1016/j.chemgeo.2003.10.010.

Boucher, O., Friedlingstein, P., Collins, B., and Shine, K. P. (2009). The indirect global warming potential and global temperature change potential due to methane oxidation. *Environmental Research Letters* 4, 044007. doi:10.1088/1748-9326/4/4/044007.

Bowles, M. W., Samarkin, V. A., and Joye, S. B. (2011). Improved measurement of microbial activity in deep-sea sediments at in situ pressure and methane concentration: Measuring activity in deep-sea sediments. *Limnology and Oceanography: Methods* 9, 499–506. doi:10.4319/lom.2011.9.499.

Boyd, J. A., Jungbluth, S. P., Leu, A. O., Evans, P. N., Woodcroft, B. J., Chadwick, G. L., et al. (2019). Divergent methyl-coenzyme M reductase genes in a deep-subseafloor Archaeoglobi. *The ISME Journal*, 1. doi:10.1038/s41396-018-0343-2.

Bradley, J. A., Amend, J. P., and LaRowe, D. E. (2019). Survival of the fewest: Microbial dormancy and maintenance in marine sediments through deep time. *Geobiology* 17, 43–59. doi:10.1111/gbi.12313.

Brazelton, W. J., and Baross, J. A. (2009). Abundant transposases encoded by the metagenome of a hydrothermal chimney biofilm. *ISME J* 3, 1420–1424. doi:10.1038/ismej.2009.79.

Brazelton, W. J., Schrenk, M. O., Kelley, D. S., and Baross, J. A. (2006). Methane- and Sulfur-Metabolizing Microbial Communities Dominate the Lost City Hydrothermal Field Ecosystem. *Appl. Environ. Microbiol.* 72, 6257–6270. doi:10.1128/AEM.00574-06.

Briggs, B. R., Pohlman, J. W., Torres, M., Riedel, M., Brodie, E. L., and Colwell, F. S. (2011). Macroscopic Biofilms in Fracture-Dominated Sediment That Anaerobically Oxidize Methane. *Applied and Environmental Microbiology* 77, 6780–6787. doi:10.1128/AEM.00288-11.

Burdige, D. J. (2006). *Geochemistry Of Marine Sediments*. Princeton University Press Available at: http://bookendin.info/david-jay-burdige-geochemistry-of-marine-sediments-pdf-books-files-freely.pdf [Accessed February 5, 2019].

Caldwell, S. L., Laidler, J. R., Brewer, E. A., Eberly, J. O., Sandborgh, S. C., and Colwell, F. S. (2008). Anaerobic Oxidation of Methane: Mechanisms, Bioenergetics, and the Ecology of Associated Microorganisms. *Environ. Sci. Technol.* 42, 6791–6799. doi:10.1021/es800120b.

Caporaso, J. G., Lauber, C. L., Walters, W. A., Berg-Lyons, D., Lozupone, C. A., Turnbaugh, P. J., et al. (2011). Global patterns of 16S rRNA diversity at a depth of millions of sequences per sample. *Proceedings of the National Academy of Sciences* 108, 4516–4522. doi:10.1073/pnas.1000080107.

Carr, S. A., Orcutt, B. N., Mandernack, K. W., and Spear, J. R. (2015). Abundant Atribacteria in deep marine sediment from the Adélie Basin, Antarctica. *Front Microbiol* 6, 872. doi:10.3389/fmicb.2015.00872.

Case, D. H., Ijiri, A., Morono, Y., Tavormina, P., Orphan, V. J., and Inagaki, F. (2017). Aerobic and Anaerobic Methanotrophic Communities Associated with Methane Hydrates Exposed on the Seafloor: A High-Pressure Sampling and Stable Isotope-Incubation Experiment. *Front. Microbiol.* 8. doi:10.3389/fmicb.2017.02569.

Castelle, C. J., Wrighton, K. C., Thomas, B. C., Hug, L. A., Brown, C. T., Wilkins, M. J., et al. (2015). Genomic Expansion of Domain Archaea Highlights Roles for Organisms from New Phyla in Anaerobic Carbon Cycling. *Current Biology* 25, 690–701. doi:10.1016/j.cub.2015.01.014.

Ceramicola, S., Praeg, D., Cova, A., Accettella, D., and Zecchin, M. (2014). Seafloor distribution and last glacial to postglacial activity of mud volcanoes on the Calabrian accretionary prism, Ionian Sea. *Geo-Mar Lett* 34, 111–129. doi:10.1007/s00367-013-0354-y.

Chen, Y., Li, Y.-L., Zhou, G.-T., Li, H., Lin, Y.-T., Xiao, X., et al. (2014). Biomineralization mediated by anaerobic methane-consuming cell consortia. *Sci. Rep.* 4. doi:10.1038/srep05696.

Cheng, T.-W., Chang, Y.-H., Tang, S.-L., Tseng, C.-H., Chiang, P.-W., Chang, K.-T., et al. (2012). Metabolic stratification driven by surface and subsurface interactions in a terrestrial mud volcano. *The ISME Journal* 6, 2280–2290. doi:10.1038/ismej.2012.61.

Clarke, K. R. (1993). Non-parametric multivariate analyses of changes in community structure. *Australian Journal of Ecology* 18, 117–143. doi:10.1111/j.1442-9993.1993.tb00438.x.

Clarke, K. R., and Warwick, R. M. (2001). Change in marine communities: an approach to statistical analysis and interpretation, 2nd edition.

Claypool, G. E., and Kaplan, I. R. (1974). "The Origin and Distribution of Methane in Marine Sediments," in *Natural Gases in Marine Sediments*, ed. I. R. Kaplan (Boston, MA: Springer US), 99–139. doi:10.1007/978-1-4684-2757-8_8.

Cline, J. D. (1969). Spectrophotometric Determination of Hydrogen Sulfide in Natural Waters1. *Limnology and Oceanography* 14, 454–458. doi:10.4319/lo.1969.14.3.0454.

Coelho, F. J. R. C., Louvado, A., Domingues, P. M., Cleary, D. F. R., Ferreira, M., Almeida, A., et al. (2016). Integrated analysis of bacterial and microeukaryotic communities from differentially active mud volcanoes in the Gulf of Cadiz. *Sci Rep* 6. doi:10.1038/srep35272.

Colwell, F. S., and D'Hondt, S. (2013). Nature and Extent of the Deep Biosphere. *Reviews in Mineralogy and Geochemistry* 75, 547–574. doi:10.2138/rmg.2013.75.17.

Conrad, R. (1999). Contribution of hydrogen to methane production and control of hydrogen concentrations in methanogenic soils and sediments. *FEMS Microbiol Ecol* 28, 193–202. doi:10.1111/j.1574-6941.1999.tb00575.x.

Cordes, E. E., Cunha, M. R., Galéron, J., Mora, C., Roy, K. O.-L., Sibuet, M., et al. (2010). The influence of geological, geochemical, and biogenic habitat heterogeneity on seep biodiversity. *Marine Ecology* 31, 51–65. doi:10.1111/j.1439-0485.2009.00334.x.

Corinaldesi, C., Dell'Anno, A., and Danovaro, R. (2012). Viral infections stimulate the metabolism and shape prokaryotic assemblages in submarine mud volcanoes. *ISME J* 6, 1250–1259. doi:10.1038/ismej.2011.185.

Crump, B. C., Peranteau, C., Beckingham, B., and Cornwell, J. C. (2007). Respiratory Succession and Community Succession of Bacterioplankton in Seasonally Anoxic Estuarine Waters. *Appl. Environ. Microbiol.* 73, 6802–6810. doi:10.1128/AEM.00648-07.

Culberson, C. H., and Pytkowicz, R. M. (1973). Ionization of water in seawater. *Marine Chemistry* 1, 309–316. doi:10.1016/0304-4203(73)90020-0.

Dale, A. W., Regnier, P., and Cappellen, P. V. (2006). Bioenergetic Controls on Anaerobic Oxidation of Methane (AOM) in Coastal Marine Sediments: A Theoretical Analysis. *Am J Sci* 306, 246–294. doi:10.2475/ajs.306.4.246.

Dale, A. W., Van Cappellen, P., Aguilera, D. R., and Regnier, P. (2008). Methane efflux from marine sediments in passive and active margins: Estimations from bioenergetic reaction–transport simulations. *Earth and Planetary Science Letters* 265, 329–344. doi:10.1016/j.epsl.2007.09.026.

Dalsgaard, T., Thamdrup, B., and Canfield, D. E. (2005). Anaerobic ammonium oxidation (anammox) in the marine environment. *Research in Microbiology* 156, 457–464. doi:10.1016/j.resmic.2005.01.011.

Danczak, R. E., Yabusaki, S. B., Williams, K. H., Fang, Y., Hobson, C., and Wilkins, M. J. (2016). Snowmelt Induced Hydrologic Perturbations Drive Dynamic Microbiological and Geochemical Behaviors across a Shallow Riparian Aquifer. *Front. Earth Sci.* 4. doi:10.3389/feart.2016.00057.

Dedysh, S. N., and Knief, C. (2018). "Diversity and Phylogeny of Described Aerobic Methanotrophs," in *Methane Biocatalysis: Paving the Way to Sustainability*, eds. M. G. Kalyuzhnaya and X.-H. Xing (Cham: Springer International Publishing), 17–42. doi:10.1007/978-3-319-74866-5_2.

Dell'Anno, A., Stefano, B., and Danovaro, R. (2002). Quantification, base composition, and fate of extracellular DNA in marine sediments. *Limnology and Oceanography* 47, 899–905. doi:10.4319/lo.2002.47.3.0899.

Deming, J. W., and Baross, J. A. (1993). Deep-sea smokers: Windows to a subsurface biosphere? *Geochimica et Cosmochimica Acta* 57, 3219–3230.

Deusner, C., Meyer, V., and Ferdelman, T. G. (2010). High-pressure systems for gas-phase free continuous incubation of enriched marine microbial communities performing anaerobic oxidation of methane. *Biotechnol. Bioeng.* 105, 524–533. doi:10.1002/bit.22553.

D'Hondt, S., Jørgensen, B. B., and Miller, D. J. (2003). Ocean Drilling Program Leg 201 Initial Reports: 1. Leg 201 Summary. Available at: http://www-odp.tamu.edu/publications/201_IR/chap_01/chap_01.htm [Accessed February 5, 2019].

D'Hondt, S., Jørgensen, B. B., Miller, D. J., Batzke, A., Blake, R., Cragg, B. A., et al. (2004). Distributions of Microbial Activities in Deep Subseafloor Sediments. *Science* 306, 2216–2221. doi:10.1126/science.1101155.

Dick, G. J., and Tebo, B. M. (2010). Microbial diversity and biogeochemistry of the Guaymas Basin deep-sea hydrothermal plume. *Environmental Microbiology* 12, 1334–1347. doi:10.1111/j.1462-2920.2010.02177.x.

Du, Z.-J., Wang, Y., Dunlap, C., Rooney, A. P., and Chen, G.-J. (2014). Draconibacterium orientale gen. nov., sp. nov., isolated from two distinct marine environments, and proposal of Draconibacteriaceae fam. nov. *INTERNATIONAL JOURNAL OF SYSTEMATIC AND EVOLUTIONARY MICROBIOLOGY* 64, 1690–1696. doi:10.1099/ijs.0.056812-0.

Eggleston, H. S., Buendia, L., Miwa, K., Ngara, T., and Tanabe, K. (2006). IPCC Guidelines for National Greenhouse Gas Inventories.

Emerson, J. B., Roux, S., Brum, J. R., Bolduc, B., Woodcroft, B. J., Jang, H. B., et al. (2018). Host-linked soil viral ecology along a permafrost thaw gradient. *Nature Microbiology* 3, 870. doi:10.1038/s41564-018-0190-y.

Engelhardt, T., Kallmeyer, J., Cypionka, H., and Engelen, B. (2014). High virus-to-cell ratios indicate ongoing production of viruses in deep subsurface sediments. *The ISME Journal* 8, 1503–1509. doi:10.1038/ismej.2013.245.

Environmental Monitoring Systems Laboratory (1996). DETERMINATION OF METALS AND TRACE ELEMENTS IN WATER AND WASTES BY INDUCTIVELY COUPLED PLASMA-ATOMIC EMISSION SPECTROMETRY. Elsevier doi:10.1016/B978-0-8155-1398-8.50010-0.

Esser, D. S., Leveau, J. H. J., and Meyer, K. M. (2015). Modeling microbial growth and dynamics. *Appl Microbiol Biotechnol* 99, 8831–8846. doi:10.1007/s00253-015-6877-6.

Etiope, G., Lassey, K. R., Klusman, R. W., and Boschi, E. (2008). Reappraisal of the fossil methane budget and related emission from geologic sources. *Geophys. Res. Lett.* 35, L09307. doi:10.1029/2008GL033623.

Etiope, G., and Milkov, A. V. (2004). A new estimate of global methane flux from onshore and shallow submarine mud volcanoes to the atmosphere. *Env Geol* 46, 997–1002. doi:10.1007/s00254-004-1085-1.

Ettwig, K. F., Butler, M. K., Le Paslier, D., Pelletier, E., Mangenot, S., Kuypers, M. M. M., et al. (2010). Nitrite-driven anaerobic methane oxidation by oxygenic bacteria. *Nature* 464, 543–548. doi:10.1038/nature08883.

Ettwig, K. F., Zhu, B., Speth, D., Keltjens, J. T., Jetten, M. S. M., and Kartal, B. (2016). Archaea catalyze iron-dependent anaerobic oxidation of methane. *PNAS* 113, 12792–12796. doi:10.1073/pnas.1609534113.

Evans, J., Sheneman, L., and Foster, J. (2006). Relaxed Neighbor Joining: A Fast Distance-Based Phylogenetic Tree Construction Method. *J Mol Evol* 62, 785–792. doi:10.1007/s00239-005-0176-2.

Evans, P. N., Parks, D. H., Chadwick, G. L., Robbins, S. J., Orphan, V. J., Golding, S. D., et al. (2015). Methane metabolism in the archaeal phylum Bathyarchaeota revealed by genome-centric metagenomics. *Science* 350, 434–438. doi:10.1126/science.aac7745.

Excoffier, L., Smouse, P. E., and Quattro, J. M. (1992). Analysis of molecular variance inferred from metric distances among DNA haplotypes: application to human mitochondrial DNA restriction data. *Genetics* 131, 479–491.

Ferrucci, F., Gaudiosi, G., Hirn, A., and Nicolich, R. (1991). Ionian Basin and Calabria Arc: Some new elements from DSS data. *Tectonophysics* 195, 411–419. doi:10.1016/0040-1951(91)90223-F.

Franzosa, E. A., McIver, L. J., Rahnavard, G., Thompson, L. R., Schirmer, M., Weingart, G., et al. (2018). Species-level functional profiling of metagenomes and metatranscriptomes. *Nature Methods* 15, 962. doi:10.1038/s41592-018-0176-y.

Fredrickson, J. K., McKinley, J. P., Bjornstad, B. N., Long, P. E., Ringelberg, D. B., White, D. C., et al. (1997). Pore-size constraints on the activity and survival of subsurface bacteria in a late cretaceous shale-sandstone sequence, northwestern New Mexico. *Geomicrobiology Journal* 14, 183–202. doi:10.1080/01490459709378043.

Freitag, T. E., and Prosser, J. I. (2009). Correlation of Methane Production and Functional Gene Transcriptional Activity in a Peat Soil. *Appl. Environ. Microbiol.* 75, 6679–6687. doi:10.1128/AEM.01021-09.

Freitag, T. E., Toet, S., Ineson, P., and Prosser, J. I. (2010). Links between methane flux and transcriptional activities of methanogens and methane oxidizers in a blanket peat bog: Methane flux and transcriptional activities in a peat bog. *FEMS Microbiology Ecology*, no-no. doi:10.1111/j.1574-6941.2010.00871.x.

Fries, M. R., Hopkins, G. D., McCarty, P. L., Forney, L. J., and Tiedje, J. M. (1997). Microbial Succession during a Field Evaluation of Phenol and Toluene as the Primary Substrates for Trichloroethene Cometabolism. *Appl. Environ. Microbiol.* 63, 1515–1522.

Fritze, D. (2004). Taxonomy of the Genus Bacillus and Related Genera: The Aerobic Endospore-Forming Bacteria. *Phytopathology* 94, 1245–1248. doi:10.1094/PHYTO.2004.94.11.1245.

Froelich, P. N., Klinkhammer, G. P., Bender, M. L., Luedtke, N. A., Heath, G. R., Cullen, D., et al. (1979). Early oxidation of organic matter in pelagic sediments of the eastern equatorial Atlantic: suboxic diagenesis. *Geochimica et Cosmochimica Acta* 43, 1075–1090. doi:10.1016/0016-7037(79)90095-4.

Fuchs, A., Lyautey, E., Montuelle, B., and Casper, P. (2016). Effects of increasing temperatures on methane concentrations and methanogenesis during experimental incubation of sediments from oligotrophic and mesotrophic lakes. *J. Geophys. Res. Biogeosci.* 121, 2016JG003328. doi:10.1002/2016JG003328.

Galperin, M. Y., Makarova, K. S., Wolf, Y. I., and Koonin, E. V. (2015). Expanded microbial genome coverage and improved protein family annotation in the COG database. *Nucleic Acids Res* 43, D261–D269. doi:10.1093/nar/gku1223.

Girguis, P. R., Cozen, A. E., and DeLong, E. F. (2005). Growth and Population Dynamics of Anaerobic Methane-Oxidizing Archaea and Sulfate-Reducing Bacteria in a Continuous-Flow Bioreactor. *Appl. Environ. Microbiol.* 71, 3725–3733. doi:10.1128/AEM.71.7.3725-3733.2005.

Girguis, P. R., Orphan, V. J., Hallam, S. J., and DeLong, E. F. (2003). Growth and Methane Oxidation Rates of Anaerobic Methanotrophic Archaea in a Continuous-Flow Bioreactor. *Appl. Environ. Microbiol.* 69, 5472–5482. doi:10.1128/AEM.69.9.5472-5482.2003.

Graham, E. B., Knelman, J. E., Schindlbacher, A., Siciliano, S., Breulmann, M., Yannarell, A., et al. (2016). Microbes as Engines of Ecosystem Function: When Does Community Structure Enhance Predictions of Ecosystem Processes? *Front. Microbiol.* 7. doi:10.3389/fmicb.2016.00214.

Graw, M. F., D'Angelo, G., Borchers, M., Thurber, A. R., Johnson, J. E., Zhang, C., et al. (2018). Energy Gradients Structure Microbial Communities Across Sediment Horizons in Deep Marine Sediments of the South China Sea. *Front. Microbiol.* 9. doi:10.3389/fmicb.2018.00729.

Haeckel, M., Suess, E., Wallmann, K., and Rickert, D. (2004). Rising methane gas bubbles form massive hydrate layers at the seafloor. *Geochimica et Cosmochimica Acta* 68, 4335–4345. doi:10.1016/j.gca.2004.01.018.

Hallam, S. J., Girguis, P. R., Preston, C. M., Richardson, P. M., and DeLong, E. F. (2003). Identification of Methyl Coenzyme M Reductase A (mcrA) Genes Associated with Methane-Oxidizing Archaea. *Appl. Environ. Microbiol.* 69, 5483–5491. doi:10.1128/AEM.69.9.5483-5491.2003.

Hallam, S. J., Putnam, N., Preston, C. M., Detter, J. C., Rokhsar, D., Richardson, P. M., et al. (2004). Reverse Methanogenesis: Testing the Hypothesis with Environmental Genomics. *Science* 305, 1457–1462. doi:10.1126/science.1100025.

Hammes, F., Vital, M., and Egli, T. (2010). Critical Evaluation of the Volumetric "Bottle Effect" on Microbial Batch Growth. *Appl. Environ. Microbiol.* 76, 1278–1281. doi:10.1128/AEM.01914-09.

Hanson, R. S., and Hanson, T. E. (1996). Methanotrophic Bacteria. *Microbiological Reviews* 60, 439–471.

Haroon, M. F., Hu, S., Shi, Y., Imelfort, M., Keller, J., Hugenholtz, P., et al. (2013). Anaerobic oxidation of methane coupled to nitrate reduction in a novel archaeal lineage. *Nature* 500, 567–570. doi:10.1038/nature12375.

Harrison, B. K., Zhang, H., Berelson, W., and Orphan, V. J. (2009). Variations in Archaeal and Bacterial Diversity Associated with the Sulfate-Methane Transition Zone in Continental Margin Sediments (Santa Barbara Basin, California). *Applied and Environmental Microbiology* 75, 1487–1499. doi:10.1128/AEM.01812-08.

Haug, T., Bogstad, B., Chierici, M., Gjøsæter, H., Hallfredsson, E. H., Høines, Å. S., et al. (2017). Future harvest of living resources in the Arctic Ocean north of the Nordic and Barents Seas: A review of possibilities and constraints. *Fisheries Research* 188, 38–57. doi:10.1016/j.fishres.2016.12.002.

Hedrich, S., Schlömann, M., and Johnson, D. B. (2011). The iron-oxidizing proteobacteria. *Microbiology* 157, 1551–1564. doi:10.1099/mic.0.045344-0.

Heitmann, T., and Blodau, C. (2006). Oxidation and incorporation of hydrogen sulfide by dissolved organic matter. *Chemical Geology* 235, 12–20. doi:10.1016/j.chemgeo.2006.05.011.

Henrichs, S. M., and Reeburgh, W. S. (1987). Anaerobic mineralization of marine sediment organic matter: Rates and the role of anaerobic processes in the oceanic carbon economy. *Geomicrobiology Journal* 5, 191–237. doi:10.1080/01490458709385971.

Hensen, C., Zabel, M., Pfeifer, K., Schwenk, T., Kasten, S., Riedinger, N., et al. (2003). Control of sulfate pore-water profiles by sedimentary events and the significance of anaerobic oxidation of methane for the burial of sulfur in marine sediments. *Geochimica et Cosmochimica Acta* 67, 2631–2647. doi:10.1016/S0016-7037(03)00199-6.

Heuer, V. B., Inagaki, F., Morono, Y., Kubo, Y., Maeda, L., Bowden, S., et al. (2017). Expedition 370 summary. 370, 20.

Hinrichs, K.-U., and Boetius, A. (2003). "The Anaerobic Oxidation of Methane: New Insights in Microbial Ecology and Biogeochemistry," in *Ocean Margin Systems*, eds. P. D. G. Wefer, D. D. Billett, D. D. Hebbeln, P. D. B. B. Jørgensen, P. D. M. Schlüter, and D. T. C. E. van Weering (Springer Berlin Heidelberg), 457–477. Available at: http://link.springer.com/chapter/10.1007/978-3-662-05127-6_28 [Accessed July 7, 2014].

Hinrichs, K.-U., Hayes, J. M., Sylva, S. P., Brewer, P. G., and DeLong, E. F. (1999). Methane-consuming archaebacteria in marine sediments. *Nature* 398, 802–805. doi:10.1038/19751.

Hiraishi, A. (2008). Biodiversity of Dehalorespiring Bacteria with Special Emphasis on Polychlorinated Biphenyl/Dioxin Dechlorinators. *Microbes Environ.* 23, 1–12. doi:10.1264/jsme2.23.1.

Hoehler, T. M., Alperin, M. J., Albert, D. B., and Martens, C. S. (1994). Field and laboratory studies of methane oxidation in an anoxic marine sediment: Evidence for a methanogen-sulfate reducer consortium. *Global Biogeochem. Cycles* 8, 451–463. doi:10.1029/94GB01800.

Hoehler, T. M., and Jørgensen, B. B. (2013). Microbial life under extreme energy limitation. *Nat Rev Micro* 11, 83–94. doi:10.1038/nrmicro2939.

Holmes, D. E., Nicoll, J. S., Bond, D. R., and Lovley, D. R. (2004). Potential Role of a Novel Psychrotolerant Member of the Family Geobacteraceae, Geopsychrobacter electrodiphilus gen. nov., sp. nov., in Electricity Production by a Marine Sediment Fuel Cell. *Appl. Environ. Microbiol.* 70, 6023–6030. doi:10.1128/AEM.70.10.6023-6030.2004.

Hong, W.-L., Sauer, S., Panieri, G., Ambrose, W. G., James, R. H., Plaza-Faverola, A., et al. (2016). Removal of methane through hydrological, microbial, and geochemical processes in the shallow sediments of pockmarks along eastern Vestnesa Ridge (Svalbard). *Limnol. Oceanogr.*, n/a-n/a. doi:10.1002/lno.10299.

Hong, W.-L., Torres, M. E., Carroll, J., Crémière, A., Panieri, G., Yao, H., et al. (2017). Seepage from an arctic shallow marine gas hydrate reservoir is insensitive to momentary ocean warming. *Nat Commun* 8, 15745. doi:10.1038/ncomms15745.

Hong, W.-L., Torres, M. E., Portnov, A., Waage, M., Haley, B., and Lepland, A. (2018). Variations in Gas and Water Pulses at an Arctic Seep: Fluid Sources and Methane Transport. *Geophysical Research Letters* 45, 4153–4162. doi:10.1029/2018GL077309.

Horsfield, B., Schenk, H. J., Zink, K., Ondrak, R., Dieckmann, V., Kallmeyer, J., et al. (2006). Living microbial ecosystems within the active zone of catagenesis: Implications for feeding the deep biosphere. *Earth and Planetary Science Letters* 246, 55–69. doi:10.1016/j.epsl.2006.03.040.

Hoshino, T., Toki, T., Ijiri, A., Morono, Y., Machiyama, H., Ashi, J., et al. (2017). Atribacteria from the Subseafloor Sedimentary Biosphere Disperse to the Hydrosphere through Submarine Mud Volcanoes. *Front. Microbiol.* 8. doi:10.3389/fmicb.2017.01135.

Hu, B. -l., Shen, L. -d., Lian, X., Zhu, Q., Liu, S., Huang, Q., et al. (2014). Evidence for nitrite-dependent anaerobic methane oxidation as a previously overlooked microbial methane sink in wetlands. *Proceedings of the National Academy of Sciences* 111, 4495–4500. doi:10.1073/pnas.1318393111.

Hug, L. A., Baker, B. J., Anantharaman, K., Brown, C. T., Probst, A. J., Castelle, C. J., et al. (2016). A new view of the tree of life. *Nature Microbiology*, 16048. doi:10.1038/nmicrobiol.2016.48.

Ijiri, A., Inagaki, F., Kubo, Y., Adhikari, R. R., Hattori, S., Hoshino, T., et al. (2018). Deep-biosphere methane production stimulated by geofluids in the Nankai accretionary complex. *Science Advances* 4, eaao4631. doi:10.1126/sciadv.aao4631.

Inagaki, F. (2004). Sulfurovum lithotrophicum gen. nov., sp. nov., a novel sulfur-oxidizing chemolithoautotroph within the -Proteobacteria isolated from Okinawa Trough hydrothermal sediments. *INTERNATIONAL JOURNAL OF SYSTEMATIC AND EVOLUTIONARY MICROBIOLOGY* 54, 1477–1482. doi:10.1099/ijs.0.03042-0.

Isaksen, M. F., and Teske, A. (1996). Desulforhopalus vacuolatus gen. nov., sp. nov., a new moderately psychrophilic sulfate-reducing bacterium with gas vacuoles isolated from a temperate estuary. *Arch Microbiol* 166, 160–168. doi:10.1007/s002030050371.

Joye, S. B., Boetius, A., Orcutt, B. N., Montoya, J. P., Schulz, H. N., Erickson, M. J., et al. (2004). The anaerobic oxidation of methane and sulfate reduction in sediments from Gulf of Mexico cold seeps. *Chemical Geology* 205, 219–238. doi:10.1016/j.chemgeo.2003.12.019.

Kallmeyer, J., Pockalny, R., Adhikari, R. R., Smith, D. C., and D'Hondt, S. (2012). Global distribution of microbial abundance and biomass in subseafloor sediment. *PNAS* 109, 16213–16216. doi:10.1073/pnas.1203849109.

Kastner, M., Solomon, E. A., Harris, R. N., and Torres, M. E. (2014). *Developments in Marine Geology*. Elsevier.

Kawagucci, S., Miyazaki, J., Morono, Y., Seewald, J. S., Wheat, C. G., and Takai, K. (2018). Cool, alkaline serpentinite formation fluid regime with scarce microbial habitability and possible abiotic synthesis beneath the South Chamorro Seamount. *Progress in Earth and Planetary Science* 5, 74. doi:10.1186/s40645-018-0232-3.

Kawai, M., Futagami, T., Toyoda, A., Takaki, Y., Nishi, S., Hori, S., et al. (2014). High frequency of phylogenetically diverse reductive dehalogenase-homologous genes in deep subseafloor sedimentary metagenomes. *Front Microbiol* 5. doi:10.3389/fmicb.2014.00080.

Keegan, K. P., Glass, E. M., and Meyer, F. (2016). "MG-RAST, a Metagenomics Service for Analysis of Microbial Community Structure and Function," in *Microbial Environmental Genomics (MEG)* Methods in Molecular Biology., eds. F. Martin and S. Uroz (New York, NY: Springer New York), 207–233. doi:10.1007/978-1-4939-3369-3_13.

Kellermann, M. Y., Wegener, G., Elvert, M., Yoshinaga, M. Y., Lin, Y.-S., Holler, T., et al. (2012). Autotrophy as a predominant mode of carbon fixation in anaerobic methane-oxidizing microbial communities. *PNAS* 109, 19321–19326. doi:10.1073/pnas.1208795109.

Kessler, J. D., Valentine, D. L., Redmond, M. C., Du, M., Chan, E. W., Mendes, S. D., et al. (2011). A Persistent Oxygen Anomaly Reveals the Fate of Spilled Methane in the Deep Gulf of Mexico. *Science*, 1199697. doi:10.1126/science.1199697.

Kim, J.-H., Torres, M. E., Haley, B. A., Ryu, J.-S., Park, M.-H., Hong, W.-L., et al. (2016). Marine silicate weathering in the anoxic sediment of the Ulleung Basin: Evidence and consequences. *Geochemistry, Geophysics, Geosystems* 17, 3437–3453. doi:10.1002/2016GC006356.

Kleindienst, S., Ramette, A., Amann, R., and Knittel, K. (2012). Distribution and in situ abundance of sulfate-reducing bacteria in diverse marine hydrocarbon seep sediments. *Environmental Microbiology* 14, 2689–2710. doi:10.1111/j.1462-2920.2012.02832.x.

Knab, N. J., Cragg, B. A., Hornibrook, E. R. C., Holmkvist, L., Borowski, C., Parkes, R. J., et al. (2008). Regulation of anaerobic methane oxidation in sediments of the Black Sea. *Biogeosciences Discussions* 5, 2305–2341.

Knittel, K., and Boetius, A. (2009). Anaerobic Oxidation of Methane: Progress with an Unknown Process. *Annual Review of Microbiology* 63, 311–334. doi:10.1146/annurev.micro.61.080706.093130.

Knittel, K., Boetius, A., Lemke, A., Eilers, H., Lochte, K., Pfannkuche, O., et al. (2003). Activity, Distribution, and Diversity of Sulfate Reducers and Other Bacteria in Sediments above Gas Hydrate (Cascadia Margin, Oregon). *Geomicrobiology Journal* 20, 269–294. doi:10.1080/01490450303896.

Knittel, K., Lösekann, T., Boetius, A., Kort, R., and Amann, R. (2005). Diversity and Distribution of Methanotrophic Archaea at Cold Seeps. *Appl. Environ. Microbiol.* 71, 467–479. doi:10.1128/AEM.71.1.467-479.2005.

Kondo, R., Nedwell, D. B., Purdy, K. J., and Silva, S. Q. (2004). Detection and Enumeration of Sulphate-Reducing Bacteria in Estuarine Sediments by Competitive PCR. *Geomicrobiology Journal* 21, 145–157. doi:10.1080/01490450490275307.

Konstantinidis, K. T., and Tiedje, J. M. (2004). Trends between gene content and genome size in prokaryotic species with larger genomes. *PNAS* 101, 3160–3165. doi:10.1073/pnas.0308653100.

Kopf, A., and Deyhle, A. (2002). Back to the roots: boron geochemistry of mud volcanoes and its implications for mobilization depth and global B cycling. *Chemical Geology* 192, 195–210. doi:10.1016/S0009-2541(02)00221-8.

Kopf, A. J. (2002). Significance of Mud Volcanism. *Rev. Geophys.* 40, 1005. doi:10.1029/2000RG000093.

Kopf, A. J. (2003). Global methane emission through mud volcanoes and its past and present impact on the Earth's climate. *Int J Earth Sci (Geol Rundsch)* 92, 806–816. doi:10.1007/s00531-003-0341-z.

Kozich, J. J., Westcott, S. L., Baxter, N. T., Highlander, S. K., and Schloss, P. D. (2013). Development of a Dual-Index Sequencing Strategy and Curation Pipeline for Analyzing Amplicon Sequence Data on the MiSeq Illumina Sequencing Platform. *Appl Environ Microbiol* 79, 5112–5120. doi:10.1128/AEM.01043-13.

Krauze, P., Kämpf, H., Horn, F., Liu, Q., Voropaev, A., Wagner, D., et al. (2017). Microbiological and Geochemical Survey of CO2-Dominated Mofette and Mineral Waters of the Cheb Basin, Czech Republic. *Front. Microbiol.* 8. doi:10.3389/fmicb.2017.02446.

Krüger, M., Wolters, H., Gehre, M., Joye, S. B., and Richnow, H.-H. (2008). Tracing the slow growth of anaerobic methane-oxidizing communities by 15N-labelling techniques. *FEMS Microbiology Ecology* 63, 401–411. doi:10.1111/j.1574-6941.2007.00431.x.

Krukenberg, V., Riedel, D., Gruber-Vodicka, H. R., Buttigieg, P. L., Tegetmeyer, H. E., Boetius, A., et al. Gene expression and ultrastructure of meso- and thermophilic methanotrophic consortia. *Environmental Microbiology*, n/a-n/a. doi:10.1111/1462-2920.14077.

Latour, P., Hong, W.-L., Sauer, S., Sen, A., Gilhooly III, W. P., Lepland, A., et al. (2018). Dynamic interactions between iron and sulfur cycles from Arctic methane seeps. *Biogeosciences Discussions*, 1–48. doi:10.5194/bg-2018-223.

Lazar, C. S., John Parkes, R., Cragg, B. A., L'Haridon, S., and Toffin, L. (2012). Methanogenic activity and diversity in the centre of the Amsterdam Mud Volcano, Eastern Mediterranean Sea. *FEMS Microbiol Ecol* 81, 243–254. doi:10.1111/j.1574-6941.2012.01375.x.

Lee, M. D., Walworth, N. G., Sylvan, J. B., Edwards, K. J., and Orcutt, B. N. (2015). Microbial Communities on Seafloor Basalts at Dorado Outcrop Reflect Level of Alteration and Highlight Global Lithic Clades. *Front Microbiol* 6. doi:10.3389/fmicb.2015.01470.

Leloup, J., Quillet, L., Oger, C., Boust, D., and Petit, F. (2004). Molecular quantification of sulfate-reducing microorganisms (carrying dsrAB genes) by competitive PCR in estuarine sediments. *FEMS Microbiol Ecol* 47, 207–214. doi:10.1016/S0168-6496(03)00262-9.

Leonte, M., Kessler, J. D., Kellermann, M. Y., Arrington, E. C., Valentine, D. L., and Sylva, S. P. (2017). Rapid rates of aerobic methane oxidation at the feather edge of gas hydrate stability in the waters of Hudson Canyon, US Atlantic Margin. *Geochimica et Cosmochimica Acta* 204, 375–387. doi:10.1016/j.gca.2017.01.009.

Lever, M. A., Torti, A., Eickenbusch, P., Michaud, A. B., Šantl-Temkiv, T., and Jørgensen, B. B. (2015). A modular method for the extraction of DNA and RNA, and the separation of

DNA pools from diverse environmental sample types. *Front Microbiol* 6. doi:10.3389/fmicb.2015.00476.

Li, D., Liu, C.-M., Luo, R., Sadakane, K., and Lam, T.-W. (2015). MEGAHIT: an ultra-fast single-node solution for large and complex metagenomics assembly via succinct de Bruijn graph. *Bioinformatics* 31, 1674–1676. doi:10.1093/bioinformatics/btv033.

Li, X., Song, L., Wang, G., Ren, L., Yu, D., Chen, G., et al. (2016). Complete genome sequence of a deeply branched marine Bacteroidia bacterium Draconibacterium orientale type strain FH5T. *Marine Genomics* 26, 13–16. doi:10.1016/j.margen.2016.01.002.

Lidstrom, M. E. (2006). "Aerobic Methylotrophic Prokaryotes," in *The Prokaryotes*, eds. M. Dworkin, S. Falkow, E. Rosenberg, K.-H. Schleifer, and E. Stackebrandt (New York, NY: Springer New York), 618–634. doi:10.1007/0-387-30742-7_20.

Lin, Y.-T., Tu, T.-H., Wei, C.-L., Rumble, D., Lin, L.-H., and Wang, P.-L. (2018). Steep redox gradient and biogeochemical cycling driven by deeply sourced fluids and gases in a terrestrial mud volcano. *FEMS Microbiol Ecol* 94. doi:10.1093/femsec/fiy171.

Lloyd, K. G., Alperin, M. J., and Teske, A. (2011). Environmental evidence for net methane production and oxidation in putative ANaerobic MEthanotrophic (ANME) archaea: Methanogenesis and methanotrophy in ANME-1 archaea. *Environmental Microbiology* 13, 2548–2564. doi:10.1111/j.1462-2920.2011.02526.x.

Loher, M., Ceramicola, S., Wintersteller, P., Meinecke, G., Sahling, H., and Bohrmann, G. (2018a). Mud Volcanism in a Canyon: Morpho-Dynamic Evolution of the Active Venere mud volcano and its Interplay With Squillace Canyon, Central Mediterranean. *Geochemistry, Geophysics, Geosystems*. doi:10.1002/2017GC007166.

Loher, M., Marcon, Y., Pape, T., Römer, M., Wintersteller, P., dos Santos Ferreira, C., et al. (2018b). Seafloor sealing, doming, and collapse associated with gas seeps and authigenic carbonate structures at Venere mud volcano, Central Mediterranean. *Deep Sea Research Part I: Oceanographic Research Papers* 137, 76–96. doi:10.1016/j.dsr.2018.04.006.

Loher, M., Pape, T., Marcon, Y., Römer, M., Wintersteller, P., Praeg, D., et al. (2018c). Mud extrusion and ring-fault gas seepage – upward branching fluid discharge at a deep-sea mud volcano. *Scientific Reports* 8, 6275. doi:10.1038/s41598-018-24689-1.

López-Rodríguez, C., De Lange, G. J., Comas, M., Martínez-Ruiz, F., Nieto, F., Sapart, C. J., et al. (2019). Recent, deep-sourced methane/mud discharge at the most active mud volcano in the western Mediterranean. *Marine Geology* 408, 1–17. doi:10.1016/j.margeo.2018.11.013.

Lozupone, C. A., Hamady, M., Kelley, S. T., and Knight, R. (2007). Quantitative and Qualitative β Diversity Measures Lead to Different Insights into Factors That Structure Microbial Communities. *Appl. Environ. Microbiol.* 73, 1576–1585. doi:10.1128/AEM.01996-06.

Luton, P. E., Wayne, J. M., Sharp, R. J., and Riley, P. W. (2002). The mcrA gene as an alternative to 16S rRNA in the phylogenetic analysis of methanogen populations in landfillb. *Microbiology* 148, 3521–3530. doi:10.1099/00221287-148-11-3521.

Maillacheruvu, K. Y., and Parkin, G. F. (1996). Kinetics of growth, substrate utilization and sulfide toxicity for propionate, acetate, and hydrogen utilizers in anaerobic systems. *Water Environment Research* 68, 1099–1106. doi:10.2175/106143096X128126.

Makarova, K. S., Wolf, Y. I., and Koonin, E. V. (2013). Comparative genomics of defense systems in archaea and bacteria. *Nucleic Acids Res* 41, 4360–4377. doi:10.1093/nar/gkt157.

Markowitz, V. M., Chen, I.-M. A., Chu, K., Szeto, E., Palaniappan, K., Pillay, M., et al. (2014). IMG/M 4 version of the integrated metagenome comparative analysis system. *Nucleic Acids Res* 42, D568–D573. doi:10.1093/nar/gkt919.

Martin, J. B., Kastner, M., Henry, P., Pichon, X. L., and Lallement, S. (1996). Chemical and isotopic evidence for sources of fluids in a mud volcano field seaward of the Barbados accretionary wedge. *Journal of Geophysical Research: Solid Earth* 101, 20325–20345. doi:10.1029/96JB00140.

Marzocchi, U., Trojan, D., Larsen, S., Meyer, R. L., Revsbech, N. P., Schramm, A., et al. (2014). Electric coupling between distant nitrate reduction and sulfide oxidation in marine sediment. *The ISME Journal* 8, 1682–1690. doi:10.1038/ismej.2014.19.

Mau, S., Römer, M., Torres, M. E., Bussmann, I., Pape, T., Damm, E., et al. (2017). Widespread methane seepage along the continental margin off Svalbard - from Bjørnøya to Kongsfjorden. *Sci Rep* 7. doi:10.1038/srep42997.

Mazzini, A., and Etiope, G. (2017). Mud volcanism: An updated review. *Earth-Science Reviews* 168, 81–112. doi:10.1016/j.earscirev.2017.03.001.

McGlynn, S. E., Chadwick, G. L., Kempes, C. P., and Orphan, V. J. (2015). Single cell activity reveals direct electron transfer in methanotrophic consortia. *Nature* 526, 531–535. doi:10.1038/nature15512.

Meulepas, R. J. W., Jagersma, C. G., Gieteling, J., Buisman, C. J. N., Stams, A. J. M., and Lens, P. N. L. (2009). Enrichment of anaerobic methanotrophs in sulfate-reducing membrane bioreactors. *Biotechnol. Bioeng.* 104, 458–470. doi:10.1002/bit.22412.

Meyerdierks, A., Kube, M., Kostadinov, I., Teeling, H., Glöckner, F. O., Reinhardt, R., et al. (2010). Metagenome and mRNA expression analyses of anaerobic methanotrophic

archaea of the ANME-1 group. *Environmental Microbiology* 12, 422–439. doi:10.1111/j.1462-2920.2009.02083.x.

Milkov, A. V. (2004). Global estimates of hydrate-bound gas in marine sediments: how much is really out there? *Earth-Science Reviews* 66, 183–197. doi:10.1016/j.earscirev.2003.11.002.

Milkov, A. V., Vogt, P. R., Crane, K., Lein, A. Y., Sassen, R., and Cherkashev, G. A. (2004). Geological, geochemical, and microbial processes at the hydrate-bearing Håkon Mosby mud volcano: a review. *Chemical Geology* 205, 347–366. doi:10.1016/j.chemgeo.2003.12.030.

Mills, H. J., Reese, B. K., and Peter, C. S. (2012). Characterization of Microbial Population Shifts during Sample Storage. *Frontiers in Microbiology* 3. doi:10.3389/fmicb.2012.00049.

Miroshnichenko, M. L., Tourova, T. P., Kolganova, T. V., Kostrikina, N. A., Chernych, N., and Bonch-Osmolovskaya, E. A. (2008). Ammonifex thiophilus sp. nov., a hyperthermophilic anaerobic bacterium from a Kamchatka hot spring. *International Journal of Systematic and Evolutionary Microbiology* 58, 2935–2938. doi:10.1099/ijs.0.2008/000182-0.

Mondav, R., Woodcroft, B. J., Kim, E.-H., McCalley, C. K., Hodgkins, S. B., Crill, P. M., et al. (2014). Discovery of a novel methanogen prevalent in thawing permafrost. *Nature Communications* 5, 3212. doi:10.1038/ncomms4212.

Müller, A. L., Kjeldsen, K. U., Rattei, T., Pester, M., and Loy, A. (2015). Phylogenetic and environmental diversity of DsrAB-type dissimilatory (bi)sulfite reductases. *ISME J* 9, 1152–1165. doi:10.1038/ismej.2014.208.

Myka, K. K., Allcock, D. J., Eloe-Fadrosh, E. A., Tryfona, T., Haag, A. F., Lauro, F. M., et al. (2017). "Adaptations of Cold- and Pressure-Loving Bacteria to the Deep-Sea Environment: Cell Envelope and Flagella," in *Microbial Ecology of Extreme Environments*, eds. C. Chénard and F. M. Lauro (Cham: Springer International Publishing), 51–80. doi:10.1007/978-3-319-51686-8_3.

Nauhaus, K., Albrecht, M., Elvert, M., Boetius, A., and Widdel, F. (2007). In vitro cell growth of marine archaeal-bacterial consortia during anaerobic oxidation of methane with sulfate. *Environmental Microbiology* 9, 187–196. doi:10.1111/j.1462-2920.2006.01127.x.

Nauhaus, K., Boetius, A., Krüger, M., and Widdel, F. (2002). In vitro demonstration of anaerobic oxidation of methane coupled to sulphate reduction in sediment from a marine gas hydrate area. *Environmental Microbiology* 4, 296–305. doi:10.1046/j.1462-2920.2002.00299.x.

Nauhaus, K., Treude, T., Boetius, A., and Kruger, M. (2005). Environmental regulation of the anaerobic oxidation of methane: a comparison of ANME-I and ANME-II communities. *Environmental Microbiology* 7, 98–106. doi:10.1111/j.1462-2920.2004.00669.x.

Nayfach, S., Bradley, P. H., Wyman, S. K., Laurent, T. J., Williams, A., Eisen, J. A., et al. (2015). Automated and Accurate Estimation of Gene Family Abundance from Shotgun Metagenomes. *PLoS Comput Biol* 11, e1004573. doi:10.1371/journal.pcbi.1004573.

Niemann, H., Duarte, J., Hensen, C., Omoregie, E., Magalhães, V. H., Elvert, M., et al. (2006a). Microbial methane turnover at mud volcanoes of the Gulf of Cadiz. *Geochimica et Cosmochimica Acta* 70, 5336–5355. doi:10.1016/j.gca.2006.08.010.

Niemann, H., Lösekann, T., de Beer, D., Elvert, M., Nadalig, T., Knittel, K., et al. (2006b). Novel microbial communities of the Haakon Mosby mud volcano and their role as a methane sink. *Nature* 443, 854–858. doi:10.1038/nature05227.

Nigro, O. D., Jungbluth, S. P., Lin, H.-T., Hsieh, C.-C., Miranda, J. A., Schvarcz, C. R., et al. (2017). Viruses in the Oceanic Basement. *mBio* 8, e02129-16. doi:10.1128/mBio.02129-16.

Nishio, Y., Ijiri, A., Toki, T., Morono, Y., Tanimizu, M., Nagaishi, K., et al. (2015). Origins of lithium in submarine mud volcano fluid in the Nankai accretionary wedge. *Earth and Planetary Science Letters* 414, 144–155. doi:10.1016/j.epsl.2015.01.018.

Nobu, M. K., Dodsworth, J. A., Murugapiran, S. K., Rinke, C., Gies, E. A., Webster, G., et al. (2016). Phylogeny and physiology of candidate phylum 'Atribacteria' (OP9/JS1) inferred from cultivation-independent genomics. *The ISME Journal* 10, 273–286. doi:10.1038/ismej.2015.97.

Nunoura, T., Oida, H., Miyazaki, J., Miyashita, A., Imachi, H., and Takai, K. (2008). Quantification of mcrA by fluorescent PCR in methanogenic and methanotrophic microbial communities. *FEMS Microbiology Ecology* 64, 240–247. doi:10.1111/j.1574-6941.2008.00451.x.

Nunoura, T., Soffientino, B., Blazejak, A., Kakuta, J., Oida, H., Schippers, A., et al. (2009). Subseafloor microbial communities associated with rapid turbidite deposition in the Gulf of Mexico continental slope (IODP Expedition 308). *FEMS Microbiol Ecol* 69, 410–424. doi:10.1111/j.1574-6941.2009.00718.x.

Orcutt, B. N., LaRowe, D. E., Biddle, J. F., Colwell, F. S., Glazer, B. T., Reese, B. K., et al. (2013). Microbial activity in the marine deep biosphere: progress and prospects. *Front Microbiol* 4. doi:10.3389/fmicb.2013.00189.

Orphan, V. J., Hinrichs, K.-U., Ussler, W., Paull, C. K., Taylor, L. T., Sylva, S. P., et al. (2001). Comparative Analysis of Methane-Oxidizing Archaea and Sulfate-Reducing Bacteria in Anoxic Marine Sediments. *Appl. Environ. Microbiol.* 67, 1922–1934. doi:10.1128/AEM.67.4.1922-1934.2001.

Orphan, V. J., House, C. H., Hinrichs, K.-U., McKeegan, K. D., and DeLong, E. F. (2002). Multiple archaeal groups mediate methane oxidation in anoxic cold seep sediments. *PNAS* 99, 7663–7668. doi:10.1073/pnas.072210299.

Orsi, W. D., Edgcomb, V. P., Christman, G. D., and Biddle, J. F. (2013). Gene expression in the deep biosphere. *Nature* 499, 205–208. doi:10.1038/nature12230.

Oulas, A., Polymenakou, P. N., Seshadri, R., Tripp, H. J., Mandalakis, M., Paez-Espino, A. D., et al. (2016). Metagenomic investigation of the geologically unique Hellenic Volcanic Arc reveals a distinctive ecosystem with unexpected physiology. *Environ Microbiol* 18, 1122–1136. doi:10.1111/1462-2920.13095.

Pachiadaki, M. G., and Kormas, K. A. (2013). Interconnectivity vs. isolation of prokaryotic communities in European deep-sea mud volcanoes. *Biogeosciences* 10, 2821–2831. doi:10.5194/bg-10-2821-2013.

Panieri, G., Polonia, A., Lucchi, R. G., Zironi, S., Capotondi, L., Negri, A., et al. (2013). Mud volcanoes along the inner deformation front of the Calabrian Arc accretionary wedge (Ionian Sea). *Marine Geology* 336, 84–98. doi:10.1016/j.margeo.2012.11.003.

Pape, T., Kasten, S., Zabel, M., Bahr, A., Abegg, F., Hohnberg, H.-J., et al. (2010). Gas hydrates in shallow deposits of the Amsterdam mud volcano, Anaximander Mountains, Northeastern Mediterranean Sea. *Geo-Mar Lett* 30, 187–206. doi:10.1007/s00367-010-0197-8.

Parkes, R. J., Cragg, B. A., Banning, N., Brock, F., Webster, G., Fry, J. C., et al. (2007). Biogeochemistry and biodiversity of methane cycling in subsurface marine sediments (Skagerrak, Denmark). *Environmental Microbiology* 9, 1146–1161. doi:10.1111/j.1462-2920.2006.01237.x.

Parkes, R. J., Cragg, B., Roussel, E., Webster, G., Weightman, A., and Sass, H. (2014). A review of prokaryotic populations and processes in sub-seafloor sediments, including biosphere:geosphere interactions. *Marine Geology* 352, 409–425. doi:10.1016/j.margeo.2014.02.009.

Paull, C. K., Ussler, W., Dallimore, S. R., Blasco, S. M., Lorenson, T. D., Melling, H., et al. (2007). Origin of pingo-like features on the Beaufort Sea shelf and their possible relationship to decomposing methane gas hydrates. *Geophys. Res. Lett.* 34, L01603. doi:10.1029/2006GL027977.

Perez-Garcia, C., Feseker, T., Mienert, J., and Berndt, C. (2009). The Håkon Mosby mud volcano: 330 000 years of focused fluid flow activity at the SW Barents Sea slope. *Marine Geology* 262, 105–115. doi:10.1016/j.margeo.2009.03.022.

Pernthaler, A., Dekas, A. E., Brown, C. T., Goffredi, S. K., Embaye, T., and Orphan, V. J. (2008). Diverse syntrophic partnerships from deep-sea methane vents revealed by direct cell capture and metagenomics. *PNAS* 105, 7052–7057. doi:10.1073/pnas.0711303105.

Pernthaler, J., and Amann, R. (2005). Fate of Heterotrophic Microbes in Pelagic Habitats: Focus on Populations. *Microbiol. Mol. Biol. Rev.* 69, 440–461. doi:10.1128/MMBR.69.3.440-461.2005.

Pett-Ridge, J., Silver, W. L., and Firestone, M. K. (2006). Redox Fluctuations Frame Microbial Community Impacts on N-cycling Rates in a Humid Tropical Forest Soil. *Biogeochemistry* 81, 95–110. doi:10.1007/s10533-006-9032-8.

Pfennig, N., and Biebl, H. (1976). Desulfuromonas acetoxidans gen. nov. and sp. nov., a new anaerobic, sulfur-reducing, acetate-oxidizing bacterium. *Archives of Microbiology* 110, 3–12. doi:10.1007/BF00416962.

Portnov, A., Smith, A. J., Mienert, J., Cherkashov, G., Rekant, P., Semenov, P., et al. (2013). Offshore permafrost decay and massive seabed methane escape in water depths >20 m at the South Kara Sea shelf. *Geophysical Research Letters* 40, 3962–3967. doi:10.1002/grl.50735.

Quast, C., Pruesse, E., Yilmaz, P., Gerken, J., Schweer, T., Yarza, P., et al. (2013). The SILVA ribosomal RNA gene database project: improved data processing and web-based tools. *Nucleic Acids Res* 41, D590–D596. doi:10.1093/nar/gks1219.

Ramírez, G. A., Jørgensen, S. L., Zhao, R., and D'Hondt, S. (2018). Minimal Influence of Extracellular DNA on Molecular Surveys of Marine Sedimentary Communities. *Front Microbiol* 9. doi:10.3389/fmicb.2018.02969.

Rasmussen, R. A., and Khalil, M. a. K. (1981). Atmospheric methane (CH4): Trends and seasonal cycles. *Journal of Geophysical Research: Oceans* 86, 9826–9832. doi:10.1029/JC086iC10p09826.

Rebata-Landa, V., and Santamarina, J. C. (2006). Mechanical limits to microbial activity in deep sediments. *Geochem. Geophys. Geosyst.* 7, Q11006. doi:10.1029/2006GC001355.

Reeburgh, W. S. (2007). Oceanic Methane Biogeochemistry. *Chem. Rev.* 107, 486–513. doi:10.1021/cr050362v.

Reed, D. C., Algar, C. K., Huber, J. A., and Dick, G. J. (2014). Gene-centric approach to integrating environmental genomics and biogeochemical models. *Proceedings of the National Academy of Sciences* 111, 1879–1884. doi:10.1073/pnas.1313713111.

Regnier, P., Dale, A. W., Arndt, S., LaRowe, D. E., Mogollón, J., and Van Cappellen, P. (2011). Quantitative analysis of anaerobic oxidation of methane (AOM) in marine sediments: A modeling perspective. *Earth-Science Reviews* 106, 105–130. doi:10.1016/j.earscirev.2011.01.002.

Roden, E. E., and Lovley, D. R. (1993). Dissimilatory Fe(III) Reduction by the Marine Microorganism Desulfuromonas acetoxidans. *Appl. Environ. Microbiol.* 59, 734–742.

Rodriguez-R, L. M., Overholt, W. A., Hagan, C., Huettel, M., Kostka, J. E., and Konstantinidis, K. T. (2015). Microbial community successional patterns in beach sands impacted by the Deepwater Horizon oil spill. *ISME J*. doi:10.1038/ismej.2015.5.

Roux, S., Brum, J. R., Dutilh, B. E., Sunagawa, S., Duhaime, M. B., Loy, A., et al. (2016). Ecogenomics and potential biogeochemical impacts of globally abundant ocean viruses. *Nature* 537, 689–693. doi:10.1038/nature19366.

Ruff, S. E., Biddle, J. F., Teske, A. P., Knittel, K., Boetius, A., and Ramette, A. (2015). Global dispersion and local diversification of the methane seep microbiome. *PNAS* 112, 4015–4020. doi:10.1073/pnas.1421865112.

Ruff, S. E., Felden, J., Gruber-Vodicka, H. R., Marcon, Y., Knittel, K., Ramette, A., et al. (2018). In situ development of a methanotrophic microbiome in deep-sea sediments. *The ISME Journal*, 1. doi:10.1038/s41396-018-0263-1.

Ruppel, C. (2011). Methane Hydrates and Contemporary Climate Change. 11.

Salter, S. J., Cox, M. J., Turek, E. M., Calus, S. T., Cookson, W. O., Moffatt, M. F., et al. (2014). Reagent and laboratory contamination can critically impact sequence-based microbiome analyses. *BMC Biology* 12, 87. doi:10.1186/s12915-014-0087-z.

Saunois, M., Bousquet, P., Poulter, B., Peregon, A., Ciais, P., Canadell, J. G., et al. (2016). The global methane budget 2000–2012. *Earth System Science Data* 8, 697–751. doi:https://doi.org/10.5194/essd-8-697-2016.

Sauter, E. J., Muyakshin, S. I., Charlou, J.-L., Schlüter, M., Boetius, A., Jerosch, K., et al. (2006). Methane discharge from a deep-sea submarine mud volcano into the upper water column by gas hydrate-coated methane bubbles. *Earth and Planetary Science Letters* 243, 354–365. doi:10.1016/j.epsl.2006.01.041.

Scheibe, T. D., Mahadevan, R., Fang, Y., Garg, S., Long, P. E., and Lovley, D. R. (2009). Coupling a genome-scale metabolic model with a reactive transport model to describe *in situ* uranium bioremediation. *Microbial Biotechnology* 2, 274–286. doi:10.1111/j.1751-7915.2009.00087.x.

Schloss, P. D. (2008). Evaluating different approaches that test whether microbial communities have the same structure. *ISME J* 2, 265–275. doi:10.1038/ismej.2008.5.

Schloss, P. D., Westcott, S. L., Ryabin, T., Hall, J. R., Hartmann, M., Hollister, E. B., et al. (2009). Introducing mothur: Open-Source, Platform-Independent, Community-Supported Software for Describing and Comparing Microbial Communities. *Appl. Environ. Microbiol.* 75, 7537–7541. doi:10.1128/AEM.01541-09.

Schouten, S., Wakeham, S. G., Hopmans, E. C., and Sinninghe Damste, J. S. (2003). Biogeochemical Evidence that Thermophilic Archaea Mediate the Anaerobic Oxidation

of Methane. *Applied and Environmental Microbiology* 69, 1680–1686. doi:10.1128/AEM.69.3.1680-1686.2003.

Seeberg-Elverfeldt, J., Schlüter, M., Feseker, T., and Kölling, M. (2005). Rhizon sampling of porewaters near the sediment-water interface of aquatic systems. *Limnology and Oceanography: Methods* 3, 361–371. doi:10.4319/lom.2005.3.361.

Seifert, R., Nauhaus, K., Blumenberg, M., Krüger, M., and Michaelis, W. (2006). Methane dynamics in a microbial community of the Black Sea traced by stable carbon isotopes in vitro. *Organic Geochemistry* 37, 1411–1419. doi:10.1016/j.orggeochem.2006.03.007.

Sen, A., Åström, E. K. L., Hong, W.-L., Portnov, A., Waage, M., Serov, P., et al. (2018). Geophysical and geochemical controls on the megafaunal community of a high Arctic cold seep. *Biogeosciences Discussions*, 1–52. doi:10.5194/bg-2017-540.

Serov, P., Portnov, A., Mienert, J., Semenov, P., and Ilatovskaya, P. (2015). Methane release from pingo-like features across the South Kara Sea shelf, an area of thawing offshore permafrost. *Journal of Geophysical Research: Earth Surface* 120, 1515–1529. doi:10.1002/2015JF003467.

Serov, P., Vadakkepuliyambatta, S., Mienert, J., Patton, H., Portnov, A., Silyakova, A., et al. (2017). Postglacial response of Arctic Ocean gas hydrates to climatic amelioration. *PNAS* 114, 6215–6220. doi:10.1073/pnas.1619288114.

Seyfried, W. E., Janecky, D. R., and Mottl, M. J. (1984). Alteration of the oceanic crust: Implications for geochemical cycles of lithium and boron. *Geochimica et Cosmochimica Acta* 48, 557–569. doi:10.1016/0016-7037(84)90284-9.

Shakhova, N., Semiletov, I., Salyuk, A., Yusupov, V., Kosmach, D., and Gustafsson, Ö. (2010). Extensive Methane Venting to the Atmosphere from Sediments of the East Siberian Arctic Shelf. *Science* 327, 1246–1250. doi:10.1126/science.1182221.

Sharon, I., Kertesz, M., Hug, L. A., Pushkarev, D., Blauwkamp, T. A., Castelle, C. J., et al. (2015). Accurate, multi-kb reads resolve complex populations and detect rare microorganisms. *Genome Res.*, gr.183012.114. doi:10.1101/gr.183012.114.

Sheik, C. S., Reese, B. K., Twing, K. I., Sylvan, J. B., Grim, S. L., Schrenk, M. O., et al. (2018). Identification and Removal of Contaminant Sequences From Ribosomal Gene Databases: Lessons From the Census of Deep Life. *Front. Microbiol.* 9. doi:10.3389/fmicb.2018.00840.

Sibuet, M., and Olu, K. (1998). Biogeography, biodiversity and fluid dependence of deep-sea cold-seep communities at active and passive margins. *Deep Sea Research Part II: Topical Studies in Oceanography* 45.

Slobodkina, G. B., Baslerov, R. V., Novikov, A. A., Bonch-Osmolovskaya, E. A., and Slobodkin, A. I. (2017). Thermodesulfitimonas autotrophica gen. nov., sp. nov., a thermophilic, obligate sulfite-reducing bacterium isolated from a terrestrial hot spring. *International Journal of Systematic and Evolutionary Microbiology* 67, 301–305. doi:10.1099/ijsem.0.001619.

Smith, A. R., Fisk, M. R., Thurber, A. R., Flores, G. E., Mason, O. U., Popa, R., et al. (2016). Deep Crustal Communities of the Juan de Fuca Ridge Are Governed by Mineralogy. *Geomicrobiology Journal*, 00–00. doi:10.1080/01490451.2016.1155001.

Solden, L., Lloyd, K., and Wrighton, K. (2016). The bright side of microbial dark matter: lessons learned from the uncultivated majority. *Current Opinion in Microbiology* 31, 217–226. doi:10.1016/j.mib.2016.04.020.

Sousa, F. L., Neukirchen, S., Allen, J. F., Lane, N., and Martin, W. F. (2016). Lokiarchaeon is hydrogen dependent. *Nature Microbiology* 1, 16034. doi:10.1038/nmicrobiol.2016.34.

Sparrow, K. J., Kessler, J. D., Southon, J. R., Garcia-Tigreros, F., Schreiner, K. M., Ruppel, C. D., et al. (2018). Limited contribution of ancient methane to surface waters of the U.S. Beaufort Sea shelf. *Science Advances* 4, eaao4842. doi:10.1126/sciadv.aao4842.

Spielhagen, R. F., Werner, K., Sørensen, S. A., Zamelczyk, K., Kandiano, E., Budeus, G., et al. (2011). Enhanced Modern Heat Transfer to the Arctic by Warm Atlantic Water. *Science* 331, 450–453. doi:10.1126/science.1197397.

Spring, S., Bunk, B., Spröer, C., Rohde, M., and Klenk, H.-P. (2018). Genome biology of a novel lineage of planctomycetes widespread in anoxic aquatic environments. *Environmental Microbiology* 0. doi:10.1111/1462-2920.14253.

Starnawski, P., Bataillon, T., Ettema, T. J. G., Jochum, L. M., Schreiber, L., Chen, X., et al. (2017). Microbial community assembly and evolution in subseafloor sediment. *PNAS*, 201614190. doi:10.1073/pnas.1614190114.

Stegen, J. C., Fredrickson, J. K., Wilkins, M. J., Konopka, A. E., Nelson, W. C., Arntzen, E. V., et al. (2016). Groundwater–surface water mixing shifts ecological assembly processes and stimulates organic carbon turnover. *Nature Communications* 7, 11237. doi:10.1038/ncomms11237.

Stegen, J. C., Lin, X., Konopka, A. E., and Fredrickson, J. K. (2012). Stochastic and deterministic assembly processes in subsurface microbial communities. *The ISME Journal* 6, 1653–1664. doi:10.1038/ismej.2012.22.

Stepanauskas, R. (2012). Enigmatic life underneath us: genomic analysis of deep subsurface microorganisms. DOE Joint Genome Institute doi:10.25585/1488075.

Stewart, F. J., Dalsgaard, T., Young, C. R., Thamdrup, B., Revsbech, N. P., Ulloa, O., et al. (2012). Experimental Incubations Elicit Profound Changes in Community Transcription in OMZ Bacterioplankton. *PLoS ONE* 7, e37118. doi:10.1371/journal.pone.0037118.

Stokke, R., Roalkvam, I., Lanzen, A., Haflidason, H., and Steen, I. H. (2012). Integrated metagenomic and metaproteomic analyses of an ANME-1-dominated community in marine cold seep sediments. *Environmental Microbiology* 14, 1333–1346. doi:10.1111/j.1462-2920.2012.02716.x.

Stumm, W., and Morgan, J. J. (1996). *Aquatic Chemistry: Chemical Equilibria and Rates in Natural Waters, 3rd ed.* Wiley-Interscience.

Summons, R. E., Franzmann, P. D., and Nichols, P. D. (1998). Carbon isotopic fractionation associated with methylotrophic methanogenesis. *Organic Geochemistry* 28, 465–475. doi:10.1016/S0146-6380(98)00011-4.

Sun, R., and Duan, Z. (2007). An accurate model to predict the thermodynamic stability of methane hydrate and methane solubility in marine environments. *Chemical Geology* 244, 248–262. doi:10.1016/j.chemgeo.2007.06.021.

Suzuki, D., Li, Z., Cui, X., Zhang, C., and Katayama, A. (2014). Reclassification of Desulfobacterium anilini as Desulfatiglans anilini comb. nov. within Desulfatiglans gen. nov., and description of a 4-chlorophenol-degrading sulfate-reducing bacterium, Desulfatiglans parachlorophenolica sp. nov. *International Journal of Systematic and Evolutionary Microbiology* 64, 3081–3086. doi:10.1099/ijs.0.064360-0.

Sylvan, J. B., Toner, B. M., and Edwards, K. J. (2012). Life and Death of Deep-Sea Vents: Bacterial Diversity and Ecosystem Succession on Inactive Hydrothermal Sulfides. *mBio* 3, e00279-11. doi:10.1128/mBio.00279-11.

Tavormina, P. L., Ussler, W., Joye, S. B., Harrison, B. K., and Orphan, V. J. (2010). Distributions of putative aerobic methanotrophs in diverse pelagic marine environments. *The ISME Journal* 4, 700–710. doi:10.1038/ismej.2009.155.

Teske, A., Hinrichs, K.-U., Edgcomb, V., Gomez, A. de V., Kysela, D., Sylva, S. P., et al. (2002). Microbial Diversity of Hydrothermal Sediments in the Guaymas Basin: Evidence for Anaerobic Methanotrophic Communities. *Appl. Environ. Microbiol.* 68, 1994–2007. doi:10.1128/AEM.68.4.1994-2007.2002.

Timmers, P. H. A., Gieteling, J., Widjaja-Greefkes, H. C. A., Plugge, C. M., Stams, A. J. M., Lens, P. N. L., et al. (2015). Growth of Anaerobic Methane-Oxidizing Archaea and Sulfate-Reducing Bacteria in a High-Pressure Membrane Capsule Bioreactor. *Appl. Environ. Microbiol.* 81, 1286–1296. doi:10.1128/AEM.03255-14.

Torres, M. E., Mix, A. C., and Rugh, W. D. (2005). Precise δ13C analysis of dissolved inorganic carbon in natural waters using automated headspace sampling and continuous-flow

mass spectrometry. *Limnology and Oceanography: Methods* 3, 349–360. doi:10.4319/lom.2005.3.349.

Torti, A., Lever, M. A., and Jørgensen, B. B. (2015). Origin, dynamics, and implications of extracellular DNA pools in marine sediments. *Marine Genomics* 24, 185–196. doi:10.1016/j.margen.2015.08.007.

Treude, T., Boetius, A., Knittel, K., Wallmann, K., and Barker Jørgensen, B. (2003). Anaerobic oxidation of methane above gas hydrates at Hydrate Ridge, NE Pacific Ocean. *Marine Ecology Progress Series* 264, 1–14. doi:10.3354/meps264001.

Valentine, D. L. (2002). Biogeochemistry and microbial ecology of methane oxidation in anoxic environments: a review. *Antonie Van Leeuwenhoek* 81, 271–282. doi:10.1023/A:1020587206351.

Valenzuela, E. I., Prieto-Davó, A., López-Lozano, N. E., Hernández-Eligio, A., Vega-Alvarado, L., Juárez, K., et al. (2017). Anaerobic methane oxidation driven by microbial reduction of natural organic matter in a tropical wetland. *Appl. Environ. Microbiol.*, AEM.00645-17. doi:10.1128/AEM.00645-17.

Van Dover, C. L., Aharon, P., Bernhard, J. M., Caylor, E., Doerries, M., Flickinger, W., et al. (2003). Blake Ridge methane seeps: characterization of a soft-sediment, chemosynthetically based ecosystem. *Deep Sea Research Part I: Oceanographic Research Papers* 50, 281–300. doi:10.1016/S0967-0637(02)00162-0.

Vandieken, V. (2006). Desulfuromonas svalbardensis sp. nov. and Desulfuromusa ferrireducens sp. nov., psychrophilic, Fe(III)-reducing bacteria isolated from Arctic sediments, Svalbard. *INTERNATIONAL JOURNAL OF SYSTEMATIC AND EVOLUTIONARY MICROBIOLOGY* 56, 1133–1139. doi:10.1099/ijs.0.63639-0.

Vanwonterghem, I., Evans, P. N., Parks, D. H., Jensen, P. D., Woodcroft, B. J., Hugenholtz, P., et al. (2016). Methylotrophic methanogenesis discovered in the archaeal phylum Verstraetearchaeota. *Nature Microbiology* 1, 16170. doi:10.1038/nmicrobiol.2016.170.

Voogd, B. D., Truffert, C., Chamot-rooke, N., Huchon, P., Lallemant, S., and Pichon, X. L. (1992). Two-ships deep seismic soundings in the basin of the eastern Mediterranean Sea (Pasiphae cruise), Geophys. *J. Int*, 536–552.

Wakeham, S. G., Hopmans, E. C., Schouten, S., and Sinninghe Damsté, J. S. (2004). Archaeal lipids and anaerobic oxidation of methane in euxinic water columns: a comparative study of the Black Sea and Cariaco Basin. *Chemical Geology* 205, 427–442. doi:10.1016/j.chemgeo.2003.12.024.

Wang, F.-P., Zhang, Y., Chen, Y., He, Y., Qi, J., Hinrichs, K.-U., et al. (2013). Methanotrophic archaea possessing diverging methane-oxidizing and electron-transporting pathways. *The ISME journal*. Available at:

http://www.nature.com/ismej/journal/vaop/ncurrent/full/ismej2013212a.html [Accessed May 20, 2014].

Wang, F.-P., Zhang, Y., Chen, Y., He, Y., Qi, J., Hinrichs, K.-U., et al. (2014). Methanotrophic archaea possessing diverging methane-oxidizing and electron-transporting pathways. *ISME J* 8, 1069–1078. doi:10.1038/ismej.2013.212.

Wang, G., Jagadamma, S., Mayes, M. A., Schadt, C. W., Megan Steinweg, J., Gu, L., et al. (2015). Microbial dormancy improves development and experimental validation of ecosystem model. *ISME J* 9, 226–237. doi:10.1038/ismej.2014.120.

Wankel, S. D., Adams, M. M., Johnston, D. T., Hansel, C. M., Joye, S. B., and Girguis, P. R. (2012). Anaerobic methane oxidation in metalliferous hydrothermal sediments: influence on carbon flux and decoupling from sulfate reduction. *Environmental Microbiology* 14, 2726–2740. doi:10.1111/j.1462-2920.2012.02825.x.

Wegener, G., Krukenberg, V., Ruff, S. E., Kellermann, M. Y., and Knittel, K. (2016). Metabolic Capabilities of Microorganisms Involved in and Associated with the Anaerobic Oxidation of Methane. *Front Microbiol* 7. doi:10.3389/fmicb.2016.00046.

Weinberger, A. D., Wolf, Y. I., Lobkovsky, A. E., Gilmore, M. S., and Koonin, E. V. (2012). Viral Diversity Threshold for Adaptive Immunity in Prokaryotes. *mBio* 3. doi:10.1128/mBio.00456-12.

Welander, P. V., and Metcalf, W. W. (2008). Mutagenesis of the C1 Oxidation Pathway in Methanosarcina barkeri: New Insights into the Mtr/Mer Bypass Pathway. *Journal of Bacteriology* 190, 1928–1936. doi:10.1128/JB.01424-07.

Werne, J. P., Haese, R. R., Zitter, T., Aloisi, G., Bouloubassi, I., Heijs, S., et al. (2004). Life at cold seeps: a synthesis of biogeochemical and ecological data from Kazan mud volcano, eastern Mediterranean Sea. *Chemical Geology* 205, 367–390. doi:10.1016/j.chemgeo.2003.12.031.

Westbrook, G. K., Thatcher, K. E., Rohling, E. J., Piotrowski, A. M., Pälike, H., Osborne, A. H., et al. (2009). Escape of methane gas from the seabed along the West Spitsbergen continental margin: ARCTIC METHANE GAS PLUMES. *Geophysical Research Letters* 36, n/a-n/a. doi:10.1029/2009GL039191.

White, J. R., Nagarajan, N., and Pop, M. (2009). Statistical Methods for Detecting Differentially Abundant Features in Clinical Metagenomic Samples. *PLoS Comput Biol* 5. doi:10.1371/journal.pcbi.1000352.

Whiticar, M. J. (1999). Carbon and hydrogen isotope systematics of bacterial formation and oxidation of methane. *Chemical Geology* 161, 291–314. doi:10.1016/S0009-2541(99)00092-3.

Widdel, F., and Bak, F. (1992). “Gram-Negative Mesophilic Sulfate-Reducing Bacteria,” in *The Prokaryotes*, eds. A. Balows, H. G. Trüper, M. Dworkin, W. Harder, and K.-H. Schleifer (Springer New York), 3352–3378. doi:10.1007/978-1-4757-2191-1_21.

Winkel, M., Mitzscherling, J., Overduin, P. P., Horn, F., Winterfeld, M., Rijkers, R., et al. (2018). Anaerobic methanotrophic communities thrive in deep submarine permafrost. *Scientific Reports* 8, 1291. doi:10.1038/s41598-018-19505-9.

Woycheese, K. M., Meyer-Dombard, D. R., Cardace, D., Argayosa, A. M., and Arcilla, C. A. (2015). Out of the dark: transitional subsurface-to-surface microbial diversity in a terrestrial serpentinizing seep (Manleluag, Pangasinan, the Philippines). *Front. Microbiol* 6, 44. doi:10.3389/fmicb.2015.00044.

Xia, Y., Wang, Y., Wang, Y., Chin, F. Y. L., and Zhang, T. (2016). Cellular adhesiveness and cellulolytic capacity in Anaerolineae revealed by omics-based genome interpretation. *Biotechnology for Biofuels* 9, 111. doi:10.1186/s13068-016-0524-z.

Xie, W., Wang, F., Guo, L., Chen, Z., Sievert, S. M., Meng, J., et al. (2011). Comparative metagenomics of microbial communities inhabiting deep-sea hydrothermal vent chimneys with contrasting chemistries. *ISME J* 5, 414–426. doi:10.1038/ismej.2010.144.

Yoshinaga, M. Y., Holler, T., Goldhammer, T., Wegener, G., Pohlman, J. W., Brunner, B., et al. (2014). Carbon isotope equilibration during sulphate-limited anaerobic oxidation of methane. *Nature Geoscience* 7, 190–194. doi:10.1038/ngeo2069.

You, C.-F., Chan, L. H., Spivack, A. J., and Gieskes, J. M. (1995). Lithium, boron, and their isotopes in sediments and pore waters of Ocean Drilling Program Site 808, Nankai Trough: Implications for fluid expulsion in accretionary prisms. *Geology* 23, 37. doi:10.1130/0091-7613(1995)023<0037:LBATII>2.3.CO;2.

You, C.-F., Spivack, A. J., Smith, J. H., and Gieskes, J. M. (1993). Mobilization of boron in convergent margins: Implications for the boron geochemical cycle. *Geology* 21, 207. doi:10.1130/0091-7613(1993)021<0207:MOBICM>2.3.CO;2.

Zeebe, R. E., and Wolf-Gladrow, D. (2001). *CO2 in Seawater: Equilibrium, Kinetics, Isotopes*. Gulf Professional Publishing.

Zhang, Y., Henriet, J.-P., Bursens, J., and Boon, N. (2010). Stimulation of in vitro anaerobic oxidation of methane rate in a continuous high-pressure bioreactor. *Bioresource Technology* 101, 3132–3138. doi:10.1016/j.biortech.2009.11.103.

Zhang, Y., Maignien, L., Stadnitskaia, A., Boeckx, P., Xiao, X., and Boon, N. (2014). Stratified Community Responses to Methane and Sulfate Supplies in Mud Volcano Deposits: Insights from an In Vitro Experiment. *PLoS ONE* 9, e113004. doi:10.1371/journal.pone.0113004.

Zhang, Y., Maignien, L., Zhao, X., Wang, F., and Boon, N. (2011). Enrichment of a microbial community performing anaerobic oxidation of methane in a continuous high-pressure bioreactor. *BMC microbiology* 11, 137.

Zhou, J., Bruns, M. A., and Tiedje, J. M. (1996). DNA recovery from soils of diverse composition. *Appl. Environ. Microbiol.* 62, 316–322.

Zhou, J., He, Z., Yang, Y., Deng, Y., Tringe, S. G., and Alvarez-Cohen, L. (2015). High-Throughput Metagenomic Technologies for Complex Microbial Community Analysis: Open and Closed Formats. *mBio* 6, e02288-14. doi:10.1128/mBio.02288-14.

Zhu, G., Jetten, M. S. M., Kuschk, P., Ettwig, K. F., and Yin, C. (2010). Potential roles of anaerobic ammonium and methane oxidation in the nitrogen cycle of wetland ecosystems. *Appl Microbiol Biotechnol* 86, 1043–1055. doi:10.1007/s00253-010-2451-4.

Zinder, S. H. (1993). “Physiological Ecology of Methanogens,” in *Methanogenesis: Ecology, Physiology, Biochemistry & Genetics* Chapman & Hall Microbiology Series., ed. J. G. Ferry (Boston, MA: Springer US), 128–206. doi:10.1007/978-1-4615-2391-8_4.

Zobell, C. E. (1938). Studies on the bacterial flora of marine bottom sediments. *Journal of Sedimentary Research* 8, 10–18. doi:10.1306/D4268FD6-2B26-11D7-8648000102C1865D.